Geoinformatic and Hydrologic Analysis using Open Source Data for Floods Management in Pakistan

POLITECNICO DI TORINO

Ph.D. in Environment and Territory

Geoinformatic and Hydrologic Analysis using Open Source Data for Floods Management in Pakistan

Muhammad Adnan Shahid

Matr. 189983

Tutor: Prof. Piero Boccardo

Ph.D. Dissertation

April 2015

Abstract

There is being observed high variability in the spatial and temporal rainfall patterns under changing climate, enhancing both the intensity and frequency of the natural disasters like floods. Pakistan, a country which is highly prone to climate change, is recently facing the challenges of both flooding and severe water shortage as the surface water storage capacity is too limited to cope with heavy flows during rainy months. Thus, an effective and timely predication and management of high flows is a dire need to address both flooding and long term water shortage issues.

The work of this thesis was aimed at developing and evaluating different open source data based methodologies for floods detection and analysis in Pakistan. Specifically, the research work was conducted for developing and evaluating a hydrologic model being able to run in real time based on satellite rainfall data, as well as to perform flood hazard mapping by analyzing seasonality of flooded areas using MODIS classification approach.

In the first phase, TRMM monthly rainfall data (TMPA 3B43) was evaluated for Pakistan by comparison with rain gauge data, as well as by further focusing on its analysis and evaluation for different time periods and climatic zones of Pakistan. In the next phase, TRMM rainfall data and other open source datasets like digital soil map and global land cover map were utilized to develop and evaluate an event-based hydrologic model using HEC-HMS, which may be able to be run in real time for predicting peak flows due to any extreme rainfall event. Finally, to broaden the study canvas from a river catchment to the whole country scale, MODIS automated water bodies classification approach with MODIS daily surface reflectance products was utilized to develop a historical archive of reference water bodies and perform seasonal analysis of flooded areas for Pakistan. The approach was found well capable for its application for floods detection in plain areas of Pakistan.

The open source data based hydrologic modeling approach devised in this study can be helpful for conducting similar rainfall-runoff modeling studies for the other river catchments and predicting peak flows at a river catchment scale, particularly in mountainous topography. Similarly, the outcomes of MODIS classification analysis regarding reference and seasonal water and flood hazard maps may be helpful for planning any management interventions in the flood prone areas of Pakistan.

First of all, thanks to Almighty ALLAH who gave me courage to pursue my Ph.D. studies and produce this dissertation; I would not be able to do anything without His blessings. Afterwards, I extend my sincere thanks to my supervisor Prof. Piero Boccardo and all the research team at ITHACA, especially Franca Disabato, Adriana, Elena and Walther, for their valuable guidance and support. I would also like to pay my gratitude to all friends for their consistent support during my stay in Italy. I have no words to pay thanks to my parents and all family members in Pakistan for their continuous prayers and moral support. These acknowledgements cannot be completed without mentioning Higher Education Commission of Pakistan; I am highly obliged for the financial support provided by HEC in the form of scholarship to conduct my Ph.D. research abroad.

Contents

Sr. #	Description	Page No.
1	**Chapter 1: Introduction**	**1**
1.1	Natural Hazards and their Impacts	1
1.2	Disaster Risk Management	3
1.3	Floods as Natural Disaster	5
1.4	Climate Change Impacts and Occurrence of Floods – Global Perspective	6
1.5	Climate Change Impacts: Floods and other Water-related Issues of Pakistan	7
1.6	Geoinformatics and Floods Management	10
1.6.1	Early Flood Warnings – ITHACA's Extreme Rainfall Detection System (ERDS)	10
1.6.2	Hydrologic Modeling at a River Catchment Scale	13
1.6.3	Detection of Flood Inundated Areas	14
1.7	Objectives of Current Dissertation	14
2	**Chapter 2: Performance Evaluation of TRMM Precipitation Estimates for Pakistan**	**17**
2.1	Overview of the Chapter	17
2.2	Literature Review and Problem Statement	18
2.3	Description of Satellite Rainfall Data	20
2.3.1	Instruments and Input Datasets	21
2.3.2	Stages of TMPA Products Development	24
2.4	Methodology for Evaluation of TRMM Data for Pakistan	26
2.4.1	Calibration using Regression Analysis	28
2.4.2	Statistical Evaluation	30
2.5	Results and Discussion	30
2.5.1	Calibration and Evaluation of TRMM datasets all over the Pakistan	30
2.5.2	Calibration and Evaluation based on three different Climatic Zones	36
2.6	Conclusions	41
3	**Chapter 3: Hydrologic Modeling at River Catchment Scale (Chenab River Catchment)**	**45**
3.1	Overview of the Chapter	45
3.2	Literature Review and Problem Statement	46
3.2.1	Description of HEC-HMS Model	47
3.3	Description of Study Area – Chenab River Catchment	50
3.4	Datasets Utilized	51
3.4.1	Digital Elevation Model	51
3.4.2	Soil and Land Use Data	52
3.4.3	Hydro-climatic Data	53
3.5	Data Pre-processing using HEC-GeoHMS	53

3.5.1	Computation of Curve Number Grid	55
3.6	HEC-HMS Model Implementation	57
3.7	Model Calibration and Validation	59
3.8	Results and Discussion	60
3.9	Conclusions	68
4	**Chapter 4: Reference Water Bodies and Flood Hazard Delineation using MODIS**	**69**
4.1	Overview of the Chapter	69
4.2	Literature Review and Problem Statement	70
4.3	Description of MODIS Data System	73
4.3.1	MODIS Sensor and Bands	73
4.3.2	MODIS Products and their Levels and Formats	75
4.3.3	MODIS Products Utilized in Current Study	77
4.4	Methodology and Implementation of Procedures	78
4.4.1	Downloading of Data	78
4.4.2	Data Pre-processing and Classification	79
4.4.3	Time Compositing	81
4.4.4	Masking of Areas	82
4.4.5	Use of Automated Procedures and Processing Times Considerations	83
4.5	Results and Discussion	84
4.5.1	Reference and Seasonal Water and Flooded Areas Analysis on Annual Basis	84
4.5.2	Seasonal Reference Water and Flooded Areas Analysis for Monsoon Season	86
4.5.3	Areas under Water on Decadal and Monthly Basis	91
4.5.4	Comparison of Flood Inundated Areas with the Observed Peak Flows and TRMM Rainfall	93
4.6	Conclusions	99
	Summary and Conclusion	**101**
	References	**105**
	Appendices	**115**
	Appendix A. Hydrologic Response of Individual Sub-basins	115
	Appendix B. Reference Water and Flood Hazard Maps on Decadal Basis for Summer/ Monsoon Season	124

Chapter 1

Introduction

This doctoral research has been conducted in the work context of ITHACA (Information Technology for Humanitarian Assistance, Cooperation and Action). ITHACA Research Center is a project developed jointly by World Food Program (WFP), Politecnico di Torino and Higher Institute on Territorial Systems for Innovation (SiTI), with the objectives of establishing historical data patterns, developing forecasting models, and applying satellite imagery to rapidly determine and monitor the areas affected by natural disasters like floods, hurricanes, earthquakes, etc. The work of this thesis is particularly focused on methodologies for floods detection and management and their application for Pakistan. In this chapter, basic introduction regarding climate change impacts, natural hazards, climate change scenarios for Pakistan, and application of different geoinformatic techniques have been described, followed by the formulation of the objectives of the thesis.

1.1 Natural Hazards and their Impacts

Natural hazards are the physical events occurring naturally, which may cause severe damage and disturbance to human life. According to United Nations International Strategy for Disaster Reduction Secretariat (UNISDR), a hazard may be defined as a potentially damaging physical event that may cause the loss of life or injury, property damage, social and economic disturbance and/or environmental degradation. When a hazard results in a serious disorder of the functioning of a community or a society causing widespread human, material, economic and/or environmental losses, which exceed the ability of the affected community or society to compete with it using its own resources, it is termed as a disaster (UNISDR, 2009).

Natural hazards can be divided into different categories viz. biological (viral and bacterial infectious diseases, etc.), geophysical (earthquake, volcano, dry mass movement), hydrological (floods, wet mass movement), meteorological (storms) and climatological (extreme temperature, drought, wildfire). It has been observed that the frequency of occurrence of the natural hazards is on gradual rise, possibly due to global warming and climate change impacts. As reported by Guha-sapir et al. (2014), Figure 1.1 shows the trends of occurrence of natural disasters, excluding biological disasters and their victims since 1990.

It can be seen that there is a major and continuous rise in number of disasters from 1990 to 2000 and almost a steady trend afterwards up to 2013.

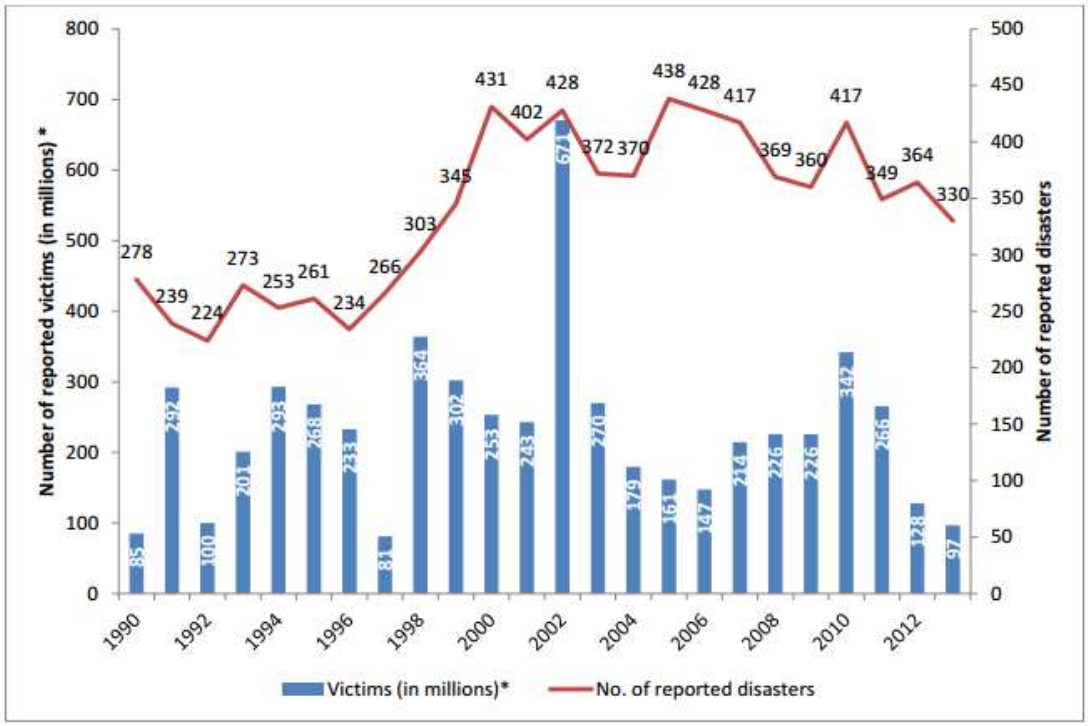

Figure 1.1: Trends of occurrence and victims of natural disasters (Guha-sapir et al., 2014)

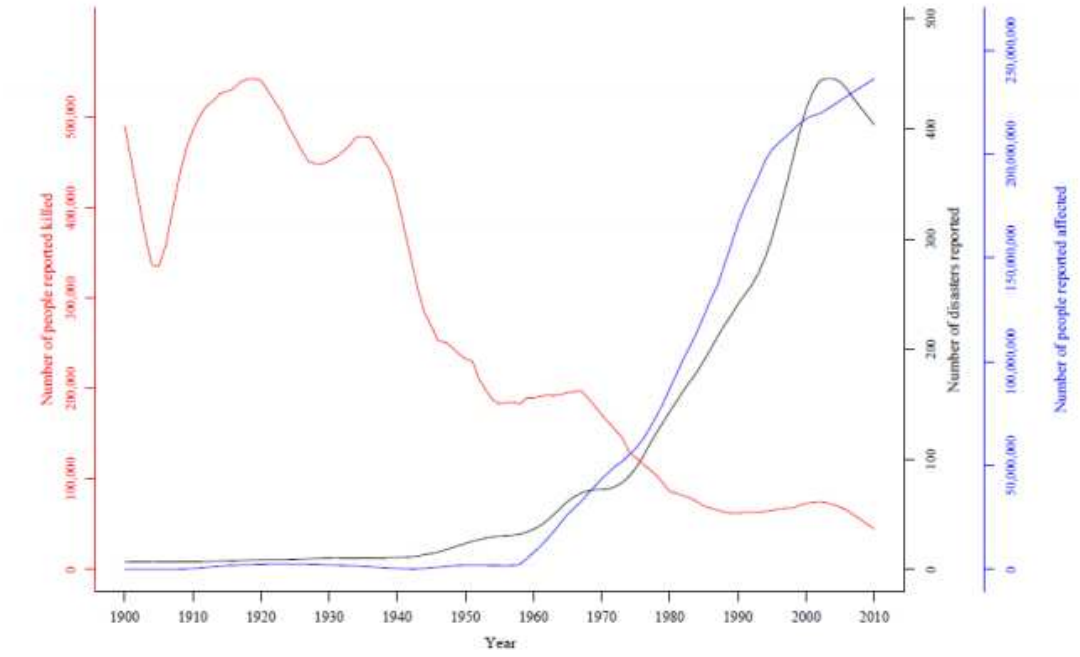

Figure 1.2: Natural disasters summary: 1900−2010 (EM-DAT, 2010)

Figure 1.2 further highlights the trend of occurrence of natural disasters and associated economic losses since 1900; along with loss of life associated with these disasters, which has

been continuously decreased. This remarkable decline in loss of life in comparison to occurred disasters points out to the increasingly effective role of disaster management activities, which can significantly contribute to reduce the impacts of hazards on human life. It can be concluded that although more people are vulnerable to disasters due to increased population and extension of populated areas into the danger zones, risk management activities in terms of early warnings and timely evacuations and other preparedness activities can significantly limit the human loss of life.

1.2 Disaster Risk Management

Disaster Risk Management can be defined as an integrated approach for designing, implementing, and evaluating strategies, policies, and measures to (i) improve the understanding of disaster risk, (ii) foster disaster risk reduction, and (iii) promote continuous improvement in disaster preparedness, response and recovery practices with the overall objective of increasing human security, well-being, quality of life, resilience and sustainable development (IPCC, 2012). In more simple form, it can be defined as a systematic approach to identify, assess and reduce the risks of a disaster. It should not be confused with conventional emergency management, because its scope is much broader with the potential of its initiatives in almost every sector of development and humanitarian work.

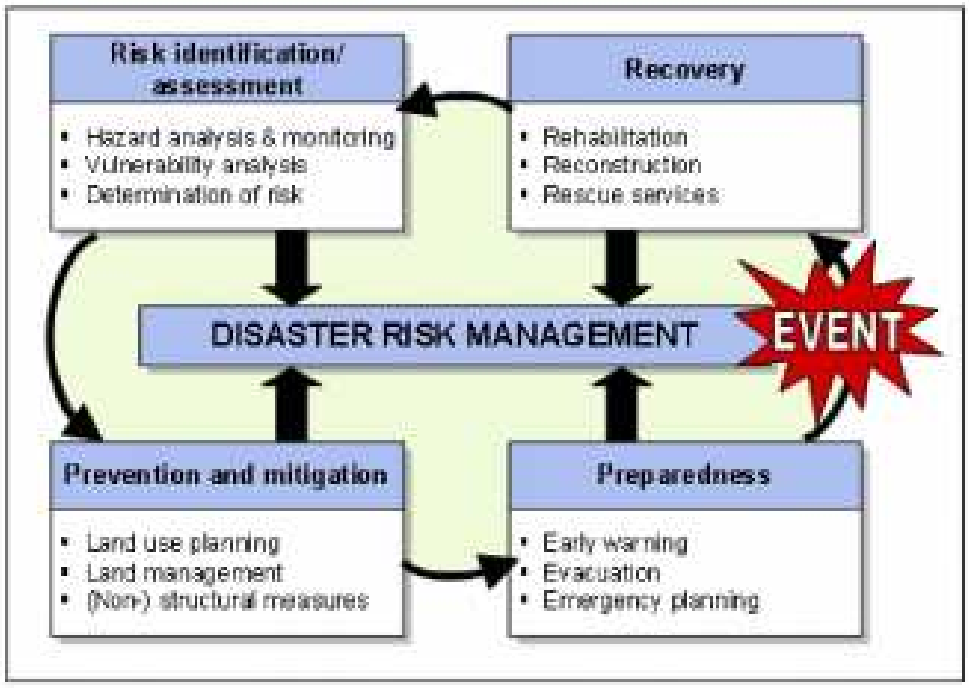

Figure 1.3: Key elements or phases of Disaster Risk Management Cycle (Source: FIG, 2006).

Disaster risk management cycle consists of different main elements or phases, which have been shown in Figure 1.3, as elaborated by (FIG, 2006). These can be briefly explained as follows:

1) Risk identification and assessment phase:

This phase consists of determining and analyzing the potential, origin and other characteristics of a hazard like frequency of occurrence and magnitude of consequences. The activities are normally comprised of statistical analysis of historical events to determine the return periods (frequency of occurrence) and amount of risks associated with events of different magnitudes for their vulnerability analysis.

2) Prevention and mitigation phase:

This is also a pre-event or normal situation phase based on the analysis of previous events, which comprises of application of risk reduction measures. This may include land use planning and land management keeping in view the previous disasters for the prevention and mitigation of future disasters. It also includes the planning and implementation of structural interventions like dams and dikes, or non-structural measures like disaster legislation.

3) Preparedness phase:

This phase comprises of activities just before or during the initial stages of occurrence of an event. The activities include timely and effective warnings, as well as evacuation and emergency planning.

4) Recovery phase:

This is a post-disaster phase, comprising of decisions and actions like rehabilitation, reconstruction and rescue services, with the objective to restore the living conditions of the affected population.

The activities described in different phases of disaster risk management cycle play an important role to effectively reduce the impacts of a natural hazard in terms of loss of life, infrastructure, etc. Importance of research in this area for further refining these activities cannot be overlooked, particularly regarding effective early warnings or alerts.

1.3 Floods as Natural Disaster

Flood can be defined as a temporary covering by water of a land, which is not normally under water. This includes floods from rivers, mountain torrents, and from the sea in coastal areas. Floods endanger human lives directly and by causing health risks in the form of infections and water-borne diseases, as well as cause heavy economic losses. In addition to such socio-economic damages, floods cause severe environmental impacts, e.g. inundation of sensitive installments having quantities of chemicals, and destruction of wetlands. De Groeve et al. (2007) have reported that floods are the most frequent ones of all the natural disasters and cause most human suffering and loss. As reported by Guha-sapir et al. (2014), Figure 1.4 shows the number of different categories of disasters occurred in 2013, as well as the number of people affected by them.

It can be seen that hydrological disasters like floods are almost 50% of the total, but the number of victims in case of such disasters is only 33% of total; while number of victims due to meteorological disasters like storms/extreme rainfalls is more than 50%. This indicates that more effective and forecast-based advance alerts, and in turn the management activities, are needed for sudden disasters like storms; whereas, relatively more lead time is available for providing alerts and planning mitigation activities in case of floods occurring downstream, based on forecast and near-real time rainfall data in upstream areas. However, meteorological disasters like extreme rainfalls and storms and hydrological disasters like floods are very much inter-related and Figure 1.4 shows that collectively more than 80% of natural disasters as well as number of victims are due to such hydro-meteorological disasters. Moreover, due to their inter-related nature, effective alerts regarding extreme rainfall events can be helpful for planning management activities for both types of disasters.

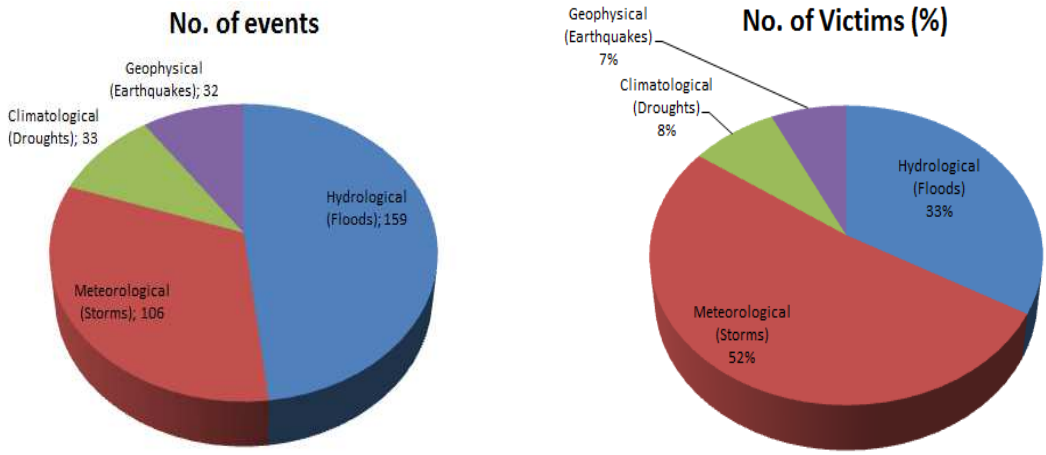

Figure 1.4: No. of events with percent victims of different types of disasters occurred in 2013.

1.4 Climate Change Impacts and Occurrence of Floods – Global Perspective

An unprecedented climate change has been observed since 1950s in the form of global atmospheric and oceanic warming, depleting snow and ice resources, changing precipitation patterns, and rising sea levels. It has been observed with high confidence that permafrost temperatures have increased in most regions since the early 1980s in response to increased surface temperature, with continued shrinkage of glaciers almost worldwide and decrease in spring snow cover extent in the northern hemisphere. These changes in climate have strong impacts and in many regions, changing precipitation patterns or melting snow and ice are bringing alterations in the hydrological systems and affecting water resources in terms of quantity and quality. It is worth mentioning that changes are not only limited to the average values of different climatic parameters, but have also been observed in extreme weather and climate events; including a decrease in cold temperature extremes, an increase in warm temperature extremes, an increase in extreme high sea levels and an increase in the number of heavy precipitation events in a number of regions. There are likely more land regions where the number of heavy precipitation events has increased than where it has decreased. Such increasing trends in extreme precipitation and discharge in some catchments imply greater risks of flooding at regional scale (IPCC, 2014).

In addition to observed climate changes, it has been predicted in IPCC fifth assessment report that global mean surface temperature will continue to increase by the end of the 21st century (2081-2100), and this increase relative to 1986-2005 is likely to be in the range of 0.3°C–4.8°C under different emission scenarios. There will be more frequent hot and fewer cold temperature extremes over most land areas on daily and seasonal timescales, and it is very likely that heat waves will occur with a higher frequency and longer duration. Changes in precipitation will not be uniform over the globe; however, there is medium confidence that increases in heavy precipitation will occur in some regions despite projected decreases in total precipitation. It is very likely that extreme precipitation events over most of the mid-latitude land masses and over wet tropical regions will become more intense and more frequent (IPCC, 2014). Moreover, projected precipitation and temperature changes imply possible changes in floods, and there is medium confidence that projected increases in heavy rainfall would contribute to increases in local flooding in some catchments or regions. Similarly, there is high confidence that changes in heat waves, glacial retreat, and/or permafrost degradation

will affect high mountain phenomena such as slope instabilities, movements of mass, and glacial lake outburst floods (IPCC, 2012).

1.5 Climate Change Impacts: Floods and other Water-related Issues of Pakistan

Pakistan, like many other countries of Asia, is a densely populated country with agriculture as its backbone, but facing the issues of severe climate impacts and limiting water resources. Major part of the country lies within the Indus basin, which is one of the ten major river systems of High Mountain Hindu Kush–Himalaya (HKH) region and originates from Karakoram Mountains, the west most part of HKH region. After the Indus Water Treaty between India and Pakistan in 1960, Pakistan was deprived of the water rights of three eastern tributaries of Indus River, whereas the rights of three western rivers including Indus, Jhelum and Chenab, were given to Pakistan (Figure 1.5).

Figure 1.5: Indus River along with its tributaries flowing through Pakistan (FAO-Aquastat, 2012).

The Indus Water Treaty brought a major change in the irrigation system of Pakistan with the construction of mega reservoirs and barrages on western rivers and excavation of link canals to divert water to the eastern rivers for irrigating the agricultural lands under the command of

these rivers. However, it created an imbalance in the natural flows; the eastern rivers depend on the waters of western rivers for feeding their irrigation canals in dry winter months, but contribute to the already heavy flows and flood situation in the country during summer and rainy months after heavy rainfalls and flood situation on Indian side.

The HKH or Himalayan region is characterized by a diversity of climate, with monsoon system weakening from east to west and rarely penetrating as far as the Karakoram. Catchments in the eastern and central Himalaya, covering the areas of Bangladesh, Nepal, India, etc., receive more than 70% of their annual rainfall in the summer monsoon period; whereas catchments to the west of the Sutlej River, an eastern tributary of Indus River, receive precipitation due to monsoon as well as westerly winds effect (Bookhagen & Burbank, 2010). Thus, in Pakistan, main source of precipitation in plain areas of Punjab and Sind is the monsoon rainfall in summer, while the northern areas receive major precipitation in the form of snow due to westerly winds. As a result of such precipitation distribution, Indus River, as it emerges onto the Punjab plains, receives more than 80% of its flow from glaciers and snowmelt. Direct runoff due to monsoonal rainfall, mainly from southern foothills of Himalayan divide, also makes a supplementary contribution to Indus River flows and its proportion increases progressively towards east in case of neighboring Indus tributaries of Jhelum, Chenab, Ravi and Sutlej (Archer and Fowler, 2004).

Under the changing climate, there has been observed as well as projected major seasonal variation in rainfall amounts, which are increasing in summer months from March to August and decreasing in the winter months. In addition to seasonal variation, there has been observed an 80-100 Km westward shift of monsoonal rainfall, indicating that there is high probability of occurrence of heavy rainfall events and increase in monsoonal rainfall contribution to the western rivers of Pakistan viz. Indus, Jhelum and Chenab. This, along with increased glacier and snowmelt contribution under increasing temperatures, points out towards heavy flows in summer and subsequent rainy months in Indus River and its tributaries flowing through Pakistan. It will create a further imbalance in the seasonal flows, indicating that northwest areas of Pakistan (central parts of KPK & north-western parts of Punjab) along with Sind province are extremely vulnerable to floods in the peak flow months of July, August and September (Hanif, 2011). A recent example of such extreme impacts is the Flood-2010, when Pakistan as a whole received 70.5% and KPK received 179.1% above normal

rainfall in the month of July due to interaction and confluence of the monsoonal and westerly winds systems over the northwest Pakistan (Figure 1.6).

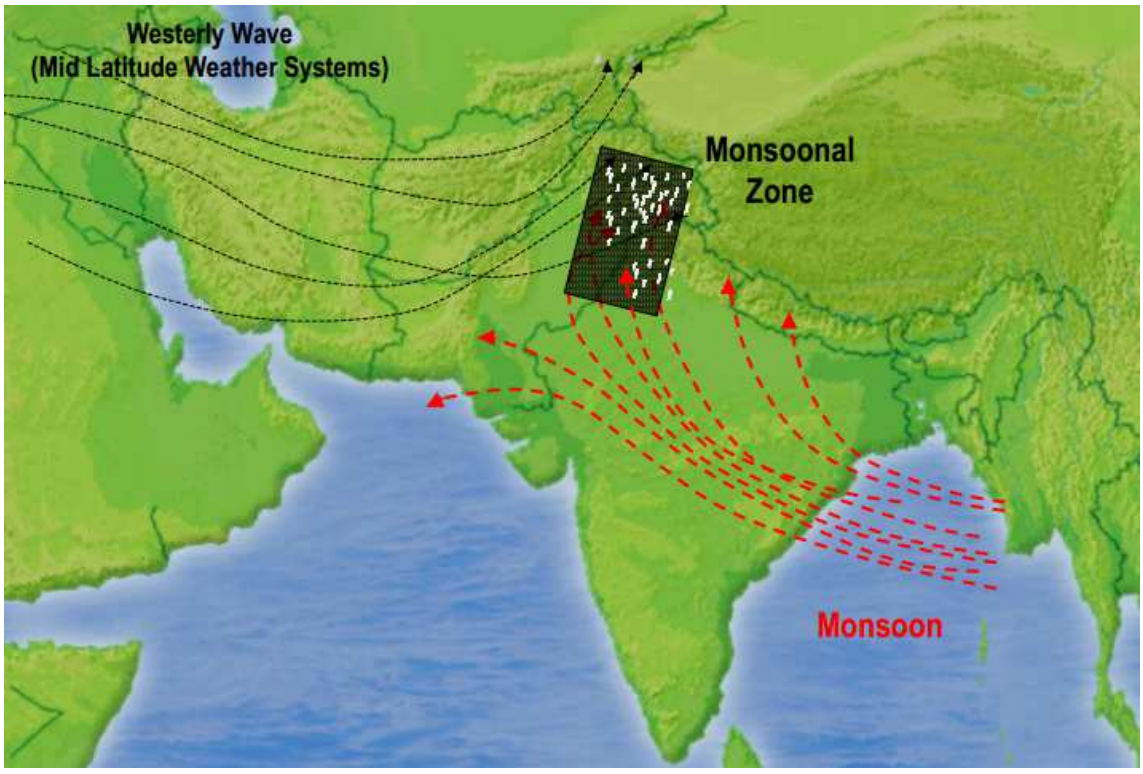

Figure 1.6: Confluence of two wave systems causing heavy rainfall and floods in 2010.

In addition to the high vulnerability to floods, Pakistan is also facing the issue of severe water shortage and in turn the risks of drought in its Baluchistan province, as well as in the desert areas of Punjab and Sind provinces. Reasons for this dual menace of floods and water shortage are high seasonal differences in rivers flows and absence of strategies to bridge this gap and normalize the availability of water over the whole year. Regardless of the heavy flows in the late summer and rainy months, Pakistan has to face the water shortage problem in rest of the year due to very limited surface water storage capacity, which is only 15% of the annual river flow (Qureshi, 2011) with carry over capacity of only 30 days as compared to 900 days of Colorado, 500 days of South Africa and 120-220 days of India (Briscoe & Qamar, 2005).

Moreover, under the long-term future climate change impacts, it has been predicted that there will be excessive glacier melt of the Karakoram glaciers due to a rise in temperatures and the flow of the Indus River at Besham Qila (upstream Terbela reservoir) will be increased by 50%. But thereafter, there will be great reduction in flows, which will be reduced to nearly 40% of their value for 2000 by the end of this century (Rees & Collins, 2005). The increase in

flows during the second decade of the century will be 6.4 BCM annually, after which there will be a steady decline of 27 BCM in the next 80 years (Qureshi, 2011). Therefore, it is highly important to plan long-term strategies like construction of new reservoirs for increasing storage capacity to capture extra flows and use them for dry months. In addition, planning and implementation of a complete framework of flood risk management activities is highly needed including effective early warning systems and evacuation, response and rehabilitation, and land use planning and other structural measures from flood mitigation to rainwater harvesting for its beneficial use.

1.6 Geoinformatics and Floods Management

Geoinformatics plays a key role using modern techniques like GIS and remote sensing to provide suitable information for planning and management activities at regional scale. It is useful not only for general planning processes, but also for the activities in different phases of disaster risk management cycle. While dealing with natural hazards, remote sensing can be helpful regarding assessment of vulnerable areas, monitoring of the events which may cause a disaster, and assessment of damages. There is a variety of remote sensing instruments mounted on different satellite platforms to ensure measurement of a wide range of parameters viz. climatic parameters like atmospheric temperature and rainfall, topography, land use land cover change, soil moisture and other properties, snow cover, etc.

Geoinformatics can be helpful for collection and analysis of relevant data like forecast as well as near real time remotely sensed rainfall data to identify the extreme rainfall events and provide early warnings regarding floods. Similarly, another important application of remote sensing is in mapping flood-prone areas based on the analysis of historical time series of satellite imageries, as well as in providing immediate information of the areas and population affected by a current flood event using near real time satellite imageries. Some important applications of Geoinformatics, relevant to current dissertation, are explained below.

1.6.1 Early Flood Warnings – ITHACA's Extreme Rainfall Detection System (ERDS)

The World Food Program (WFP) is the United Nations Agency which is involved in risk management for fighting hunger in developing countries, where victims of natural and manmade disasters suffer from severe food shortages. To respond successfully to emergencies entailing food shortages, WFP must be able to mobilize its response quickly and efficiently,

making preparedness a critical component of any emergency operation (Horton, 2008). ITHACA (Information Technology for Humanitarian Assistance, Cooperation and Action) Research Center is a project developed jointly by WFP, Politecnico di Torino and Higher Institute on Territorial Systems for Innovation (SiTI), with the objectives of establishing historical data patterns, developing forecasting models, and applying satellite imagery to rapidly determine and monitor the areas affected by natural disasters like floods, hurricanes, earthquakes, etc.

The Extreme Rainfall Detection System (ERDS), developed and implemented by ITHACA, provides timely and meaningful alerts related to exceptional rainfalls and potential flood events by elaborating near real time and forecasted rainfall data. An important strength of this system is its near global coverage particularly focusing on developing countries and simplification due to its dependence on single input, i.e. satellite rainfall data, which is available at a time interval of 3-hours.

Hydrologic models based on complete rainfall-runoff phenomena are the conventional and standard tools for calculating flows due to rainfall and other hydro-morphological parameters in a river catchment. However, it is not possible using a complete rainfall-runoff model running worldwide due to inability to acquire all the catchment specific data needed for such models viz. hydro-morphological properties, soil type, land use, etc. Early warning systems like ERDS provide opportunity to avoid complex hydrologic processes and give alerts based on exceptional rainfall events in different parts of the globe based on the near global coverage of the input data. Another important aspect of ERDS is its Web GIS platform, having capabilities for the assessment of event magnitude/severity by the integration of monitoring and forecasting tools with vulnerable data-sets to generate value-added and event-specific information, such as countries and population affected (Ajmar et al., 2013).

Data used for the near-real time detection of heavy rainfall events in ERDS are taken from the Tropical Rainfall Measuring Mission (TRMM) Multi-satellite Precipitation Analysis (TMPA), which is available with 0.25x0.25 degrees spatial resolution, near global coverage from 50^{o}N to 50^{o}S, and 3-hourly temporal resolution. The forecasted precipitation data, being used in ERDS, are based on a deterministic weather prediction model of National Oceanic and Atmospheric Administration-Global Forecast System (NOAA-GFS), providing alerts up to 7 days in advance.

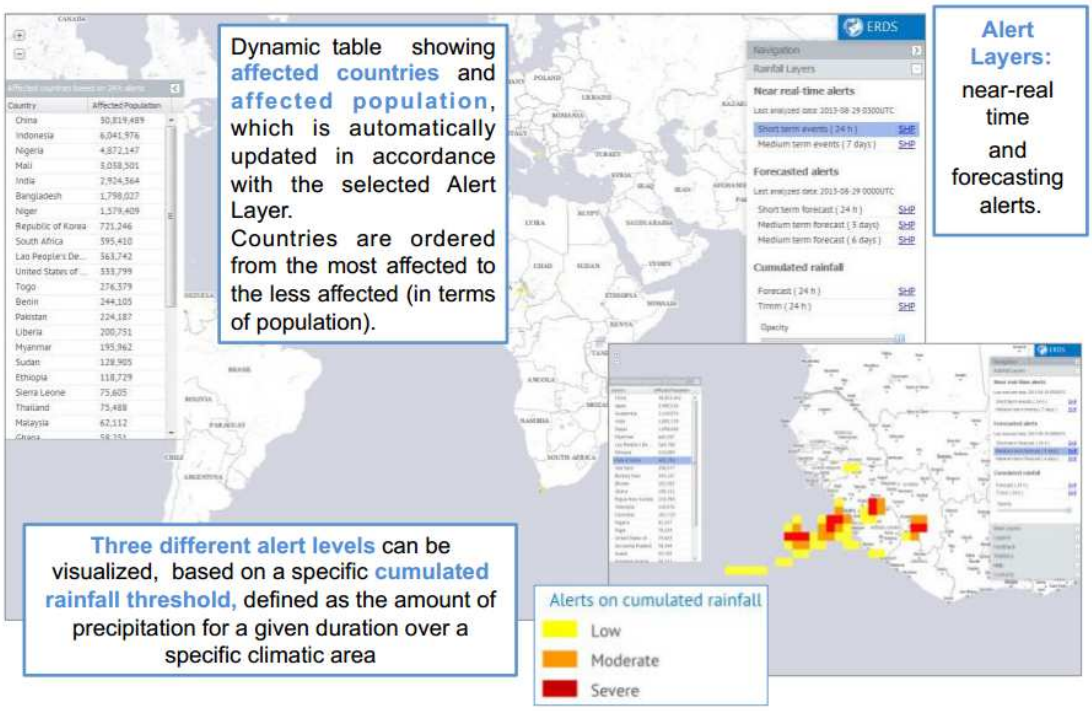

Figure 1.7: Web GIS platform of ERDS ("http://erds2.ithacaweb.org/")

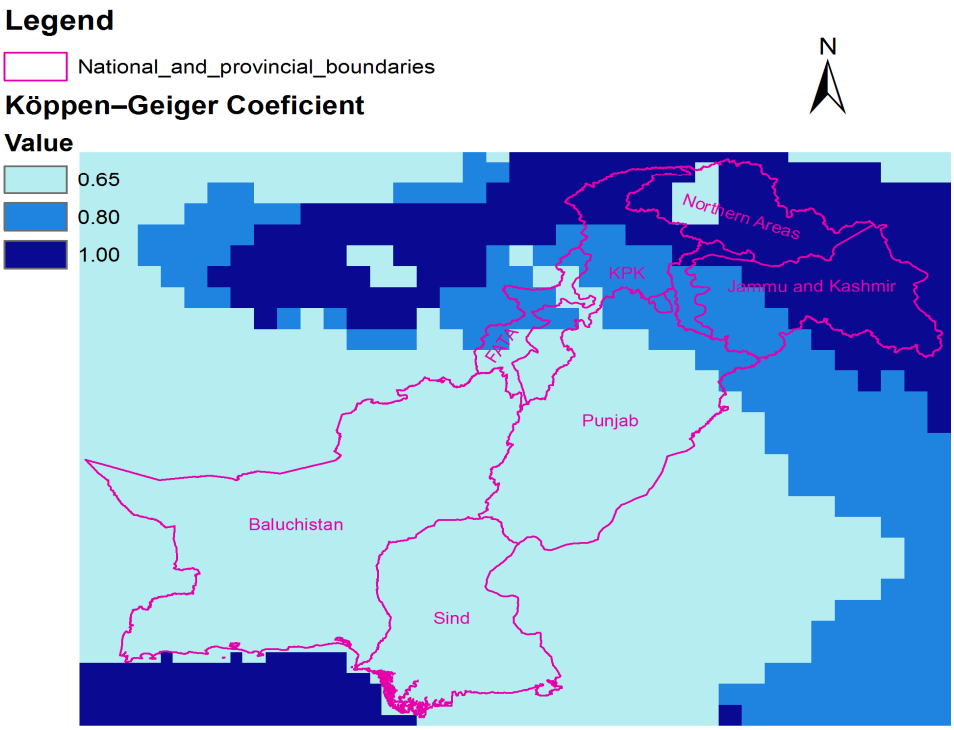

Figure 1.8 Koppen-Geiger climatic coefficients grid overlaid on Pakistan.

ERDS utilizes the standard rainfall thresholds of 80 mm, 120 mm and 200 mm for low, medium and high alerts, respectively; which are multiplied by the specific coefficients based on Koppen–Geiger climate classification system for having area-specific rainfall thresholds. Figure 1.8 shows the Koppen-Geiger coefficients grid overlaid on the area of Pakistan; it can

be seen that the upper mountainous northern areas have the coefficient values of 1.00 or 0.80 in agreement to their humid climate, while the rest of the country has coefficient value of 0.65 as a reflection of their semi-arid to arid climate.

1.6.2 Hydrologic Modeling at a River Catchment Scale

Hydrologic models are the basic tools in traditional flood warning systems for predicting flows based on the hydro-morphological and meteorological data in a river catchment. However, due to complex nature of processes involved in transforming rainfall to runoff and need for the measurement of a number of catchment dependent as well as independent parameters, it is not possible to run a hydrologic model at global scale. The alternate is the rainfall-based flood warning systems like ERDS, which can be used at near global scale to provide alerts based on the comparison of cumulated rainfall with already defined rainfall thresholds.

However, the importance of basic rainfall-runoff transformation process, and the parameters involved in it, cannot be overlooked and running hydrologic model at a river catchment scale can also be helpful for testing and refining the already used rainfall thresholds in a flood warning system. Moreover, in addition to flood warnings, hydrologic models provide the opportunity to conduct different studies regarding water resources and climate change impacts. Use of modern techniques like GIS and remote sensing has made the development and evaluation of a hydrologic model quite easier. Advancements in GIS and remote sensing have helped hydrologists calculating hydro-morphological parameters like basin slope, flow directions, sub-basins delineation, and lag time, etc., based on the analysis of Digital Elevation Model. Similarly, other basic datasets like soil map, land use map, and rainfall grid data, etc., developed and acquired using remote sensing techniques can be helpful in hydrologic modeling.

In developed world, where data availability and coordination is not a problem, many flood warning systems are based on the hydrologic modeling approach. An example is the European Flood Alert System (EFAS), which runs with the LISFLOOD hydrological rainfall-runoff model (Van Der Knijff et al. 2008; Thielen et al. 2009). Lot of work has been done in different river basins in developing countries regarding development and testing of different hydrologic models; these can be used for testing and refining of the existing rainfall-based flood warning systems having near global coverage, as well as for developing new hydrologic modeling based warning systems.

1.6.3 Detection of Flood Inundated Areas

Remote sensing techniques have great potential in floods management regarding mapping of flooded areas using post-flood real time imagery, as well as developing floodplain or flood hazard maps based on the analysis of historical archive. Applications based on free satellite data have been developed at ITHACA for automated classification of reference water bodies and their use for flood hazard management activities. During classification of water bodies using images coming from optical sensors like MODIS, the presence of cloud coverage prevents from the acquisition of earth surface, and the clouds shadows can be wrongly classified as water bodies because of their spectral response very similar to that of water. The automated classification algorithm developed at ITHACA allows classifying the data of reflectivity and compositing them temporally in order to minimize cloud coverage effects. More details about the development and testing of MODIS automated water bodies classification procedures have been presented by Disabato (2010). Such an approach to develop historical archive of water bodies can be very helpful in mapping seasonality of flooded areas.

1.7 Objectives of Current Dissertation

The general objective of this research work was to test and evaluate the potential of different open source data based methodologies for floods detection and analysis in Pakistan. Specifically, the research work was aimed at developing and evaluating a hydrologic model being able to run in real time, as well as to perform flood hazard mapping by analyzing seasonality of flooded areas using MODIS. Moreover, the outcome of this research work may be helpful to determine some critical rainfall patterns for Pakistan, which can be used to test and fine-tune the already used rainfall thresholds for Pakistan in ITHACA's Extreme Rainfall Detection System (ERDS) to provide early warnings of floods.

The specific objectives of the research work were:

- To perform testing and evaluation of TRMM rainfall data for different time periods and climatic zones of Pakistan
- To develop and evaluate a hydrologic model using HEC-HMS at river catchment level to predict peak flows in real time.

- To develop a historical archive of reference water bodies using MODIS automated water bodies' classification approach and perform analysis regarding seasonality of flooded areas.
- To test and evaluate the accuracy of MODIS classification approach by comparing peak flows and processed rainfall data with the respective flood-inundation extents as detected by MODIS.

To achieve the stated objectives, the work of thesis was divided into three phases:

At first step, monthly satellite rainfall data (TMPA 3B43) was evaluated for Pakistan by comparison with rain gauge data, as well as by further focusing on its analysis and evaluation for different time periods and climatic zones of Pakistan.

In the next phase, hydrologic modeling was performed using HEC-HMS model for Chenab river catchment, an eastern tributary of Indus River. Keeping in view the mandate of this dissertation to develop and use procedures, which are as much open source data-based as possible, TRMM rainfall data and other open source datasets like digital soil map and global land cover map were utilized to develop and evaluate an event-based hydrologic model, which may be able to be run in real time for any extreme rainfall event causing high flows or floods in the river.

In the final phase, to broaden the study canvas from a river catchment to the whole country scale, MODIS automated water bodies classification approach with MODIS daily surface reflectance products was utilized to develop a historical archive of reference water bodies and perform seasonal analysis of flooded areas for Pakistan. The comparison of MODIS flooded areas extents with respective peak flow values and TRMM precipitation helped checking and refining the classification approach, as well as developing some guidelines regarding rainfall amounts which may cause low, medium or high floods in Pakistan.

Chapter 2

Performance Evaluation of TRMM Precipitation Estimates for Pakistan

2.1 Overview of the Chapter

Increase in global average temperatures, widespread snow and glaciers melt and rising sea levels are important evidences of climate change, causing severe changes in the spatial and temporal rainfall patterns and increasing the frequency of related natural disasters like floods and droughts. This scenario highlights the importance of satellite data for effective monitoring and forecasting of such disasters. Such data become more valuable in case of developing countries where there is limited availability of local data. The most commonly used open source data for detecting critical rainfall events are taken from Tropical Rainfall Measuring Mission (TRMM) Multi-satellite Precipitation Analysis (TMPA). However, it is important to have a comparison of TRMM based rainfall estimates with locally available data to evaluate their accuracy and scope of use for a region. In this chapter, performance evaluation of TRMM monthly precipitation product (3B43) has been presented for Pakistan using 15 years data from 1998 to 2012, in comparison to the ground rainfall data for the same period. After overall performance evaluation, the study area (Pakistan) was divided into three zones based on climate and separate analysis and calibration was performed to check the accuracy and scope of use of the original as well as calibrated TRMM estimates for each zone.

The chapter starts with the problem statement and need of evaluation study, followed by the detailed description of TMPA products and their development, and explanation of methodology adopted for the calibration and evaluation. Afterwards, results regarding calibration and evaluation have been presented all over the Pakistan, as well as for different climatic zones separately. The chapter ends with detailed discussion of results and concluding remarks regarding scope of use of TRMM precipitation data for Pakistan.

2.2 Literature Review and Problem Statement

Climate change impacts in terms of increased global temperatures and high spatio-temporal variability in rainfall patterns are being witnessed worldwide. These primary impacts are providing base for several inter-related issues and emerging challenges for water resources, agriculture, energy and other socioeconomic sectors. Increased frequency and severity of natural disasters like floods and droughts are also an important aspect of the adverse climate changes. Rainfall is an important factor of the hydrologic cycle and has key role in different phenomena like surface runoff generation and hydropower potential, occurrence of floods or droughts, and sustainable agriculture and food security. Therefore, the need for reliable and high resolution, both spatial and temporal, rainfall data is crucial for sound hydrologic studies and for timely detection and management of natural disasters like floods and droughts.

Rain gauges have been, and are still being considered a reliable source for providing reasonably accurate point rainfall measurements. However, point rainfall measurements do not provide true estimation of areal rainfall (Tustison et al., 2001; Draper et al., 2009), particularly when there exist local rainfall gradients as in case of Himalayas (Barros et al., 2004; Bhatt & Nakamura, 2005; Anders et al., 2006). The areal rainfall estimation is mandatory at proper spatial and temporal scale for conducting studies at basin level (Sawunyama & Hughes, 2008). This scenario raises the importance of satellite data for effective monitoring of rainfall for conducting catchment level water studies and combating disasters. Use of such data becomes more important in case of developing countries where there is limited availability of local data in terms of sparse rain gauge network, which cannot detect rainfall variations caused by topography and orographic effects, and thus, results in erroneous estimates of areal rainfall (Andreassian et al., 2001).

Satellite-based precipitation products have become an important alternative source of information (Din et al., 2008), under the need for more accurate spatially distributed rainfall estimates (Huffman et al., 2001). Some important remotely measuring precipitation instruments are active Precipitation Radar (PR), passive Microwave Radiometer (MWR) such as Tropical Rainfall Measuring Mission (TRMM) Microwave Imager (TMI) and Infrared Radiometer (IR) sensors (Huffman et al., 2007; Ushio et al., 2009). The active PR sensor records the three dimensional structure of the rainfall distribution (Kummerow et al., 1998); IR observations provide indirect measurements at the top of clouds (Huffman et al., 2007);

while the TMI detects the radiation emitted by the water fraction in the vertical profile of the atmosphere (Kubota et al., 2007).

The TRMM Multi-satellite Precipitation Analysis (TMPA) provides high temporal (3 hourly) and reasonable spatial (0.25^o x 0.25^o) resolution products with uniform near global coverage using combination of different types of sensors and satellite datasets. However, the indirect nature of precipitation measurement by the sensors shows some uncertainties too (Hong et al., 2006; Hossain et al., 2006), associated with lack of rainfall detection, false detection and bias (Tobin & Bennett, 2010). Franchito et al. (2009) have reported both temporal (8% to 12%) and sampling (30%) errors in satellite rainfall estimates. These biases and random errors may be due to sampling frequency, diurnal cycle of rainfall, non-uniform field of view of sensors, and the uncertainties in the rain retrieval algorithms (Kousky, 1980; Bell et al., 1990; Chiu et al., 1990; Kummerow, 1998; Anagnostoub et al., 1999; Chang & Chiu, 1999). Therefore, satellite rainfall estimates are needed to be evaluated to reduce such errors, especially on regional basis instead of using global approximations (Huffman, 1997; Kummerow et al., 2000).

Many scientists have made efforts at global and regional scales for the evaluation of satellite products by comparing them with the field rainfall measurements, which showed varying accuracies in different regions and for different methods. Adeyewa & Nakamura (2003) used Global Precipitation Climatology Center global-precipitation-analyses rain gauge data for comparison with TRMM Precipitation Radar (PR) data, the threshold-matched precipitation index and the TRMM-and-other-sources ‘‘best-estimate’’ data product (3B43) for 36 months over the major climatic regions in Africa. They found close agreement of 3B43 product with the rain gauge data, and even used it as a substitute of rain gauge data over the South Atlantic Ocean for the validation of other satellite products. Ji & Stocker (2003) observed correlation of 0.56 between the satellite and rain gauge measurements. Dinku et al. (2007) estimated Nash–Sutcliffe efficiency of 0.81 and root mean square error of 25% between the satellite and rain gauge data averaged over 2.5^o grid boxes. The accuracy for a single 25km×25km pixel containing 23 rain gauges in Oklahoma was tested by Villarini & Krajewski (2007) and a correlation of 0.55 was found between the satellite and rain gauges values. Cheema & Bastiaanssen (2012) performed calibration of TRMM Precipitation Radar data for the year of 2007 over Indus basin using regression analysis and geographical differential analysis techniques. They reported decrease from pre-calibration to post-calibration deviation between

TRMM data and rain gauge data to be from 10.9% to 6.1% for annual time periods, and from 34.9% to 15.4% for monthly periods.

The objective in current study was the evaluation of TRMM monthly data (3B43) over 15 years from 1998 to 2012 for Pakistan to investigate its scope for detection and management of natural disasters like droughts and floods. Monthly rainfall products at high spatial resolution are very useful for conducting drought studies, but daily or even 3-hourly datasets (TRMM 3B42) are considered better to conduct sound rainfall-runoff studies and managing floods. However, it is worth mentioning that the TRMM research datasets also incorporate the monthly rain gauge data for automated calibration (Huffman et al., 2001). For this purpose, the available 3-hourly near real time estimates (3B42RT) are summed over the calendar month to create a monthly multi-satellite (MS) product, which is then combined to monthly gauge data using inverse-error variance weighting, as reported by Huffman (1997), to create a post-real-time monthly satellite-gauge combination (SG) product, known as TRMM 3B43 product. Then for each grid box, monthly SG/MS or 3B43/MS ratio is computed and applied to each near real time 3-hourly field in the month, producing the final 3B42 post research 3-hourly and daily products. Thus, it is believed that the evaluation of monthly product (3B43) for an area might also help in providing guidelines for the use of daily and hourly products. Further detailed description of TMPA products and their development has been presented in the following section.

2.3 Description of Satellite Rainfall Data

Precipitation is acritical weather element for determining the habitability of different parts of the Earth; however, adequate measurement of its spatial distribution is difficult with surface-based instruments due to its small-scale variability in space and time. Satellite-borne sensors play a key role in estimating precipitation and development of precipitation-sensing satellities since the last 25 years has greatly enhanced our ability to esrimate precipitation over much of the globe. But the critical issue is deciding how to combine different types of individual satellite estimates to form a single best estimate. The desired result should be a stable, long, quasi-global time series of precipitation estimates on a uniform time/space grid that has as much finest scale as possible. Regarding finest granularity, each sensor, and associated algorithms, may have strenghts and weaknesses that can affect its accuracy usually varying from region to region. Another issue is the uncoordinated constellation of precipitation

sensing satellites, although operational agencies typically strive to maintain one or two specific satellites in preferred orbits.

In comparison to the earlier datasets, Tropical Rainfall Measuring Mission (TRMM) Multi-satellite Precipitation Analysis (TMPA) was designed and developed in 1998 to use "all" available data, meaning that the potential inhomogenities of time-varying complement of inputs can be accepted in return for potentially better combination results when more high quality data are available. Another difference with the earlier datasets is that the TMPA is generated twice; first as a real time (RT) product computed about 6-9 hours after the observation time, and then as a post-real-time research product computed about 15 days after the end of a month with additionally including monthly rain gauge data. The spatial resolution of TMPA products was set as 0.25^{o}x0.25^{o} to ensure that the grid box is somewhat larger than the typical footprint size for passive microwave precipitation estimates, which are the coarsest estimates in common use. The spatial domain was set as 50^{o}N to 50^{o}S, as the entire microwave and infrared (IR) estimates tend to lose skill at higher latitudes. The temporal resolution was set as three hours, which provides following benefits:

1. It allows resolving the diurnal cycle.

2. It matches with the mandated interval for full-disk images from the international constellation of geosynchronous satellites.

3. It provides a reasonable compromise between spatial coverage and temporal frequency for gridding the synoptic microwave estimates from Low-Earth-Orbit (LEO) satellites.

2.3.1 Instruments and Input Datasets

The TMPA takes input from two different types of satellite sensors, namely microwave and IR sensors, as well as the precipitation gauge analysis for adjustments in the post-real-time research products.

1) High Quality Precipitation Sensors

Precipitation-related data obtained from sensors onboard TRMM satellite and the microwave sensors mounted on other Low Earth Orbit (LEO) satellites, are collectively known as High Quality (HQ) preciptation estimates.

Intruments or sensors onboard TRMM are Precipitation Radar (PR), TRMM Microwave Imager (TMI), Visible and Infrared Scanner (VIRS), and Lightning Imaging Sensor (LIS).

Data from the TMI and PR, as well as from other TRMM sensors where needed, are combined to produce the best rain estimate for TRMM, known as TRMM Combined Instrument (TCI) estimates, as reported by Haddad et al., (1997 a, b).

Microwave sensors mounted on different other LEO satellites include Special Sensor Microwave Imager (SSMI), Special Sensor Microwave Imager/Radiometer (SSMI/R), Advanced Microwave Scanning Radiometer for the Earth Observing System (AMSR-E), Advanced Microwave Sounding Unit-B (AMSU-B) and Microwave Humidity Sounders (MHS). Table 2.1 highlights the different datasets/sensors along with their respective satellites and algorithms, which are being used for HQ precipitation estimates in TMPA.

Table 2.1: Datasets/sensors used in HQ/microwave precipitation estimates.

Sr. No.	**Dataset/ Sensors**	**Satellite**	**Algorithm**
1	TCI (PR, TMI, and other TRMM sensors)	TRMM	TCI algorithm
2	TMI	TRMM	Goddard Profiling (GPROF) sensor specific algorithms for precipitation retrieval
3	SSMI	Defense Meteorological Satellite Program (DMSP) satellites	
4	SSMI/S	Defense Meteorological Satellite Program (DMSP) satellites	
5	AMSR-E	Aqua	
6	AMSU-B	National Oceanic and Atmospheric Administration (NOAA) series satellites	National Environmental Satellite Data and Information Service (NESDIS) algorithms for precipitation retrieval
7	MHS	Later NOAA-series satellites and European Operational Meteorological (MetOp) satellite	

Each microwave pixel-level observation from TMI, AMSR-E, SSMI and SSMI/S is converted to a precipitation estimate with sensor-specific versions of the Goddard Profiling (GPROF) algorithms (Kummerow et al., 1996; Olson et al., 1999) for subsequent use in the TMPA. GPROF is a physically-based algorithm that applies a Bayesian least-squares fit scheme to reconstruct the observed radiances for each pixel by selecting the "best" combination of thousands of numerical model-generated microwave channel upwelling radiances. Microwave pixel-level observations from AMSU-B and MHS are converted to precipitation estimates at

the National Environmental Satellite Data and Information Service (NESDIS) using operational versions of the Zhao & Weng (2002) and Weng et al. (2003) algorithms.

All of these data have a direct physical connection to the hydrometeor profiles above the surface, but each individual satellite provides a very sparse sampling of the time-space occurrence of precipitation. Even when composited into 3-hour datasets, the current "full" microwave coverage averages about 80% of the Earth's surface in the latitude band 50°N-S, and was amounted to about 40% at the beginning of the TMPA record in 1998 with three satellites.

2) Infrared Radiometer (IR) Sensors

The second major data source for the TMPA is the geo-IR data, which provides excellent time-space coverage, in contrast to the microwave data. However, all IR-based precipitation estimates share the limitation that the IR brightness temperatures (T_b) primarily represent cloud-top temperature, and implicitly cloud height. Arkin & Meisner (1987) showed that IR estimates are poorly correlated to precipitation at fine time/space scales, but relatively well-correlated at scales larger than about 1day and 2.5°x2.5° of lat./long.

The Climate Prediction Center (CPC) of NOAA merges geo-IR data from five geosynchronous satellites into half-hourly 4x4-km lat./long. grids for the domain 60°N-60°S (Janowiak et al., 2001). The dataset contains IR T_b's corrected for zenith angle viewing effects (Joyce et al., 2001) and inter-satellite calibration differences. Recently, the geosatellites being in use for TMPA include MTSat-2 operated by Multi-functional Transport Satellite (MTSat) of Japan; GOES-E and GOES-W operated by Geosynchronous Operational Environmental Satellites (GOES) of United States; and Meteosat-9 and Meteosat-7 operated by Meteorological Satellite (Meteosat) of European Community (Huffman & Bolvin, 2014).

3) Precipitation Gauge Analysis

Finally, the research TMPA employs the precipitation gauge analysis produced by the Global Precipitation Climatology Centre (GPCC), as reported by (Schneider et al., 2011). Rain gauge reports are archived from a time-varying collection of over 70,000 stations around the globe, both from Global Telecommunications System (GTS) reports and from other world-wide or national data collections.

2.3.2 Stages of TMPA Products Development

There are different types of TMPA products which can be broadly classified as real time and post-real-time research products. The research-quality TMPA products are computed in four stages:

(1) The microwave precipitation estimates are inter-calibrated and combined;

(2) IR precipitation estimates are created using the calibrated microwave precipitation;

(3) The microwave and IR estimates are combined;

(4) Precipitation gauge analysis data are integrated.

The real-time TMPA lacks the fourth step and has a few simplifications.

Stage I: HQ precipitation estimates

Each microwave precipitation data set is averaged to the 0.25° spatial grid over the time range ±90 minutes from the nominal 3-hourly observation times (00Z , 03Z, ..., 21Z). Probability matching to a "best" estimate using coincident matchups is used to adjust each sensor, similar to Miller (1972) and Krajewski & Smith (1991). Although TCI is adopted as the calibrating data source, the coincidence of TCI with any of the sensors other than TMI is sparse, so a TCI-TMI calibration was established and then applied to TMI. All the remaining sensors data are calibrated to TMI, and then adjusted to TCI using the TCI-TMI calibration. The TCI-TMI relationship is computed on a $1^{o}x1^{o}$ grid for each month with the coincident data aggregated on overlapping 3°x3° windows. The TCI-TMI calibration interval for the research product is a calendar month, and the resulting adjustments are applied to data for the same calendar month.

Once the microwave estimates are calibrated for each satellite and are quality-controlled, the grid is filled using the "best" available data to produce the High Quality (HQ) microwave combination od precipitation estimates. The rain rate in each grid box is the average of TCI alone (known as 2B31), if available in the 3-hour window. Otherwise, if there are one or more overpasses from TCI-adjusted TMI, TCI-adjusted AMSR-E, TCI-adjusted SSM/I and TCI-adjusted SSMI/S in the 3-hr window for a given grid box, all of these data are used by pixel-weighted averaging. The pixel-weighted average of AMSU-B and MHS estimates is utilized for a grid box, if no other HQ estimates are available.

Stage II: IR precipitation estimates

The IR data from different geosatellites is used to produce the “Merged 4-Km IR Tb dataset” by the Climate Prediction Center (CPC) of NOAA National Centers for Environmental Prediction, Washington, DC. The IR data from different geosatellites are zenith-angle corrected (Joyce et al., 2001), re-navigated for parallax, and merged on a global grid. In the event of duplicate data in a grid box, the value with the smaller zenith angle is taken. The data are provided on a 4-km-equivalent latitude/longitude grid over the latitude band 60°N-S, with a total grid size of 9896x3298. The CPC merged IR data is then averaged to 0.25° resolution and combined into hourly files as ±30 minutes from the nominal time.

Time-space matched HQ precipitation rates and IR Tb's are accumulated for a month into histograms of 3-hourly 0.25°x0.25° values on a l°xl° grid, aggregated to overlapping 3°x3° windows, and then used to convert IR Tb's to precipitation rates. As in the TCI-TMI calibration for the HQ, the calibration period is again the calendar month. The IR precipitation estimate is a simple "colder clouds precipitate more" approach, with the coldest 0.25°x0.25°average Tb assigned the greatest observed HQ precipitation rate, and so on, with zero precipitation assigned for all Tb's warmer than a spatially varying threshold value determined by the fractional coverage of precipitation in the microwave data. The HQ-IR calibration coefficients computed for a month are finally applied to each 3-hourly IR dataset during that month.

Stage III: HQ and IR combination

Combining HQ and IR precipitation estimates at individual 3-hourly fields is quite gaming because the quantities being sensed tend to have different fine-scale patterns. Accordingly, the more physically based HQ estimates are used preferably where available, while the remaining grid boxes are filled with HQ-calibrated IR estimates.

Stage IV: Integration with precipitation gauge analysis

Monthly precipitation gauge data is introduced as final step in elaborating the TMPA research products. The approach taken in the GPCP One-Degree Daily combination dataset is used, which is to scale the short-period estimates to sum to a monthly estimate that includes monthly gauge data (Huffman et al., 2001). All available 3-hourly merged HQ-IR estimates are summed over the calendar month to create a monthly multi-satellite (MS) product. The MS and the monthly gauge data are combined using inverse-error variance weighting

(Huffman, 1997) to create a post-real-time monthly satellite-gauge combination (SG), which is known as a separate TMPA monthly research product (3B43). Then for each grid box the monthly SG/MS ratio is computed and applied to scale each 3-hourly field in the month, producing the version 7.0 3-hourly research product (3B42). Anpther auxiliary research product is the TMPA daily research product (3B42-derived) which is generated by summing up all 3-hourly fields on daily basis.

TMPA Real Time (RT) product

In TMPA, the RT and research product systems have been designed to be as similar as possible to ensure consistency between the resulting data sets. One important difference is that the research product's calibrator, the TCI, is not available in real time. In its absence the TMI estimates are used as the RT calibrator. A second important difference is that a real-time system cannot reach into the future, so the HQ-IR calibration "month" is taken as the five trailing and one current (partial) pentads, or 5-day calendar intervals, of accumulated coincident data. As in the research product, the inter-calibration of individual microwave estimates to the TMI is handled with climatological coefficients. Then the HQ-IR calibration is recomputed for each 3-hr period to capture rapid changes in the calibration for rare heavy rain events. Third, the monthly gauge adjustment stage carried out for the research product is not possible for the RT product.

Starting from 20 January 2009, a procedure to address the second and third differences listed above was implemented. Tests showed that computing these adjustments on a climatological basis provoked fewer artifacts than attempting to use data from trailing months. Therefore, a matched histogram calibration of TMI to the TCI, computed for 10 years of coincident data, was performed to establish the climatology for each calendar month. Second, a climatological monthly calibration of TCI to the 3B43 research product is computed as a simple ratio, again on a l°xl° spatial grid and using 10 years of data. Finally, the TMI-TCI and TCI-3B43 calibrations are successively applied to the preliminary 3-hr RT multi-satellite product to create the final 3B42RT product.

2.4 Methodology for Evaluation of TRMM Data for Pakistan

Pakistan is an agriculture based country representing a region which is highly prone to climate change. Ranging from coastal areas along the Arabian Sea in south to the glaciated mountains

in north, Pakistan possesses a landscape having high diversity in terms of plains, deserts, plateaus, hills and glaciers. Geographically and from water resources point of view, the country can be divided into three major zones: the northern highlands and north-eastern Himalayan mountains contributing by snowmelt and rainfall to the mighty Indus River and its tributaries; the Indus River plain which covers major area of Pakistan including centeral and southern Punjab and Sind provinces; and the Balochistan Plateau which lies in the south-west and is mostly under drought conditions due to arid climate (Figure 2.1).

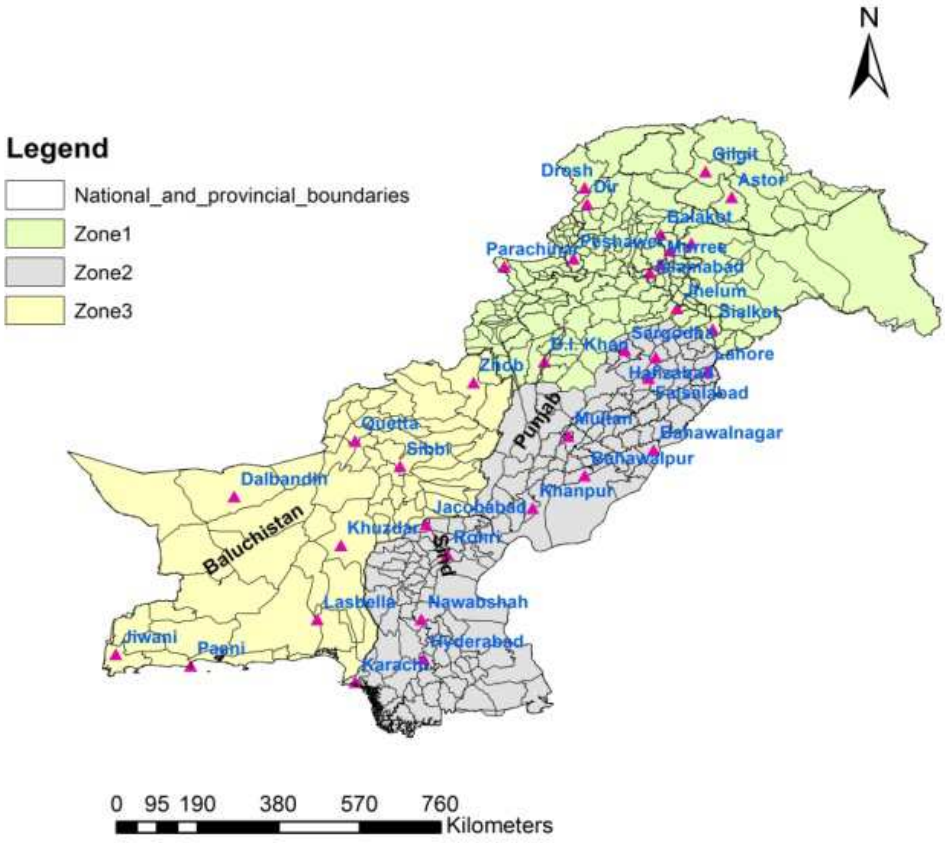

Figure 2.1: Map of Pakistan along with delineation of three zones and location of rain gauge stations used in this study.

Major part of Pakistan is under arid to semi-arid climate with relatively higher rainfalls in the northern areas and lower towards the middle and south. Two important sources of rainfall are monsoon causing heavy rainfalls and frequent flooding from June to September, and the western disturbances contributing in terms of rain and snowfall over hilly areas during winter. However, there is high variability in seasonal rainfalls with monsoon season contributing alone to about 70% of annual rainfall, and dry months of October and November with almost no rain. In addition to seasonal differences, annual rainfall also varies greatly from year to

year and occurrences of alternate flooding and drought are common. Due to a sparse rain gauge network in the country, satellite rainfall datasets like TMPA products can be very helpful for providing uniform spatial and temporal coverage throughout the country for different rainfall based studies like management of water resources, floods, droughts, etc.

In this study, the performance evaluation of TRMM monthly rainfall data (TMPA v 7.0 3B43 product) have been conducted for Pakistan. The data were downloaded and processed for 15 years from 1998 to 2012 for use in ArcMap. For its evaluation and calibration, monthly ground rainfall data were used as standard and were obtained over the same period of 15 years for 35 rain gauge stations from Pakistan Meteorological Department (PMD). Rain gauges may also have some errors, but are normally considered correct and true representative of point rainfall (Vila et al., 2009) in a basin for validation of other datasets. Moreover, use of 15 years data to have average annual and monthly rainfall values, both for satellite and rain gauge data, may be considered helpful in neutralizing any biases in both datasets.

2.4.1 Calibration using Regression Analysis

There has been found a good relationship between the TRMM rainfall estimates and rain gauge observations by many scientists (Adeyewa & Nakamura, 2003; Din et al., 2008; Cheema & Bastiaanssen, 2012). The empirical relations were developed for each month using regression analysis on data from 29 rain gauge stations and the corresponding pixels in TRMM grid data which were identified using spatial join overlay technique in ArcMap. Data for remaining six rain gauge stations were used for validation purposes only, following the calibration and validation stations ratio adopted by Cheema & Bastiaanssen (2012). To have best relationships and address the non-linearity in both datasets, second order polynomial equations were developed with zero intercept, which can be described as:

$$R_{cal} = R_{gauge} = a\,(R_{TRMM})^2 + b\,(R_{TRMM}) \qquad (1)$$

Where R_{cal} is the resulting calibrated TRMM rainfall, R_{TRMM} is the TRMM rainfall from original 3B43 product, and ‘a’ and ‘b’ are the regression coefficients for the calibration of 3B43 product for Pakistan.

In the next phase, to account for the high variability of rainfall patterns in different regions and further refining of the calibration procedure, regression analysis and calibration were performed on seasonal and annual basis by dividing the country into three climatic zones. Zone-1, including northern mountainous areas along with KP and upper Punjab provinces,

represents a very humid climate with heavy rainfall in monsoon season and snowfall in winter; zone-2, covering the areas of central and southern Punjab and Sind provinces, formulates a region with average rainfall amounts and semi-arid climate; whereas zone-3, covering Baluchistan plateau, represents mostly the dry climatic areas with very less amounts of precipitation. List of rain gauge stations used for calibration and validation purposes for the specific zones is shown in Table 2.2.

Table 2.2: List of Rain gauge stations used for calibration and validation in different zones.

Sr. No.	Zone 1: Northern Areas, KP, FATA and Upper Punjab	Zone 2: Central and Lower Punjab and Sind Provinces	Zone 3: Baluchistan Plateau
For Calibration:			
1	Astor	Bahawalnagar	Dalbandin
2	Balakot	Hafizabad	Jacobabad
3	Drosh	Hyderabad	Jiwani
4	D.I. Khan	Karachi	Khuzdar
5	Gilgit	Khanpur	Lasbella
6	Islamabad	Lahore	Quetta
7	Murree	Multan	Pasni
8	Muzaffarabad	Rohri	
9	Parachinar	Sargodha	
10	Peshawer		
11	Sialkot		
For Validation:			
1	Dir	Faisalabad	Sibbi
2	Garhi dupatta	Bahawalpur	Zhob
3	Jhelum	Nawabshah	

By the use of developed calibration equations for each month, new monthly rainfall raster, and in turn, the seasonal (six monthly) and annual raster datasets were developed using map algebra tool. The year was divided into two six monthly parts keeping in view the two prevailing cropping seasons, as well as the hydro-climatic distribution, i.e. Rabi/Winter (from October to March) representing the relatively dry winter and a bit hot spring with rainfall currents due to western disturbances, and Kharif/Summer (from April to September)

representing the hot summer and rainy season having heavy monsoon rains. Similarly, in the second zone-wise evaluation phase, zone-wise seasonal and annual calibration equations were utilized to develop calibrated monthly rainfall raster, and in turn, the seasonal (six monthly) raster datasets using map algebra tool.

2.4.2 Statistical Evaluation

For performance evaluation and validation of the original TRMM data and the calibrated rainfall maps, six remaining rain gauges' measurements and their respective pixel values were used to estimate Nash-Sutcliffe Efficiency (NSE) for each month. NSE determines the relative magnitude of noise in estimated data compared to the measured data (Nash & Sutcliffe, 1970) using following relation:

$$NSE = 1 - \frac{\sum_{i=1}^{n}(Rrgs - Rtrmm)\text{^}2}{\sum_{i=1}^{n}(Rrgs - <Rrgs>)\text{^}2} \qquad (2)$$

Where R_{rgs} is the measured/observed rainfall for a specific rain gauge, R_{trmm} is the satellite rainfall value for the respective pixel, $<R_{rgs}>$ is the mean observed rainfall, and n is the total number of observations or rain gauge stations used for the validation purpose. Value of NSE ranges from -∞ to 1; values between 0.0 and 1.0 are generally considered as acceptable, while the values less than 0.0 indicate that the observed mean is more accurate than the estimated value, which is unacceptable. NSE was calculated for each month to evaluate the accuracy of TRMM 3B43 product and the performance of calibration work using the pre-calibration and post-calibration satellite rainfall maps, respectively. Similarly, for zone-wise analysis, measurements from the reserved rain gauges in each zone and their respective pixel values were utilized to estimate seasonal NSE values without calibration, as well as based on seasonal and annual calibration equations.

2.5 Results and Discussion

The results of this study have been presented in two sections, i.e. the evaluation on monthly basis for all over the Pakistan and the evaluation for three devised climatic zones separately.

2.5.1 Calibration and Evaluation of TRMM datasets all over the Pakistan

Comparison of monthly satellite rainfall estimates with rain gauge measurements for 29 rain gauges all over the Pakistan, along with the resulting second order polynomial equations and

respective R^2 values, has been presented for both winter and summer season months in Figures 2.2 and 2.3, respectively.

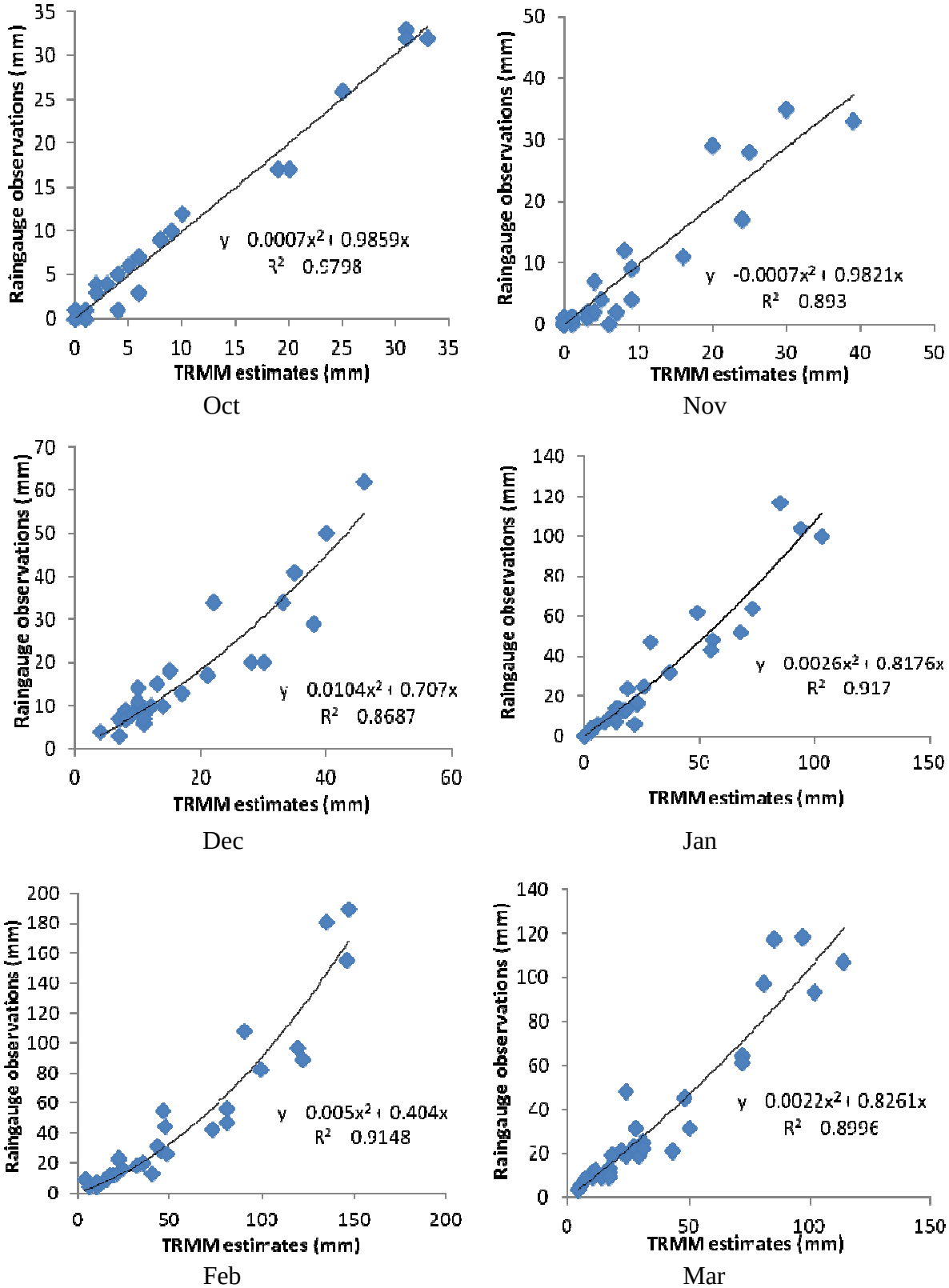

Figure 2.2: Regression analysis for 15 years' mean precipitation values of rain gauges vs TRMM 3B43 for winter season months.

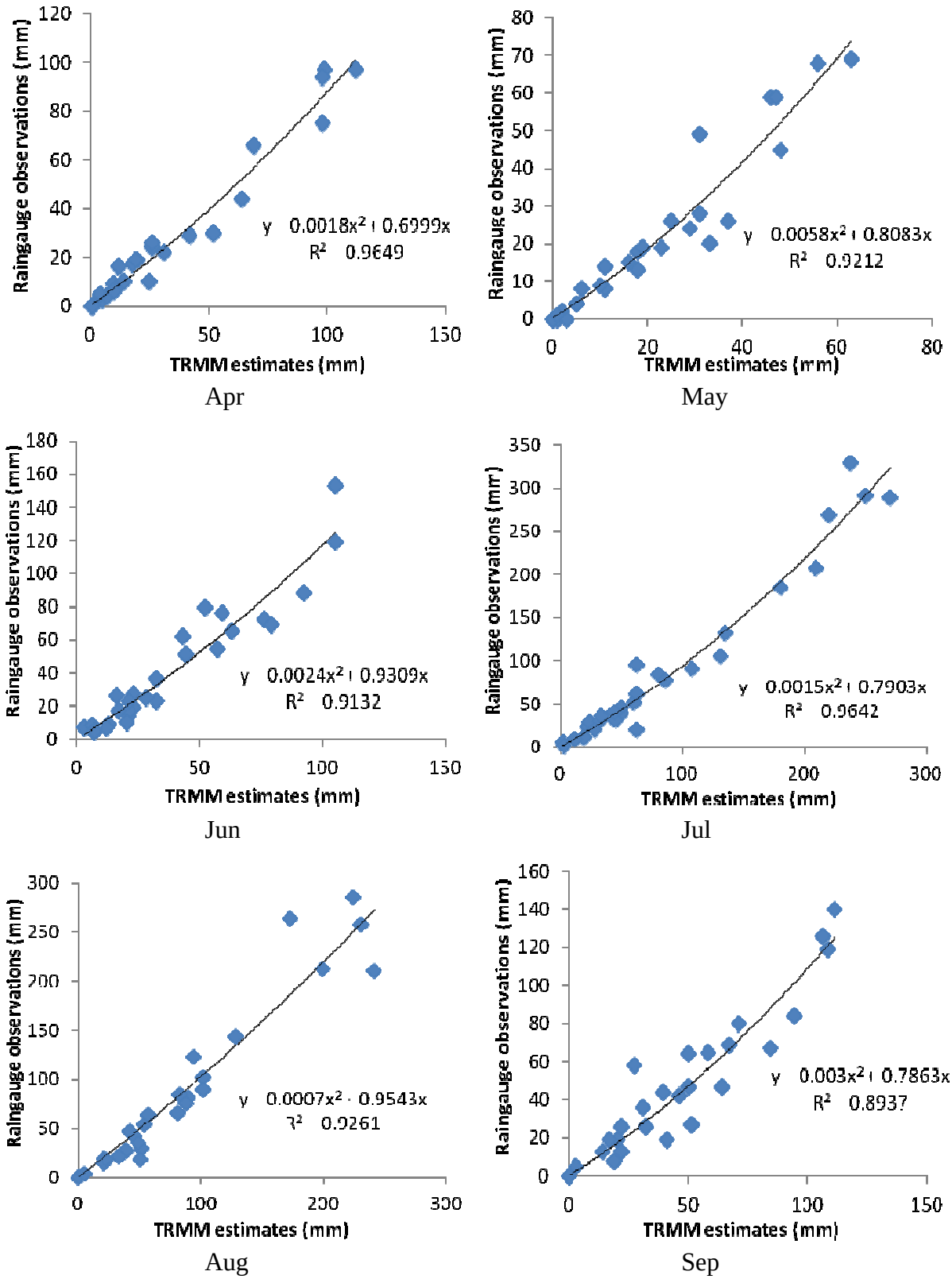

Figure 2.3: Regression analysis for 15 years' mean precipitation values of rain gauges vs TRMM 3B43 for summer season months.

For most of the months, resulting curves were of the parabolic form with their convection towards horizontal axis. This indicates that the overall TRMM satellite estimates were found

on higher side a little, but leading to the underestimation at higher rainfall values; similar trends were experienced by other scientists (Islam & Uyeda, 2008; Cheema & Bastiaanssen, 2012). However, almost linear behavior was seen for the months of October and November (Figure 2.2), as the total rainfall in these months was very low, i.e. upto 40 mm month^{-1}. Therefore, it can be seen here that these lines actually represented just the lower one-third part of the curves for other months, and thus, showed almost a linear behavior with little overestimation by the satellite. High correlation was found between two datasets for all months with R^2 values ranging from 0.87 for December to 0.98 for October.

The seasonal and annual raster maps before and after the calibration of satellite data have been shown in Figure 2.4. It can be seen that in low rainfall winter and spring season, calibration work improved the satellite data and there was found a shift of most part of south-western areas (Balochistan province) from rainfall class of 45-90 mm to that of below 45 mm. Similar little variations were found in the distribution of other classes before and after calibration. For the summer and monsoon rainfall season, the distribution of rainfall classes was found almost similar before and after calibration; and similar was the case for the whole year mapping. The upper Punjab province areas, which are at the foot hills of Himalayan Mountains, were found under heavy rainfall in summer season due to monsoon winds and orographic effects. The annual maps show that the upper Punjab foot hills areas and upper KP province are under severe climate change impacts in terms of heavy rainfall, which mostly result in flooding in the downstream areas of KP, Punjab and Sind provinces. South-western areas in Balochistan province and some desert areas in the north-eastern Sind province were found under the severe drought risks with arid climate having average annual rainfall in the range of 35-135 mm. Areas in the southern Punjab and the belt along the mutual boundary of Sind and Balochistan provinces were also found under arid to semi-arid climate with average annual rainfall in the range of 135-225 mm, thus having threat for agriculture in terms of temporary crop water stresses.

Figure 2.5 presents the monthly and annual values of Nash-Sutcliffe Efficiency (NSE) for pre and post calibration TRMM rainfall estimates. TRMM rainfall estimates even without calibration were found as a useful source of rainfall grid data in comparison to sparse rain gauge network, having NSE values in the range of 0.73 to 0.92. The calibration work performed in this study further improved the NSE values for the satellite rainfall estimates, but this improvement was only about 5% on the average.

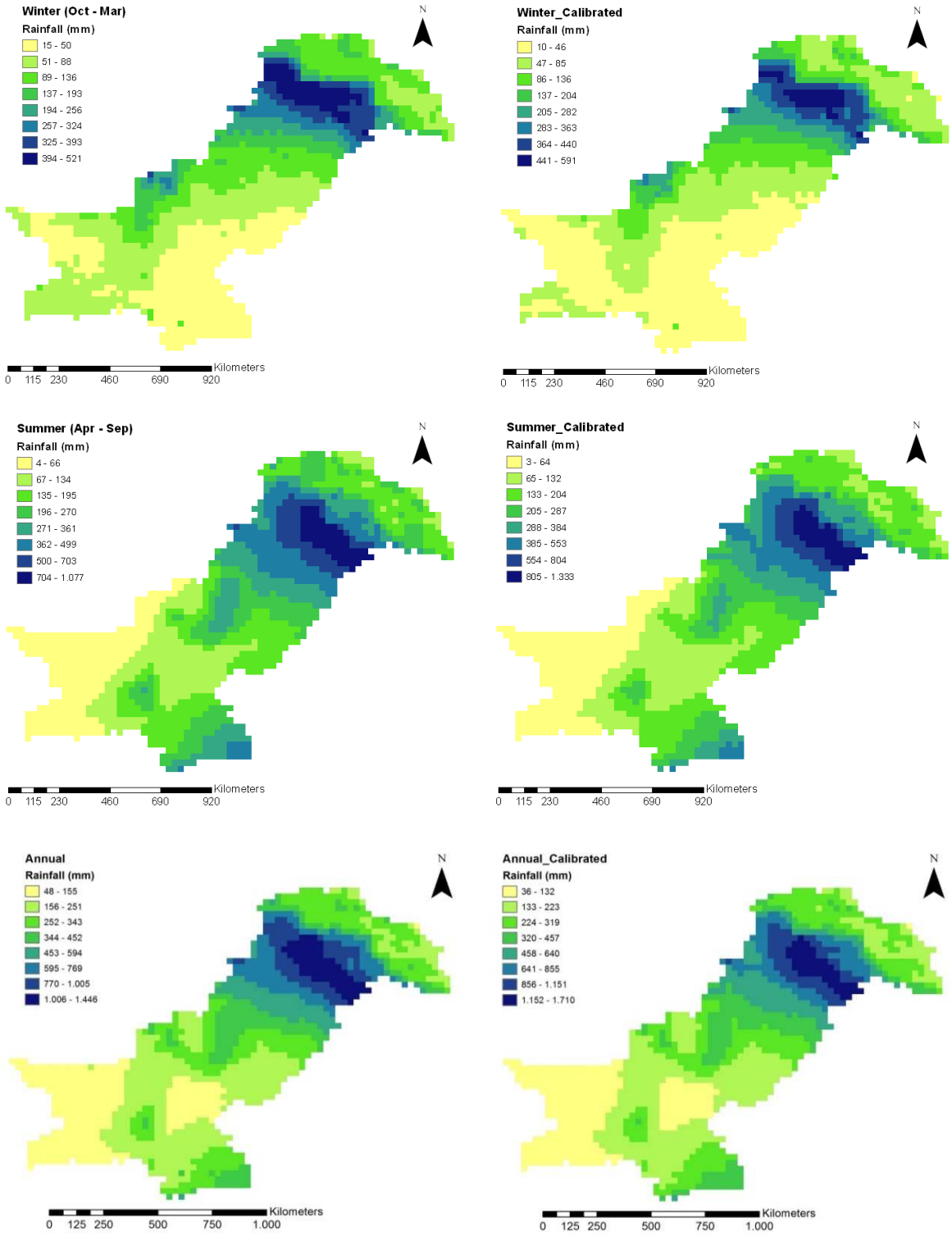

Figure 2.4: Seasonal and annual raster maps of satellite rainfall estimates before and after calibration.

It is important to mention that the NSE values were found high (0.85-0.95) in the summer and monsoon months, i.e. from April to September due to relatively heavy rainfalls during these

months, but the calibration approach even decreased the NSE values for the rainy months of July, August and September. Reasons for this extraordinary result were investigated and major deviations between rain gauge and pixel values causing low NSE values during these months were found for the mountaineous rain gauge stations, which are under high wind and orographic effects during the monsoon period. In these areas during monsoon season, there may be high variations in rainfall from pixel to pixel and even within a pixel covering an area of about 25 x 25 km^2; thus, any comparison or calibration in these areas using sparse rain gauge network may further increase the biases (Cheema & Bastiaanssen, 2012). Figure 2.5 shows that the lowest NSE values were recorded for the months of October, November and December; but the accuracy was greatly improved here by the calibration work resulting in an increase of 10-15% in the NSE values. This finding also matches with the results of Anders et al. (2006), who stated that TRMM overestimates the low rainfall, but very low rainfall rates are difficult to measure by the precipitation radar (PR) of TRMM due to detection limitation. Thus the accuracy of satellite rainfall estimates was found a little lower in these months, but greatly improved by the calibration work because high wind speeds and orographic effects were almost absent in these months.

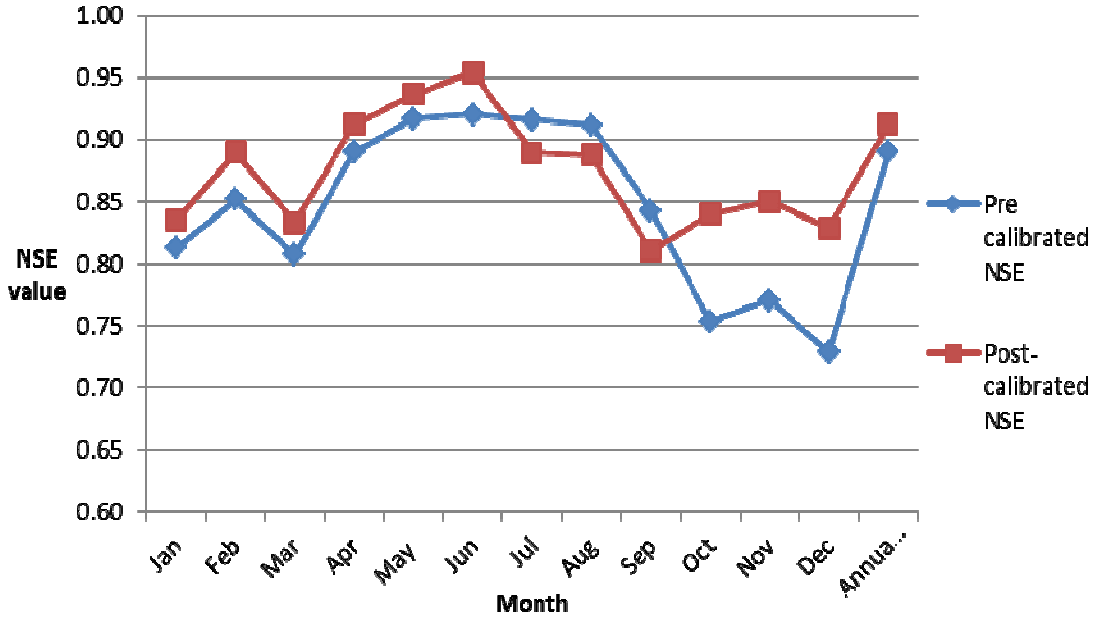

Figure 2.5: Variations in pre and post calibration monthly NSE values for all over Pakistan.

2.5.2 Calibration and Evaluation based on three different Climatic Zones

This section presents the results of TRMM evaluation by dividing the country into three zones as explained in the methodology. Figure 2.6 shows the comparison of monthly satellite

rainfall estimates with rain gauge measurements for all the three zones and regression anlaysis has been performed on seasonal and annual basis.

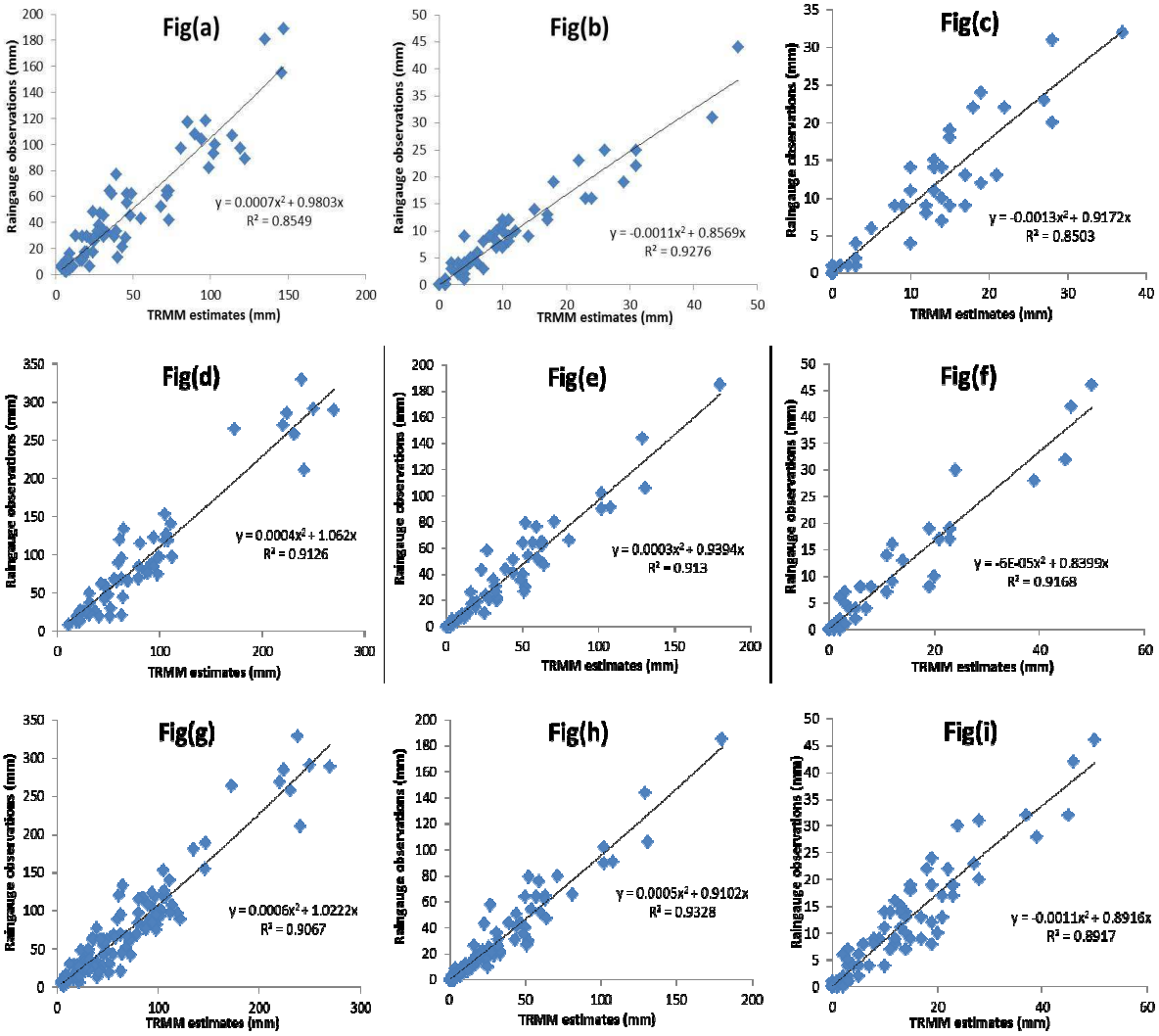

Figure 2.6: Regression analyses for (a) zone-1, (b) zone-2, and (c) zone-3 for winter; (d) zone-1, (e) zone-2, and (f) zone-3 for summer; and (g) zone-1, (h) zone-2, and (i) zone-3 for whole year.

High correlation was found between two datasets for all cases with R^2 values ranging from 0.85 to 0.93. Resulting curves along with second order polynomial equations indicate that the overall TRMM satellite estimates are on higher side a little, but leading to the underestimation at higher rainfall values as can be seen especially in Figures 2.6(a), 2.6(d) and 2.6(g) for zone-1. Almost linear behaviour with little overestimation by the satellite was seen in winter for zone-2 and in both seasons as well as on annual basis for zone-3, as the monthly rainfall in this region was very low, i.e. 40 to 50 mm.

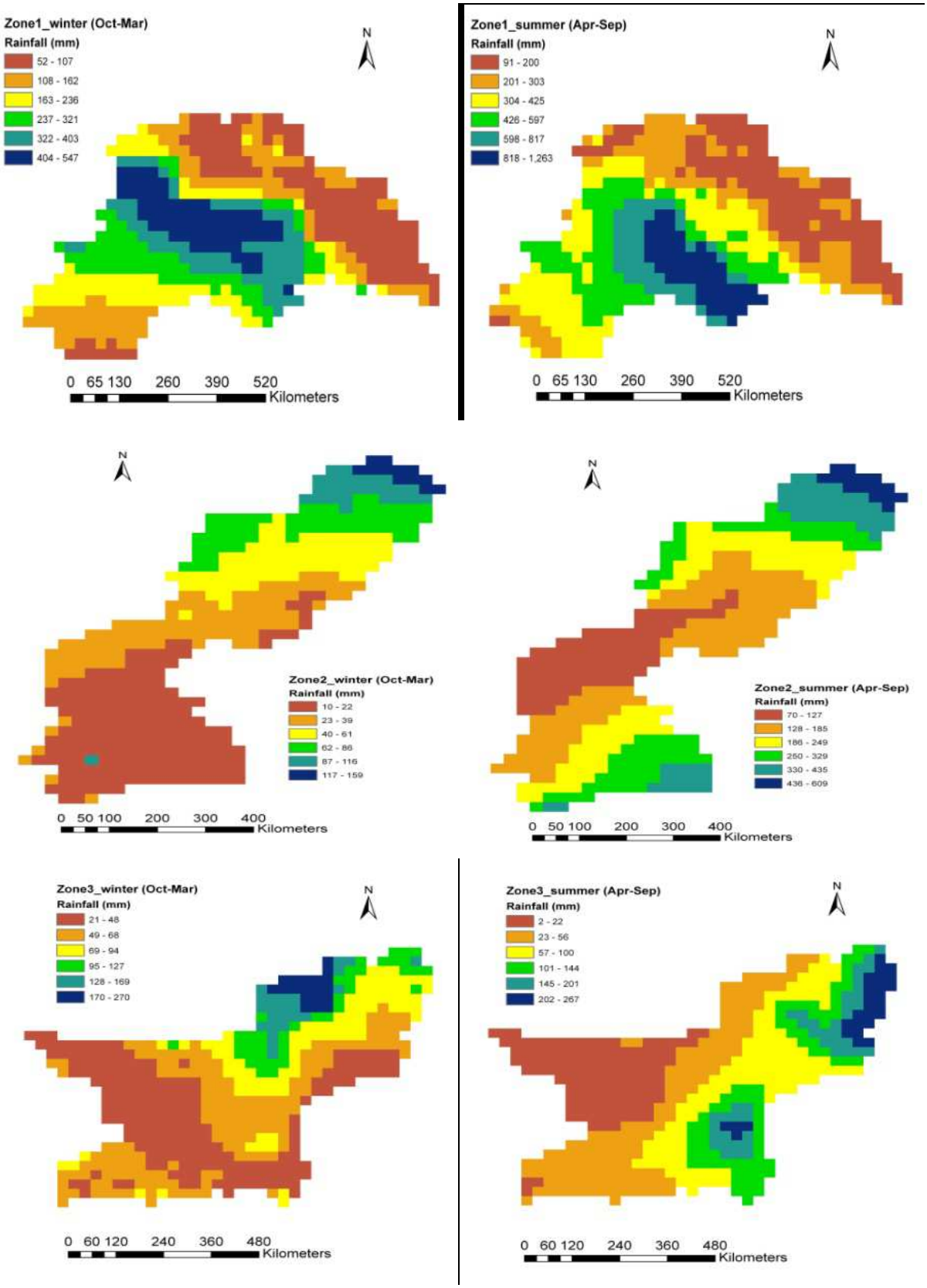

Figure 2.7: Seasonal raster maps for three zones after calibration on seasonal level.

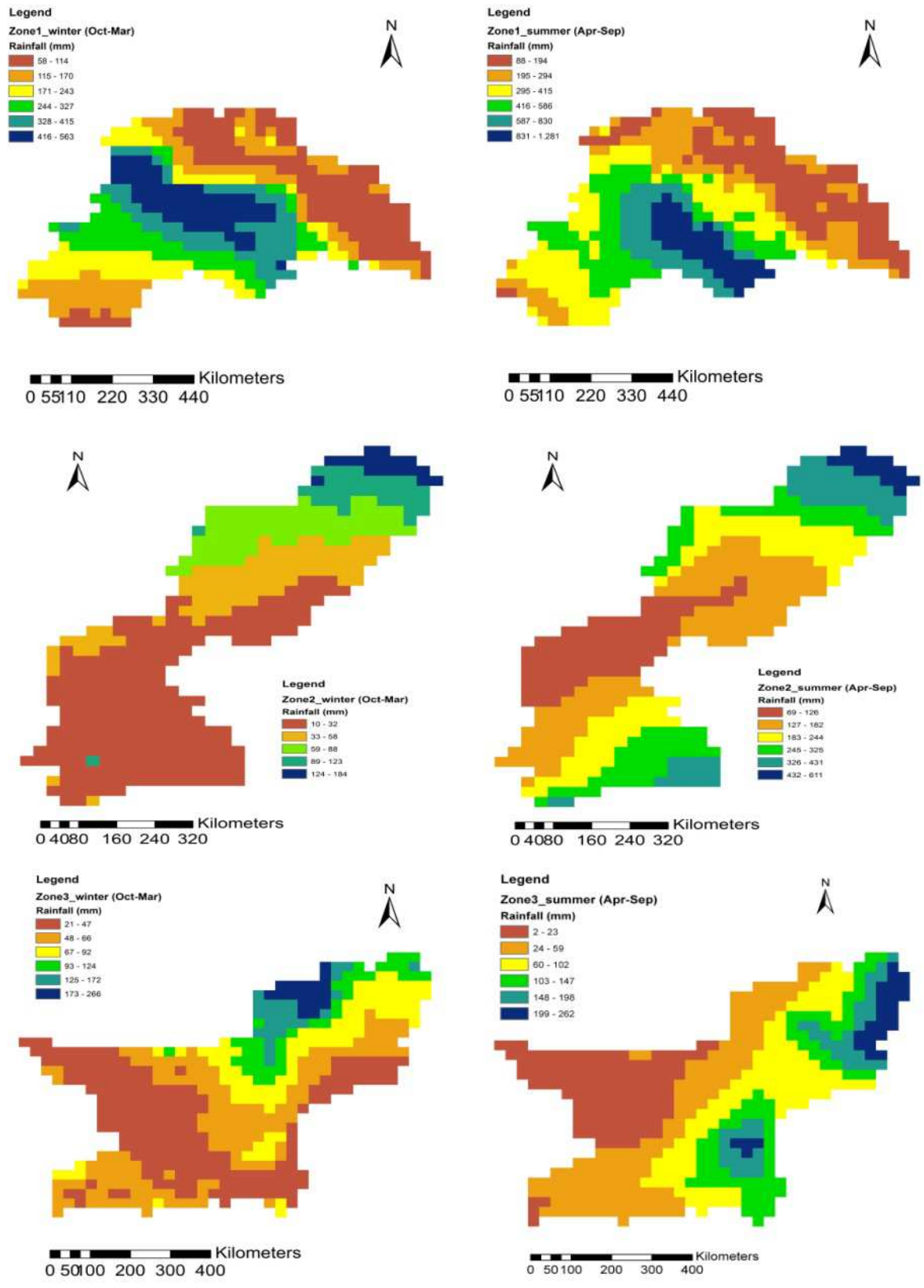

Figure 2.8: Seasonal raster maps for three zones after calibration on annual level.

There were found high spatial variations in the rainfall amounts between the three zones, as can be seen in Figures 2.7 and 2.8 for both seasonal and annual based calibration approaches respectively, which justify the delineation of the devised three zones to achieve better calibration and evaluation of satellite datasets. However, comparison of Figures 2.7 and 2.8 indicates that use of seasonal or annual based calibration approach didn't show much differences and similar results were obtained by using both methods.

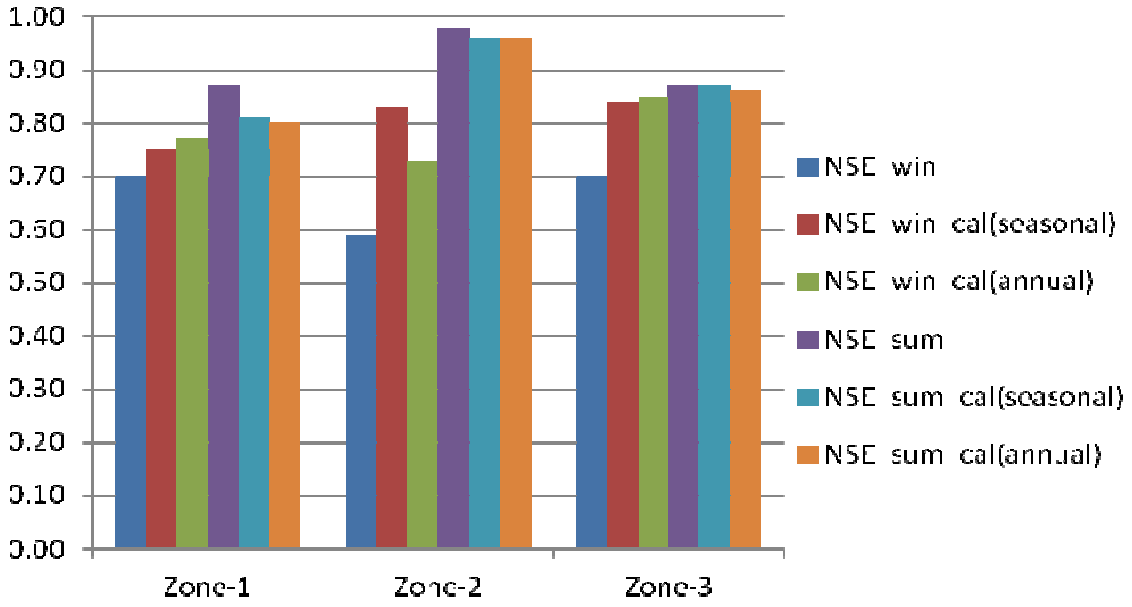

Figure 2.9: Pre and post calibration NSE values for different seasons and climatic zones of Pakistan based on seasonal and annual calibration equations.

For the performance evaluation of original TRMM estimates and the validation of calibration methodology on zonal basis, Figure 2.9 shows the comparison of seasonal NSE values before and after calibration for the three zones using both seasonal and annual based empirical equations. Like the analysis on all over Pakistan, original TRMM rainfall estimates (3B43 without calibration) were found quite reliable for their direct use on zonal basis too, having NSE values in the range of 0.59 to 0.98. For winter season, as the rainfall amounts are less and there is overestimation by satellite, NSE values were relatively less for all regions and improved by about 20% on average after calibration. However, it is important to mention that the calibration approach did not make further improvements in already high NSE values for summer season and even considerably decreased the NSE value for zone-1 which includes the areas of Himalayas and may have more biases due to steep slopes and orographic effects, as explained earlier. The calibration approach was found most suitable in zone-2 for winter season, where most of the areas are plains with semi-arid climate.

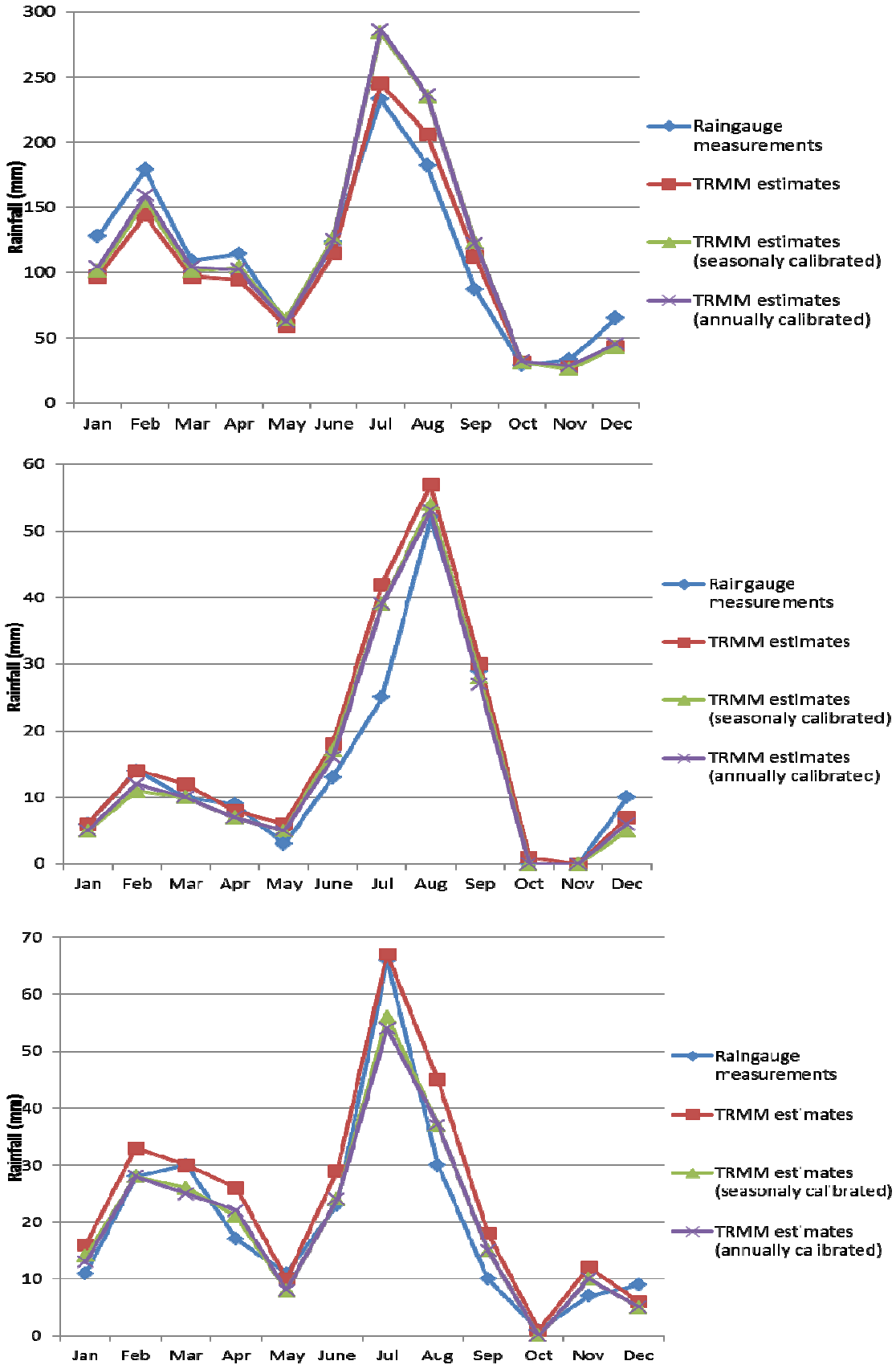

Figure 2.10: Comparison of rain gauge measurements and TRMM estimates with and without calibration for (a) Garhi-dupatta (zone-1), (b) Bahawalpur (zone-2) and (c) Zhob (zone-3).

Regarding time periods for calibration, both seasonal and annual based approaches were found to have similar effects on NSE for summer and a mixed trend for winter with minor improvements in zone-1 and zone-3 but a significant decrease in zone-2 for NSE values based on annual level as compared to those based on seasonal level.

To have further insight into deviations between two datasets throughout the year, Figure 2.10 shows the comparison of monthly rain gauge measurements and TRMM estimates with and without calibration for the three selected rain gauge stations as representative of three respective zones. Figure 2.10(a) shows that for Garhi-dupatta in zone-1 representing high altitudes, TRMM estimates were found to be underestimated for winter and spring months due to heavy precipitation amounts in the range of 120 to 180 mm, except for relatively dry winter months of November and December; and the calibration helped decreasing the deviations. However, for rainy months on this specific rain gauge station of Garhi dupatta, satellite rainfall was found a little overestimated in contradiction to the general trend of underestimation of high values, possibly due to local gradients and orographic effects during these months causing high variations from pixel to pixel and even within a pixel. This phenomenon explains why calibration further increased the biases in this region during these months and resulted in lowering the NSE values. Figure 2.10(b) shows that for Bahawlpur in zone-2, TRMM estimates were found in good agreement with rain gauge measurements throughout the year with a slight overestimation, as the rainfall values were only up to 60 mm; and calibration further decreased the biases between two datasets and resulted in improvement of NSE. Figure 2.10(c) shows that for Zhob in zone-3, TRMM again slightly overestimated the rainfall particularly for the dry winter months and calibration helped improving the NSE values.

2.6 Conclusions

Satellite rainfall datasets like TRMM/TMPA products have become an important source of high and uniform spatio-temporal resolution grid data for their use in climate change and water resources studies. Many scientists have conducted studies for the evaluation of TRMM data in different parts of the world, as well as in Indus Basin covering the major area of Pakistan. This part of the thesis work regarding TRMM evaluation was novel in this sense that 15 years data from the initiation of TRMM program, i.e. 1998 to 2012 was utilized, with the assumption that averaging of both the satellite and rain-gauge datasets over the period of 15

years will help neutralizing the errors and biases in both datasets. The study concluded that TRMM data are quite reliable for their direct and real time use for conducting any rainfall-based studies. For conducting high accuracy studies, these can be further calibrated by adopting suitable calibration techniques. However, for high mountainous areas with heavy orographic rainfalls, regional calibration should be performed very carefully and for limited areal extents using as much dense and uniformly distributed rain gauge network as possible.

These results were further elaborated by dividing the study area into three major zones based on the high variations in their average annual rainfall amounts. It was considered necessary because the results were based on the statistical parameter NSE, which is basically relative to the variation in the standard data, the observed rain gauge measurements in this case. Thus, keeping in view the high diversity in rainfall amounts from north to south in the country, it was divided into three zones so that the difference between mean and the individual rain gauge measurements is as less as possible and high NSE values, if obtained, can be confidently attributed to the agreement of satellite rainfall data with the ground measurements. However, this zonal analysis again resulted in high NSE values (0.59 – 0.98) indicating the accuracy and reliability of TRMM data for its direct use in any real time study. Calibration further improved the NSE values by about 20% for winter season in all the zones, as the rainfall amounts are less in this season and there is somewhat over-estimation by remotely sensing instruments. For summer season, the adopted calibration approach didn't enhance NSE values, but even decreased considerably in zone-1, which comprises of high mountainous regions.

The point of orographic effects due to mountainous regions was further proved in Figure 2.10(a) by comparison of rain gauge measurements with TRMM data for a hilly rain gauge station namely Garhi-dupatta. It was seen that due to high pixel to pixel and within pixel variations, the comparison with rain gauge measurements was not realistic in such areas and the application of regression equations further increased the biases instead of reducing them. A better approach in such areas may be the downscaling of TRMM data in first phase to reduce pixel size and then performing regression analysis by comparison with rain gauge data.

However, the main objective of this study was the evaluation of TRMM data for its direct use; and higher NSE values, both all over the Pakistan and on zonal basis, concluded that TRMM data is quite reliable for its direct use. Although the evaluation was made only for monthly research product (3B43), the interlink of this monthly research product with the 3-hourly or

daily research (3B42) and real time (3B42RT) products suggests that the results of this study can be considered as guidelines for the use of any TMPA product.

Chapter 3

Hydrologic Modeling at River Catchment Scale (Chenab River Catchment)

3.1 Overview of the Chapter

Investigating the hydrological response of an area to adverse climate changes and extreme rainfall events is crucial for managing land and water resources and mitigating the natural hazards like floods. Limited availability of the in situ data, especially in case of Transboundary Rivers, further highlights the need to develop and evaluate decision support systems which may predict the flows in real time using open source satellite rainfall data. This chapter presents the study conducted in the Chenab river catchment to develop and evaluate a hydrologic model using Hydrologic Engineering Center's Hydrologic Modeling System (HEC-HMS) for predicting flows based on TRMM rainfall data. The catchment was analyzed regarding hydro-morphological properties using Shuttle Radar Topography Mission's Digital Elevation Model (SRTM DEM) in HEC-GeoHMS.

As the objective was to rely on open source data as much as possible, digital soil map of the world developed by Food and Agriculture Organization (FAO) and global land cover map developed by European Space Agency were utilized to develop Curve Number grid for the catchment. These preliminary data analyses were employed to set initial values of different parameters to be used for model calibration. The model was calibrated for five rainfall events occurred in the rainy seasons of 2006, 2010 and 2013. The calibrated model was then validated for four other rainfall events of similar type in the same years.

There was found consistency between simulated and observed flows with percent difference in volume to be -6.17% to 5.47% and percent difference in peak flows to be in the range of -6.96% to 7.28%. Values of Nash-Sutcliffe Efficiency were found ranging from 0.299 to 0.909 with average value of 0.586 for all events.

The model was found well capable of capturing the hydrologic response of the catchment in result of a rainfall event. Based on the real time or forecast rainfall data, such modeling approach can be helpful in providing alerts of peak flows or floods in real time.

In the following sections, literature review along with description of model and the study area has been presented. Detailed methodology adopted in this study has been provided in the subsequent sections, with results and discussion concluding the outcomes of this chapter at the end.

3.2 Literature Review and Problem Statement

Climate change impacts in terms of increased global temperatures and high spatio-temporal variations in rainfall can be seen worldwide. These climate change indicators have strong impacts on a river catchment regarding changes in the general water resource situation as well as in the form of natural disasters like floods. This demands the real time investigation of water resources and flood situation in a river catchment, which becomes further challenging in case of limited or no availability of ground data, particularly in case of transboundary rivers.

Pakistan, a country lying in a region which is highly prone to climate change, possesses most of the rivers being shared by India as an upper riparian. River Chenab, being one of the three major western rivers, has an important contribution in water resources of Pakistan. However, major area of this river catchment upstream Marala Barrage lies either in the disputed territory of Jammu & Kashmir or in India; where the ground data availability is limited or its acquisition is difficult for Pakistan. Moreover, even if the flow data at the last gauging station on Indian side (Akhnor) is available, there is big area downstream of it which drains to River Chenab directly at Marala. This situation highlights the need for the development and evaluation of an independent system which may predict the flows in real time using open source satellite rainfall data products.

Tropical Rainfall Measuring Mission (TRMM) Multi-satellite Precipitation Analysis (TMPA) provides high temporal (3-hourly and daily) and uniform spatial (0.25^o x 0.25^o) resolution products using combination of microwave and infrared sensing instruments. Many scientists have made efforts at global and regional scales for the evaluation of satellite rainfall products by comparing them with the field rainfall measurements as well as by testing their scope of use in hydrological studies. Adeyewa & Nakamura (2003) tested TRMM 3B43 data product for 36 months over the major climatic regions in Africa and found it having close agreement with the rain gauge data, and used it as a substitute of rain gauge data over the South Atlantic Ocean for the validation of other satellite products. Dinku et al. (2007) estimated Nash–Sutcliffe Efficiency (NSE) of 0.81 and root mean square error of 25% between the satellite

and rain gauge data averaged over 2.5^{o} grid boxes. The accuracy for a single 25km×25km pixel containing 23 rain gauges in Oklahoma was tested by Villarini & Krajewski (2007) and a correlation of 0.55 was found between the satellite and rain gauges values. Cheema & Bastiaanssen (2012) performed calibration of TRMM Precipitation Radar data for the year of 2007 over Indus basin using regression analysis and geographical differential analysis techniques. They reported decrease from pre-calibration to post-calibration deviation between TRMM and rain gauge data to be from 10.9% to 6.1% for annual time periods, and from 34.9% to 15.4% for monthly periods. Shahid et al. (2014) evaluated the TRMM monthly product (3B43) for Pakistan using 15 years data from 1998 to 2012 in comparison to ground rainfall data for the same period. It was reported that TRMM data is quite reliable for its direct use with NSE values ranging from 0.73 to 0.92 for different months.

Hydrologic modeling is an important tool for the investigation of hydrological response of a river catchment based on the analysis of its geomorphologic and agro-ecological characteristics. Hydrologic models often provide a base for the traditional flood warning systems, where the objective is to provide timely alerts for the advance activation of flood mitigation measures to reduce the damages. Moreover, use of hydrologic models allows employing different open source datasets viz. digital soil map, global land use land cover map, snow cover and other satellite imageries, satellite rainfall datasets, etc. to effectively address the deficiency of ground data and conduct sound hydrologic studies. Immerzeel et al. (2009) conducted study in the Upper Indus Basin and reported that the stream flows can be predicted with a high degree of accuracy by developing and using a hydrologic model and forcing it with remotely sensed precipitation and snow cover data.

3.2.1 Description of HEC-HMS Model

HEC-HMS (Hydrologic Engineering Center–Hydrologic Modeling System) model, developed by the US Army Corps of Engineers (USACE, 2008), can be used for hydrological simulations in different types of studies. The Hydrologic Modeling System is designed to simulate the rainfall-runoff processes of dendritic watershed systems. It is applicable in a wide range of geographic areas for solving the widest possible range of problems. This includes large river basin water supply and flood hydrology, and small urban or natural watershed runoff. Hydrographs produced by the program are used directly or in conjunction with other software for studies of water availability, urban drainage, flow forecasting, future urbanization impact, reservoir spillway design, flood damage reduction, floodplain regulation, wetlands

hydrology, and systems operations. HEC-HMS provides a completely integrated work environment including a database, data entry utilities, computation engine, and results reporting tools. The graphical user interface allows the user seamless movement between the different parts of the program as shown in Figure 3.1.

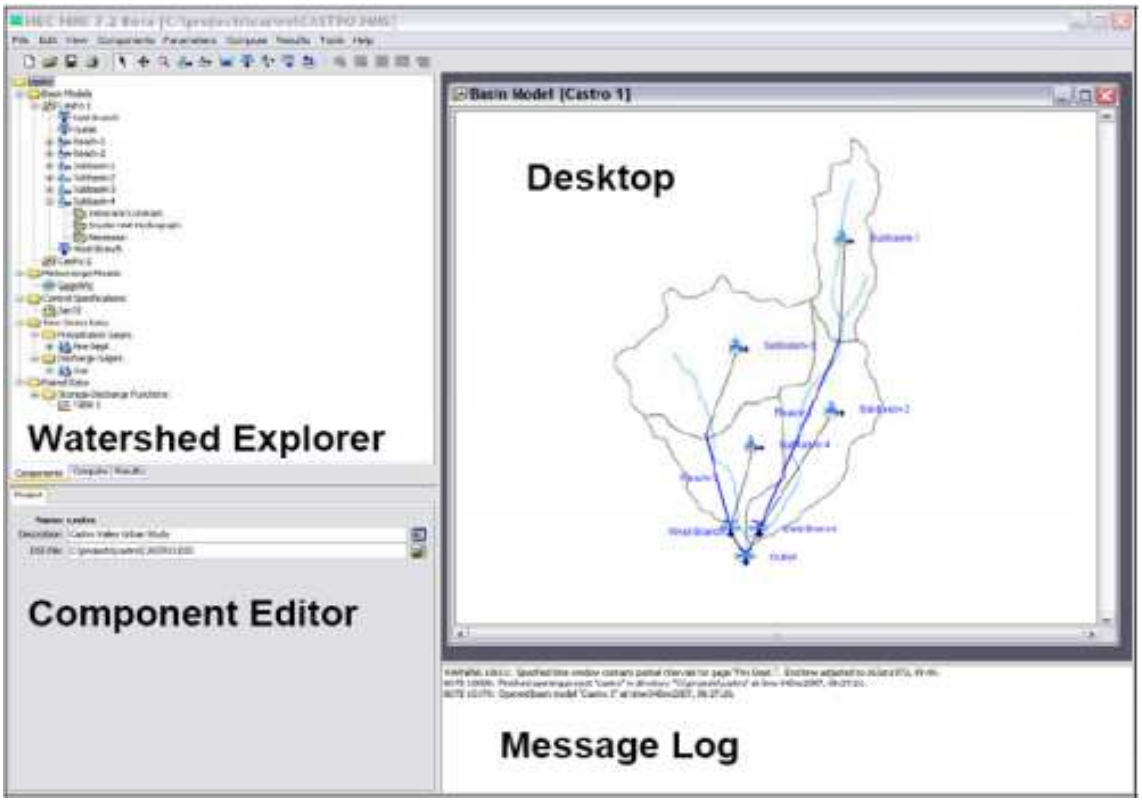

Figure 3.1: HEC-HMS User Interface.

The Geospatial Hydrologic Modeling System Extension (HEC-GeoHMS) has been developed as a geospatial hydrology toolkit for engineers and hydrologists with limited GIS experience. HEC-GeoHMS uses ArcView and the Spatial Analyst extension to develop a number of hydrologic modeling inputs for the HEC-HMS. ArcView GIS and its Spatial Analyst extension are available from the Environmental Systems Research Institute (ESRI). Analyzing digital terrain data, HEC-GeoHMS transforms the drainage paths and watershed boundaries into a hydrologic data structure that represents the drainage network. The program allows users to visualize spatial information, to document watershed characteristics, to perform spatial analysis, and to delineate sub-basins and streams. Working with HEC-GeoHMS through its interfaces, menus, tools, and context-sensitive online help allows the user to conveniently create hydrologic inputs for HEC-HMS. Figure 3.2 illustrates the relationship between GIS, HEC-GeoHMS, and HEC-HMS, with vertical dashed line separating the roles

of GIS and watershed hydrology and HEC-GeoHMS providing the connection for translating GIS spatial information into model files for HEC-HMS (Fleming & Doan, 2010).

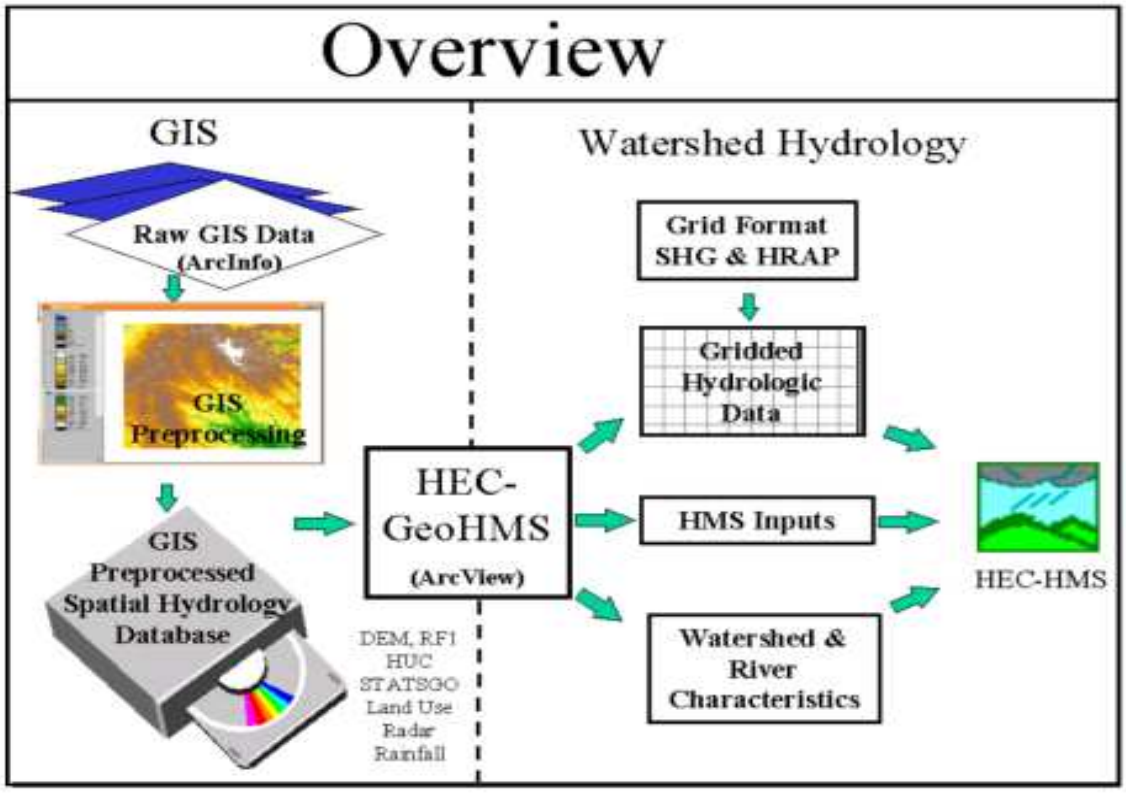

Figure 3.2: Role of HEC-GeoHMS for providing connection between GIS and HEC-HMS (Source: HEC-GeoHMS User's Manual).

Many scientists have conducted valuable hydrologic studies using HEC-HMS model. Chen et al. (2009) used HEC-HMS model employing SCS Curve Number method to predict the impacts of land use change on surface runoff in a rapidly urbanizing Xitiaoxi Basin, China. Ali et al. (2011) combined an empirical land use change model and an event based rainfall-runoff model using HEC-HMS to quantify the impacts of potential land use changes on the storm-runoff generation in the Lai Nullah Basin in Islamabad, Pakistan. The model was calibrated and validated for 5 storm events in the study area, and the results showed good consistency between the simulated and measured hydrographs at the outlet of the basin with NSE ranging from 76 to 98%. Halwatura & Najim (2013) conducted a study to calibrate and validate HEC-HMS model for Attanagalu Oya river catchment and generate long term flow data for the Oya River and tributaries; they reported that the model can reliably be used for simulating flows. Silva et al. (2014) conducted a case study of event and continuous hydrologic modeling in the Kelani River basin in Sri Lanka using HEC–HMS model. The results depicted the capability of HEC–HMS to reproduce stream flows in the basin to a high

accuracy with averaged computed NSE values of 0.91 for event–based simulations and 0.88 for continuous simulations. The study demonstrated the potential of HEC–HMS application for disaster management, flood control, and water management in medium-size river basins in tropical countries.

The current study was conducted for the development and evaluation of an event based hydrologic model in Chenab river catchment upstream Marala Barrage using HEC-HMS model and TRMM rainfall data. The study is important in this respect that most of the catchment lies in India and Marala is the first control structure on River Chenab in Pakistan. Thus the use of open source rainfall datasets like TRMM in a hydrologic modeling environment is very important for this area to independently predict peak flows in real time and provide alerts for disaster management.

3.3 Description of Study Area – Chenab River Catchment

The River Chenab originates in the Kulu and Kangra districts of the Himachal Pardesh province of India in the form of two main streams: the Chandra and the Bhaga, which arise from large snowfields on opposite sides of Baralcha pass and then join at Tandi in the state of Jammu and Kashmir, nearly 3000 m above mean sea level. The catchment of the river is elongate in shape and it covers an area of about 26,000 km^2 up to Marala Barrage (74.4636^{o}E, 32.6733^{o}N) near Sialkot in Pakistan (Figure 3.3).

Singh et al. (1995) described the spatial and seasonal variations in precipitation in Chenab river catchment in detail by dividing the area into three categories based on altitude. They reported that in Greater Himalaya ranges (higher altitudes), about 75% precipitation occurs in pre-monsoon and monsoon seasons, while about 15% precipitation occurs in winter in the form of snowfall. In Middle Himalaya ranges, about 65% precipitation occurs in pre-monsoon and monsoon periods and about 26% in winter. In Outer Himalaya ranges, about 36% precipitation occurs in winter, but most of it is not in the form of snow due to lower altitudes and tropical climate, and thus forms a major source of contribution to river flow during winter season in the form of seasonal winter rains. Snowmelt runoff starts contributing to river flows in the mid or late summer season, while during monsoon season the flow is further enhanced by monsoon rains producing higher discharges and occasional peak flows. Due to combination of rain and snow and glacier-melt runoff, about 84% of annual river flows occur in pre-monsoon and monsoon seasons (April–September), particularly in the months of June-

September (Singh et al., 1997). Thus, it is highly important to predict and simulate flows for rainfall events being occurred in these months, which may enhance the normal flows and cause flooding.

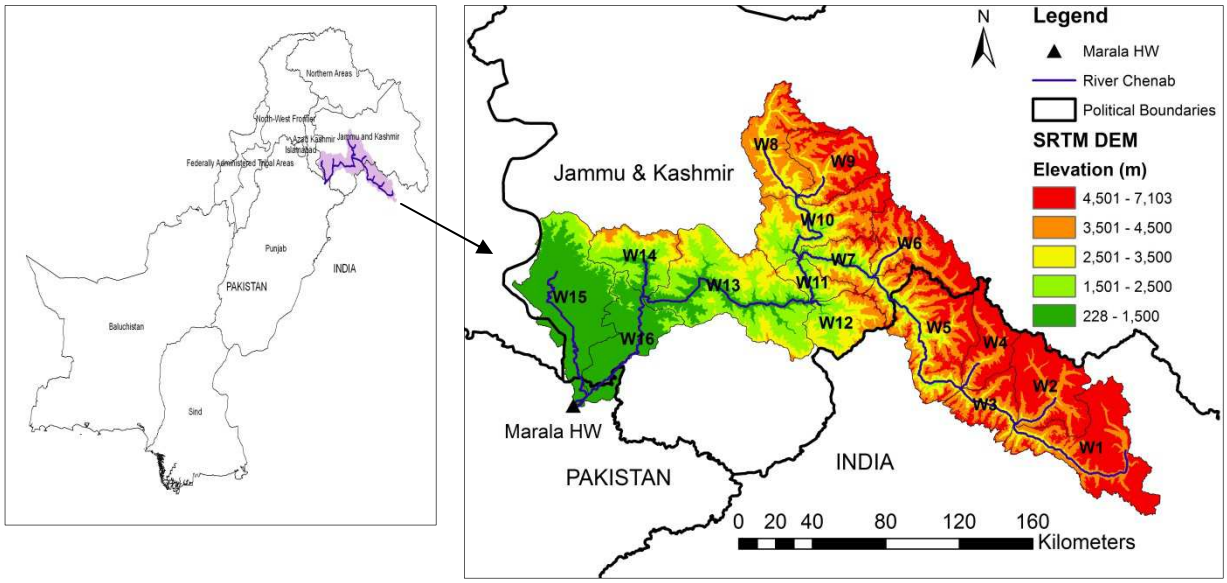

Figure 3.3: Location and topography of the study area (Chenab river catchment).

3.4 Datasets Utilized

As the objective of the research was to devise methodologies for floods management which are based on open source datasets as long as possible, the hydrologic model developed here was also based on different open source input data like topography, soil, land use, etc. Rainfall, being an important input of a hydrologic model, was also tried to be kept open source using TRMM rainfall data, so that the model can be run in real time using such data, or at least, can be helpful in providing guidelines about critical rainfall depths in extreme rainfall alerts systems which are based on such satellite rainfall products. Different datasets utilized for the development and evaluation of a hydrologic model are described below.

3.4.1 Digital Elevation Model

Topography of a region is defined by a Digital Elevation Model (DEM) that describes the elevation of any point in a given area at a specific spatial resolution. The DEM is necessary to delineate the watershed and analyze the drainage pattern of the land surface terrain. Analysis of DEM helps obtaining sub-basins and rivers parameters. In this study, Shuttle Radar Topography Mission (SRTM) DEM has been utilized, which obtained elevation data on a near-global scale, i.e. about 80% of land areas from 60°N to 54°S latitudes (Figure 3.4), to

generate the most complete high-resolution digital topographic database of Earth. SRTM is an international project spearheaded by the National Geospatial-Intelligence Agency (NGA) and the National Aeronautics and Space Administration (NASA), and SRTM DEM is available with a near-global coverage and spatial resolution of 90 m at the equator. SRTM data products have been validated on continental scales through comparison with reserved ground control points: the absolute vertical accuracy has been found better than 9 m, indicating that SRTM improved on its design goal of 16 m absolute (ITHACA, 2010, pp: 11).

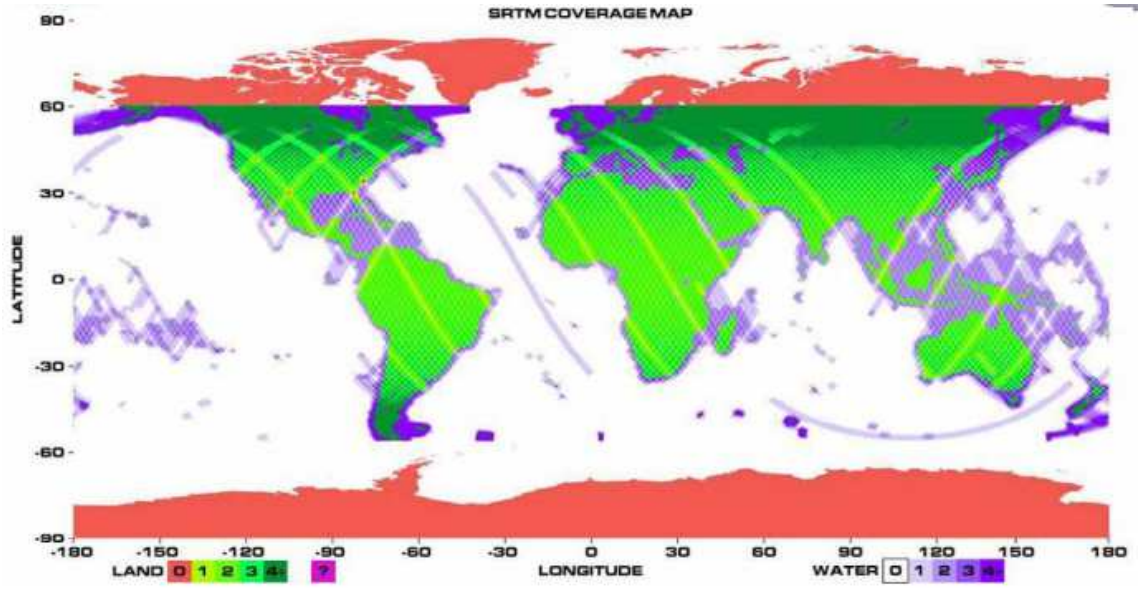

Figure 3.4: SRTM coverage map (colors of the swaths indicate the number of times the area was imaged by SRTM).

3.4.2 Soil and Land Use Data

Hydrological models require information about soil textural and physio-chemical properties. The soil information is generally used in the form of runoff curve number, soil water holding capacity, soil texture, hydraulic conductivity, etc. In this study, the soil information for the study area was obtained by downloading and employing the Digital Soil Map of World, developed and updated by Food and Agriculture Organization of United Nations in 2007 (FAO, 2007).

Land use is another important factor to define surface erosion, runoff and evapotranspiration, as well as to determine Curve Number values in a watershed. The land use information was obtained from global land cover map (GlobeCover 2009) developed and released by European Space Agency (ESA) in 2010 (ESA, 2010). The soil and land use information was used in calculating Curve Number (CN) values, as well as the initial values of different sub-basin

parameters like initial loss, constant loss rate, etc. which are to be used for loss and transform methods in the HEC-HMS model.

3.4.3 Hydro-climatic Data

Rainfall is an important input in any hydrologic study. To keep the developed hydrologic model independent of ground data, TRMM satellite rainfall data was employed in the model for its calibration and validation based on satellite data inputs. For this purpose, TMPA 3-hourly product (3B42) were downloaded and processed in Interactive Data Language (IDL) to have cumulative 3-hourly rainfall amounts on pixel basis for the study area. Finally the 3-hourly image files were processed in ArcMap to get the average rainfall amounts for the individual sub-basins of the study area for each 3-hourly field. For this purpose, model builder tool was utilized to integrate all the steps and automate the procedure for its repeated use. The step-wise procedure consisted of clipping the input file to the study area, converting it into integer and then polygon, uniting it with the sub-basins shape file, and finally getting the average TRMM rainfall values for each sub-basin using dissolve tool. The schematic diagram of the developed procedure has been shown in Figure 3.5. Flow data at a gauging station is an important parameter to compare and calibrate the model simulated flows. For this purpose, flow data for the Marala Barrage was obtained from Surface Water Hydrology Project (SWHP) of WAPDA, Pakistan.

3.5 Data Pre-processing using HEC-GeoHMS

For the hydro-morphologic analysis of the catchment, data from SRTM DEM was processed to simulate the stream network and delineate the watershed into a series of sub-basins. The SRTM DEM was first projected into UTM Zone 43 coordinates, and then different pre-processing operations like filling of sinks, simulation of flow direction, flow accumulation, stream definition and watershed and sub-basins delineation were performed using HEC-GeoHMS toolbar in ArcGIS 10.0. The project for the study area was generated which is to be used in HEC-HMS, and different input characteristics like river length, slope, basin slope, longest flow path, sub-basins centroids and centroid elevation, etc. were calculated; some of these have been shown in Figure 3.6. Other necessary steps like creation of background shape files for river and catchment were performed to be used in HEC-HMS.

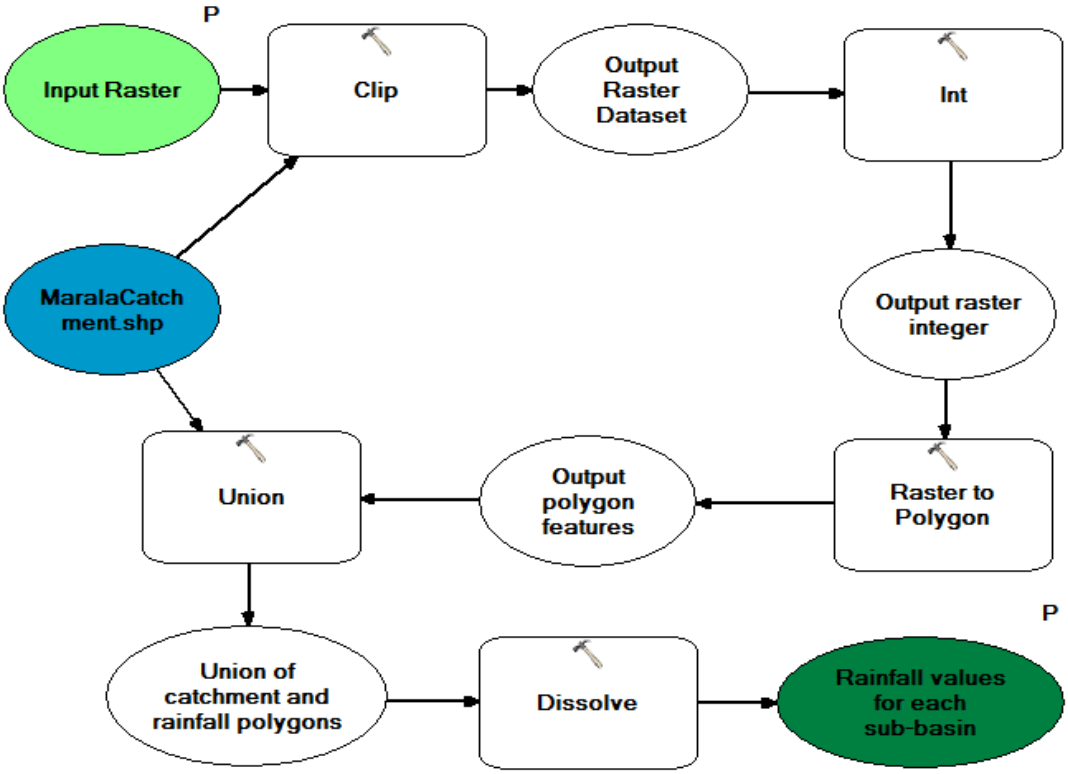

Figure 3.5: Schematic of TRMM rainfall processing in ArcMap.

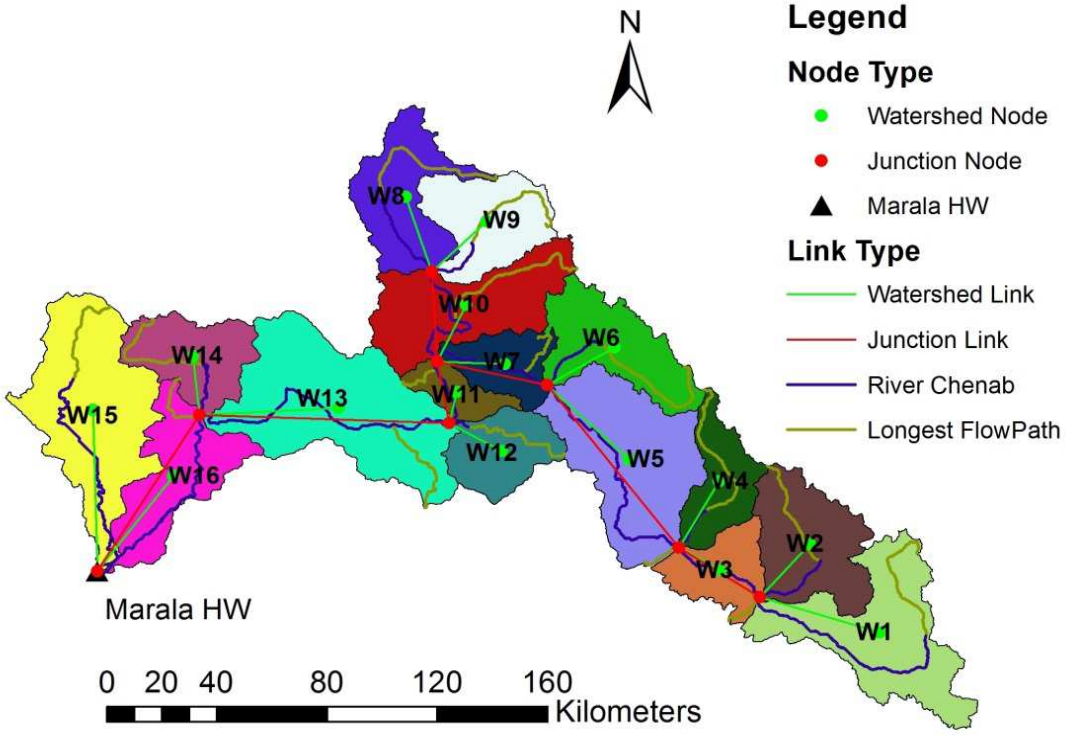

Figure 3.6: Data pre-processing and project generation in HEC-GeoHMS.

3.5.1 Computation of Curve Number Grid

Curve Number (CN) is an important hydrologic parameter used to assess the response of a basin in the form of runoff generation to a specific rainfall event. The Soil Conservation Services (SCS) CN grid was developed for the study area using soil and land use data and employing the methodology proposed by Merwade (2012). The soil information for the study area was analyzed by downloading and employing the Digital Soil Map of World, developed and updated by Food and Agriculture Organization of United Nations in 2007 (FAO, 2007). Based on the information of percent sand, silt and clay for different types of soils in the study area, a specific soil code or hydrologic soil group was assigned to each type following the guidelines provided in National Engineering Handbook of Hydrology (USDA-NRCS, 2007), as described in Table 3.1.

Table 3.1: Classification of Soil Hydrologic Groups as per guidelines of National Engineering Handbook of Hydrology (USDA-NRCS, 2007).

Soil Hydrologic Group	Percent Clay	Percent Silt	Percent Sand
A	< 10%		> 90%
B	10 – 20%	< 30%	50 – 90%
C	20 – 40%		< 50%
D	> 40%		< 50%

The land use information was explored through global land cover map (GlobeCover 2009) developed and released by European Space Agency (ESA) in 2010 (ESA, 2010). There exist 22 different land cover classes which were reclassified into four broad classes for the study area (Merwade, 2012); Table 3.2 shows in detail the different land cover classes and their reclassification into four main classes.

After the processing of soil and landuse information, Union tool was used to merge/union the soil and landuse data. The CN Lookup Table was generated with six fields namely LUValue, Description, A, B, C and D. Table was populated with columns A, B, C and D storing curve number values for corresponding soil groups and landuse category (LUValue); the numbers were obtained from TR55 of USDA-NRCS (1986) and have been presented in Table 3.3. Finally CN grid was created using HEC-GeoHMS by employing the merged soil and landuse feature class and CN Lookup Table. The developed CN grid has been shown in Figure 3.7, which was then used to calculate the mean CN values for all sub-basins. These mean CN

values were employed in estimating initial values of lag time and in turn, the time of concentration for all the sub-basins for their use in HEC-HMS.

Table 3.2: Reclassification of different land cover classes.

Original GlobeCover Classification		Revised Classification	
Number	Description	Number	Description
170	Closed (>40%) broadleaved forest or shrub land permanently flooded - Saline or brackish water	1	Water and Wetlands
180	Closed to open (>15%) grassland or woody vegetation on regularly flooded or waterlogged soil-Fresh, brackish or saline water		
210	Water bodies		
220	Permanent snow and ice		
190	Artificial surfaces and associated areas (Urban areas >50%)	2	Urban/ Residential Areas
40	Closed to open (>15%) broadleaved evergreen or semi-deciduous forest (>5m)	3	Forest
50	Closed (>40%) broadleaved deciduous forest (>5m)		
60	Open (15-40%) broadleaved deciduous forest/woodland (>5m)		
70	Closed (>40%) needle-leaved evergreen forest (>5m)		
90	Open (15-40%) needle-leaved deciduous or evergreen forest (>5m)		
100	Closed to open (>15%) mixed broadleaved and needle-leaved forest (>5m)		
110	Mosaic forest or shrub land (50-70%) / grassland (20-50%)		
130	Closed to open (>15%) (broadleaved or needle-leaved, evergreen or deciduous) shrub land (<5m)		
160	Closed to open (>15%) broadleaved forest regularly flooded (semi-permanently or temporarily) - Fresh or brackish water		
11	Post-flooding or irrigated croplands (or aquatic)	4	Agricultural Lands
14	Rain-fed croplands		
20	Mosaic cropland (50-70%) / vegetation (grassland/shrub land/forest) (20-50%)		
30	Mosaic vegetation (grassland/shrub land/forest) (50-70%) / cropland (20-50%)		
120	Mosaic grassland (50-70%) / forest or shrub land (20-50%)		
140	Closed to open (>15%) herbaceous vegetation (grassland, savannas or lichens/mosses)		
150	Sparse (<15%) vegetation		
200	Bare areas		

Table 3.3: Attributes of CN Lookup Table.

LUValue	Description	A	B	C	D
1	Water	100	100	100	100
2	Urban/ Residential	57	72	81	86
3	Forest	30	58	71	78
4	Agricultural	67	77	83	87

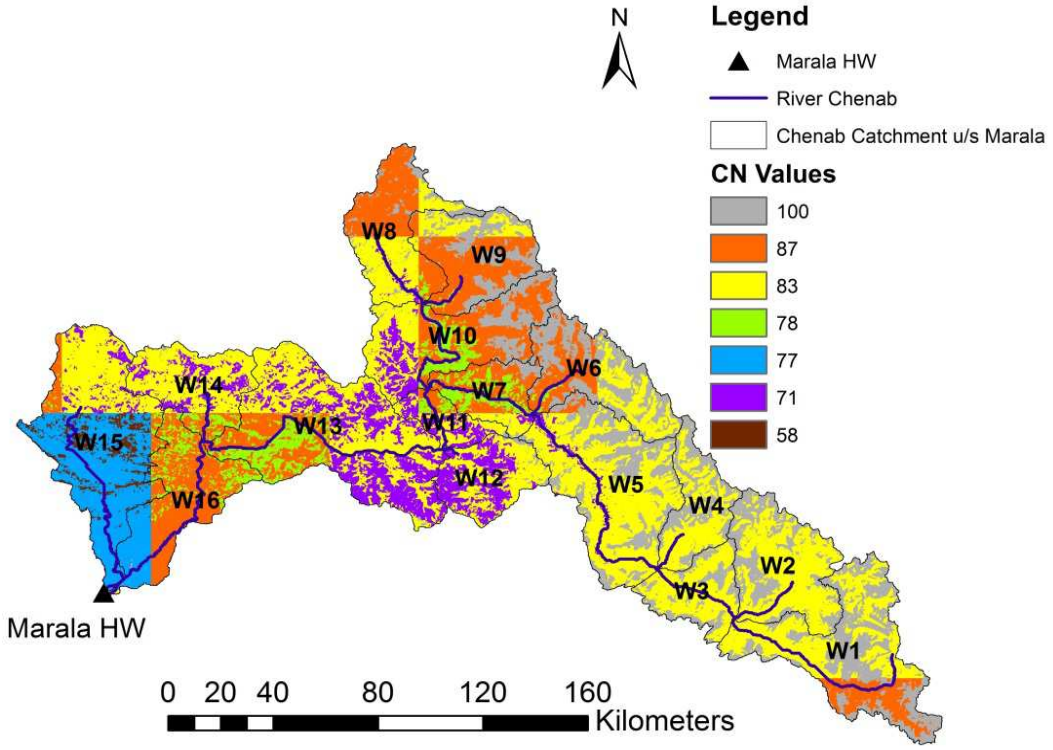

Figure 3.7: Developed CN grid for the study area.

3.6 HEC-HMS Model Impementation

HEC-HMS model was implemented through different model components viz. basin model, meteorological model, control specifications and time series data managers. Background shape files for the river and catchment were loaded into the model and basin model representing the physical watershed was constructed, which consisted of 16 sub-basins, seven reaches and eight junctions with J8 representing the outlet at Marala Barrage (Figure 3.8).

The objective in this study was to perform event-based simulations so that the model can be trained for assessing the hydrologic response of extreme rainfall events. Initial and Constant Loss method was selected to calculate the losses, and its parameters viz. initial loss (mm) and

constant loss rate (mm/hr.) were initialized based on the soil and land use type of sub-basins as per the guidelines provided in technical reference manuals of HEC-HMS model (USACE, 1994; USACE, 2000).

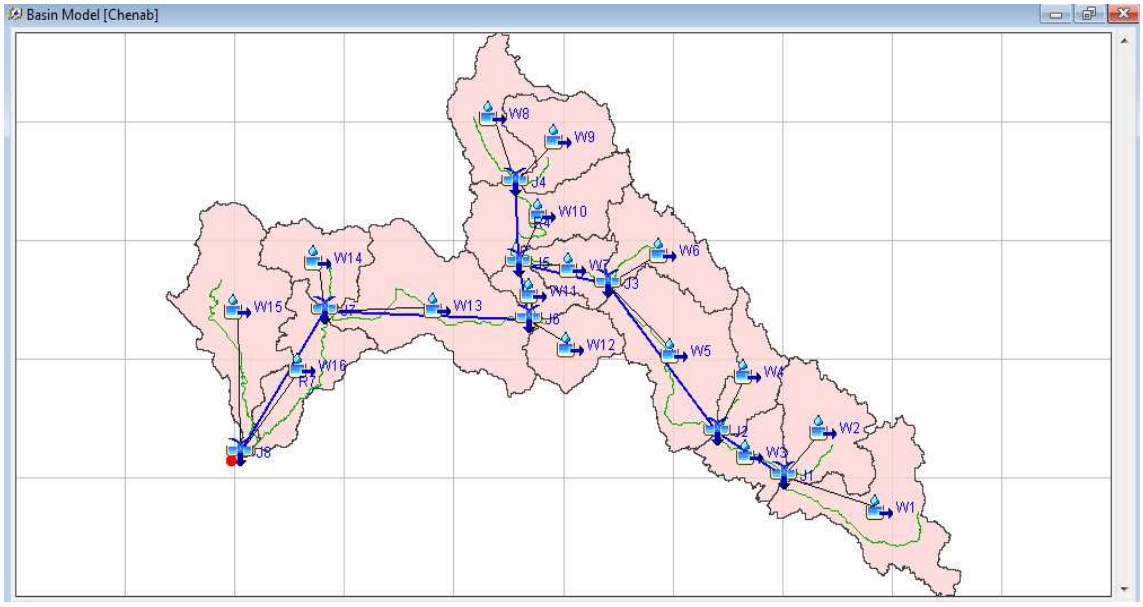

Figure 3.8: Basin model of Chenab river catchment

The Clark Unit Hydrograph transform method was employed to calculate the direct runoff due to its simplicity and less number of required parameters, i.e. only time of concentration and storage coefficient. Time of concentration (hrs.) was calculated using the SCS lag equation for lag time as follows:

$$t_l = 0.00227 \times L^{0.8} \times \left(\frac{1000}{CN} - 9\right)^{0.7} \times S^{-0.5} \qquad (3.1)$$

$$T_c = 0.6 \times t_l \qquad (3.2)$$

Where T_c, t_l, L, CN and S are the time of concentration (hrs.), lag time (hrs.), main stream length (m), Curve Number value, and sub-basin's slope (%), respectively (USDA-NRCS, 2010). The basin storage coefficient, R, is an index of the temporary storage of precipitation excess in the watershed as it drains to the outlet point. There exists a linear relationship between time of concentration and storage coefficcient, and many scientists have proposed empirical relations for the calculation of R based on time of concentration. Initial values of R for the sub-basins were calculated in this study using the empirical relation suggested by Russel et al. (1979) as follows:

$$R = c \times T_c \qquad (3.3)$$

Where c is the proportionality coefficient and its value ranges from 8-12 for densely forested areas, 1.5-2.8 for predominantly agricultural areas, and 1.1-2.1 for urban areas.

For base flow computations, recession method was employed, which is based on three parameters viz. initial flow, recession constant and base flow threshold which may be a threshold discharge value or a ratio-to-peak value. The observed discharge value at the start of each event was input as initial flow, while the recession constant value was initialized as 0.8 for all sub-basins. For base flow threshold, the minimum observed discharge value for the month in which the event occurred was input as base flow threshold discharge.

For routing of flow through the reaches, Lag method of routing was employed and the values of lag times for reaches were calculated and averaged using different empirical equations viz. Kirpich, Chow, NERC, and Watt & Chow, as described by Loukas & Quick (1996).

The meteorological model determines the way to calculate the precipitation input for the sub-basin elements. In this study, TRMM 3-hourly rainfall product (3B42) averaged over the sub-basins level was to be utilized. For this purpose, specified hyetograph meteorological model was selected and a hypothetical rain gauge was defined for each sub-basin to input 3-hourly time series of rainfall data for all sub-basins. Evapotranspiration is the combination of evaporation from ground surface and transpiration by vegetation, and is not a required input in case of event-based modeling. Moreover, as the objective in this study was to capture and simulate the peak flows due to monsoon rain events, no snowmelt mechanism was studied separately in addition to calculating base flows by initializing as the initial observed discharge value. Time series data of TRMM 3B42 rainfall product for all sub-basins and the observed flow data of Marala Barrage at the outlet (J8) of the basin model were input.

3.7 Model Calibration and Validation

All empirically calculated and initialized watershed parameters need calibration to produce a best fit between the observed and simulated flows. For this purpose, the model was calibrated using optimization trail tool by running it for five selected rainfall events viz. E1 (July 8-11, 2006), E2 (July 25-August 01, 2006), E3 (July 18-23, 2010), E4 (July 29-31, 2013) and E5 (August 01-03, 2013). The optimized parameters include initial loss (mm), constant loss rate (mm/hr.), time of concentration (hrs.), storage coefficient (hrs.), base flow recession constant and base flow ratio to peak for all the sub-basins, and lag time (min) for all the seven reaches.

In this way, total number of parameters to be optimized was 103, and Univariate Gradient method was chosen to run the optimization trail with maximum iterations set as 309 and tolerance value as 0.01. The Peak-Weighted RMS Error function was selected as objective function, which is used to determine the goodness of fit and is a modification of standard RMS error giving increased weight to flows above average and less weight to flows below average. As the base flow threshold discharge values were initialized for running the model, these were calibrated for all the events and sub-basins and were divided by the respective simulated peak flows to calculate calibrated ratio-to-peak values for their general use for any other rainfall event. The optimized parameters were then taken as input along with other known parameters and rainfall and discharge data to run and validate the model for four other events viz. E1_val (August 24-29, 2006), E2_val (September 01-05, 2006), E3_val (August 05-08, 2013) and E4_val (August 13-17, 2013).

Model performance was assessed statistically using three evaluation parameters viz. Nash–Sutcliffe Efficiency (NSE), percent deviation in runoff volumes (D_v) and percent difference in peak flow (D_p) using following equations (Nash & Sutcliffe, 1970; Ali et al., 2011):

$$NSE = 1.0 - \frac{\sum_{i=1}^{N}(Qsi - Qoi)^2}{\sum_{i=1}^{N}(Qoi - <Qo>)^2} \quad (3.4)$$

$$D_v\,(\%) = \frac{\sum_{i=1}^{N} Qsi - \sum_{i=1}^{N} Qoi}{\sum_{i=1}^{N} Qoi} \times 100 \quad (3.5)$$

$$D_p\,(\%) = \frac{Q_{sp} - Q_{op}}{Q_{op}} \times 100 \quad (3.6)$$

Where Q_{si} and Q_{oi} are the simulated and observed stream flows at time step i, $<Q_o>$ is the mean observed stream flow over the simulation period, and Q_{sp} and Q_{op} are the simulated and observed peak flows, respectively. These parameters were estimated for both calibration and validation periods.

3.8 Results and Discussion

In the developed hydrologic model, the Chenab river catchment has been divided into 16 sub-basins and the average rainfall amounts for each sub-basin were input to assess its hydrologic response in terms of flow. The individual flows of sub-basins are joined through junctions and are routed to the main outlet through reaches. The collective response of the whole catchment along with observed flows at the outlet (Marala Barrage) were used to calibrate the model for

different rainfall events. Figure 3.9 highlights the hydrologic response of some sub-basins for the first calibration event E1; four sub-basins namely W1, W8, W12 and W15 are presented in the Figure, which basically represent different categories based on elevation and climate. W1 represents the south-east side of the catchment where average elevation is more than 4500 m and glacier and snow-melt have major contribution to flows. W8 represents the northern side with elevation in the range of 3500-4500 m in most of the area, which is again a snowmelt based sub-basin. Sub-basin W12 represents the central part of the catchment with elevations ranging from 1500–3500 m, and runoff considerably contributed by the rainfall. Sub-basin W15 lies on the western downstream side of catchment with elevations less than 1500 m, and has high contributions to flows in result of heavy monsoon rains. Specifically for event E1, it is evident from Figure 3.9 that there was a contribution to flows due to rainfall too for W1, but W8 quite normally did not get much rainfall during this event and there was no excess rainfall in fact for this event to generate direct runoff from W8.

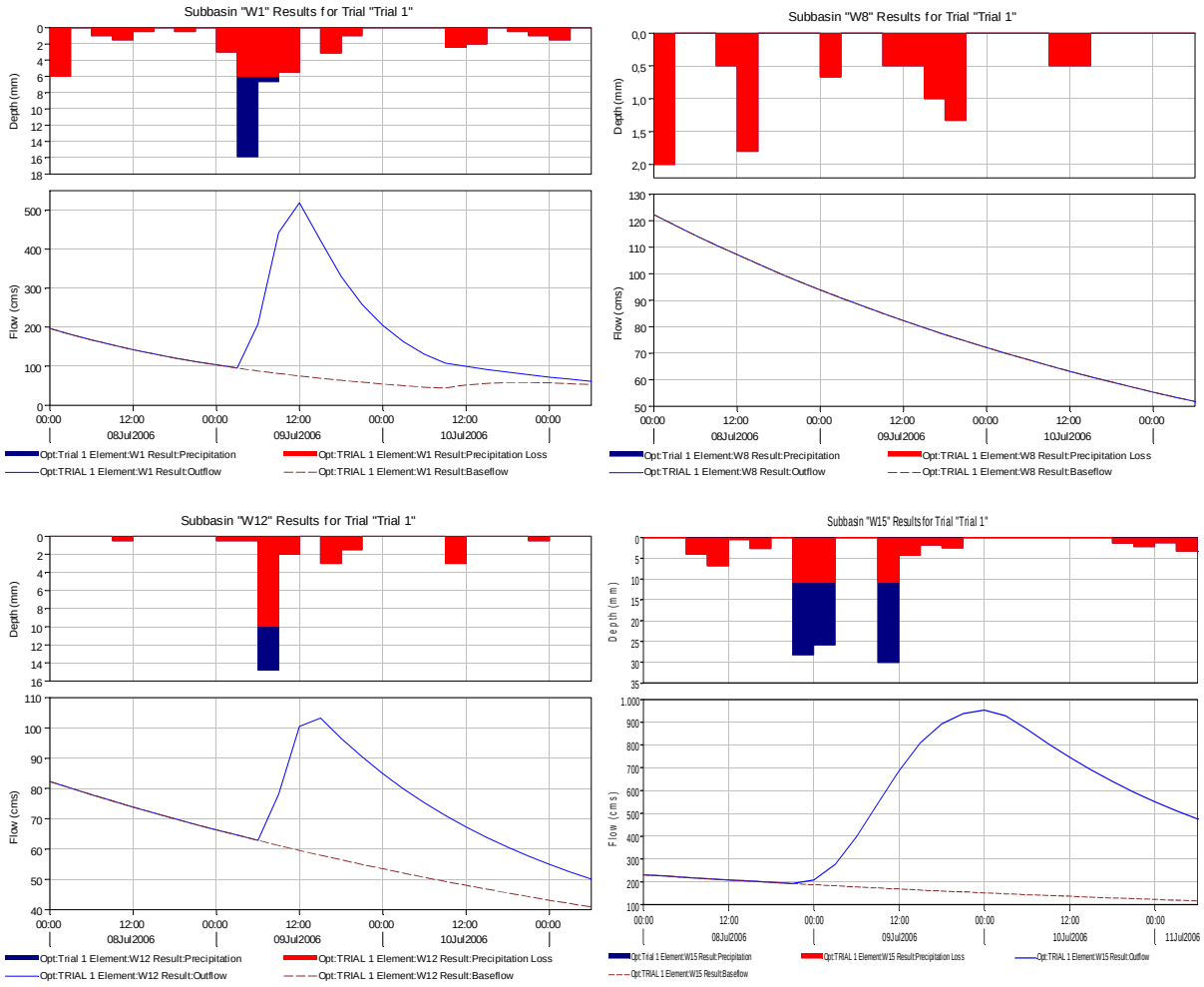

Figure 3.9: Individual response of some sub-basins for the calibration event E1; (a) Sub-basin W1, (b) W8, (c) W12, and (d) W15.

Sub-basin W12 received almost similar rainfall amount for this event as that of W1, but the peak flow generated by it was only about 100 cubic meters per second (cms) as compared to 500 cms from W1. Even the runoff in the form of base flow from both W1 (200 cms) and W8 (120 cms) was found higher than the total flow generated by W12. This is because the W12 sub-basin consists of small area (1000 km^2) as compared to those of W1 (2500 km^2) and W8 (1500 km^2), and therefore, the runoff generated from W12 for the same amount of rainfall is less than that of W1. As stated earlier, sub-basin W15 received heavy amount of rainfall and generated high peak flows as can be seen in Figure 3.9. The detailed results about individual contributions of the sub-basins for all the events have been presented in Appendix A.

The collective response of the whole catchment along with observed flows at the outlet (Marala Barrage) for all the calibration events has been shown in Figure 3.10, which presents the comparison of simulated and observed flows, as well as times of major rainfall occurrence along with peak flow times to have an idea of the lead time available under different rainfall scenarios. Although different scenarios prevail depending upon the variations in rainfall pattern for each event, it can be seen that the peak flows occurred on average about 18-24 hours after the major rainfall event. However, there was found diversity in this lead time ranging from 15 hours for E4 to about 45 hours for E3, which depends upon several factors like rainfall intensity (E.g. very high in case of E4), initial soil moisture condition, etc. in addition to morphological parameters like time of concentration and lag time.

Different parameters were optimized through these calibration events and the average values of the optimized parameters have been presented in Table 3.4. For loss parameters (initial loss and constant loss rate), however, minimum of all the calibrated events' values were selected as representative instead of averaging. Similarly while calculating average optimized values of recession constant, values less than 0.5 for any event were ignored. These adjustments were made to keep losses at lower limit and to increase the sensitivity of model regarding base flow contributions by setting high recession constant values. It is worth mentioning that high recession constant values result in quick depletion/recession of base flow and quick achievement of base flow threshold, at which the base flow contribution starts supplementing the total flow. Decision to keep losses on lower side and base flow contributions on higher side was made based on the fact that no separate estimation of flows due to snowmelt was considered. Such adjustments provided the best possible results for the validation events.

Table 3.4: Optimized parameters based on five calibrated rainfall events.

Elements	Parameters					
Sub-basins	**Initial Loss (mm)**	**Constant Loss Rate (mm/hr.)**	**Time of Con. (hrs.)**	**Storage Coefficient (hrs.)**	**Recession Constant**	**Base-flow Threshold (Ratio-to-peak)**
W1	3.1300	1.8824	6.4590	8.7013	0.6920	0.4548
W2	3.1300	2.3530	4.0787	6.601	0.7360	0.4582
W3	3.2500	2.3530	2.9200	5.802	0.8374	0.3351
W4	3.1300	2.3530	4.1627	7.116	0.7620	0.4438
W5	3.0981	1.7312	4.8865	8.772	0.9090	0.3928
W6	3.1300	0.8416	4.2695	6.837	0.9160	0.3912
W7	4.9484	0.7239	4.2886	22.530	0.9429	0.2995
W8	3.5295	1.2046	8.3223	13.969	0.8367	0.4081
W9	3.1850	0.7237	3.5515	9.852	0.7585	0.3524
W10	3.6934	0.9651	5.0556	22.2536	0.7688	0.4426
W11	3.9396	1.9301	3.4408	37.4152	0.8943	0.5229
W12	4.7060	1.6007	4.1814	23.0010	0.8461	0.4706
W13	4.9413	1.2805	9.6029	38.8694	0.8315	0.3641
W14	4.7060	1.7729	5.7838	10.2635	0.8360	0.3648
W15	4.7060	2.4264	13.2276	34.5612	0.9197	0.2772
W16	3.3333	0.8000	10.4547	23.0804	0.8442	0.1409

Reaches	**Lag Time (min)**	**Lag Time (hrs.)**	**Cum. Lag Time (hrs.)**
R7	706.980	11.783	11.783
R6	1117.012	18.617	30.400
R5	359.914	5.999	36.398
R4	434.496	7.242	43.640
R3	455.596	7.593	43.992
R2	433.146	7.219	51.211
R1	378.660	6.311	57.522

From Figure 3.10, it is evident that model captured the observed flows quite well, particularly the peak flow amounts and their timings, which is mainly emphasized in any event based modeling studies to detect the extreme flood events and provide timely alerts (Ali et al., 2011). The calibrated model was found capable of capturing peak flows and hydrograph recession curves with reasonable accuracy recording percent difference in peak flows to be in the range of -4.8% to 0.7% and NSE values ranging from 0.473 to 0.909 (Table 3.5). However, there were observed biases in the rising limbs, as can be seen particularly for E2, E4 and E5 events, indicating that model takes some time at the start of simulation to match well with the observed flows. These biases were on negative side for all events resulting in percent difference in volume to be ranging from -0.76 to -6.17 (Table 3.5), indicating that the

simulated flows were under-estimated at the start of each event and model takes some time to match well with the observed flows at the start.

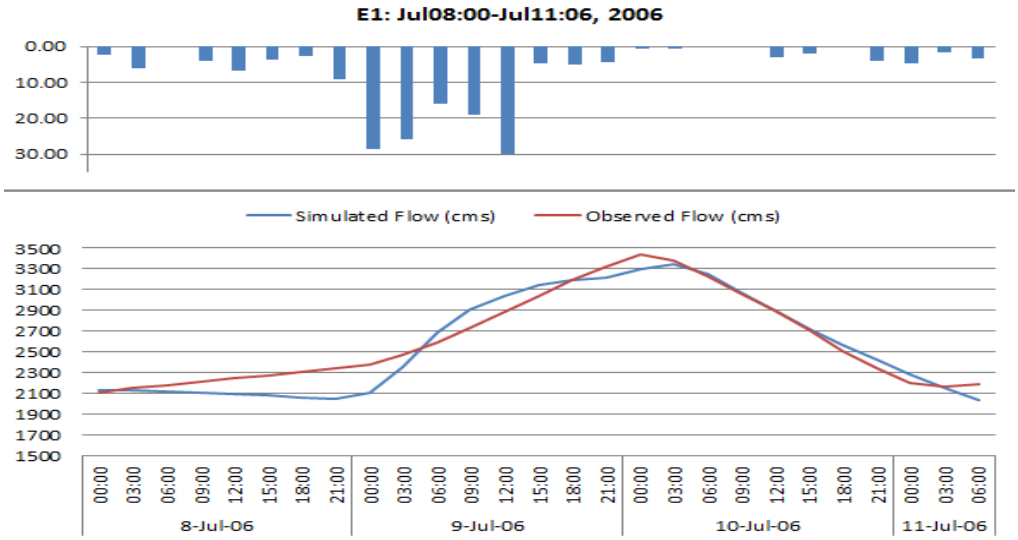

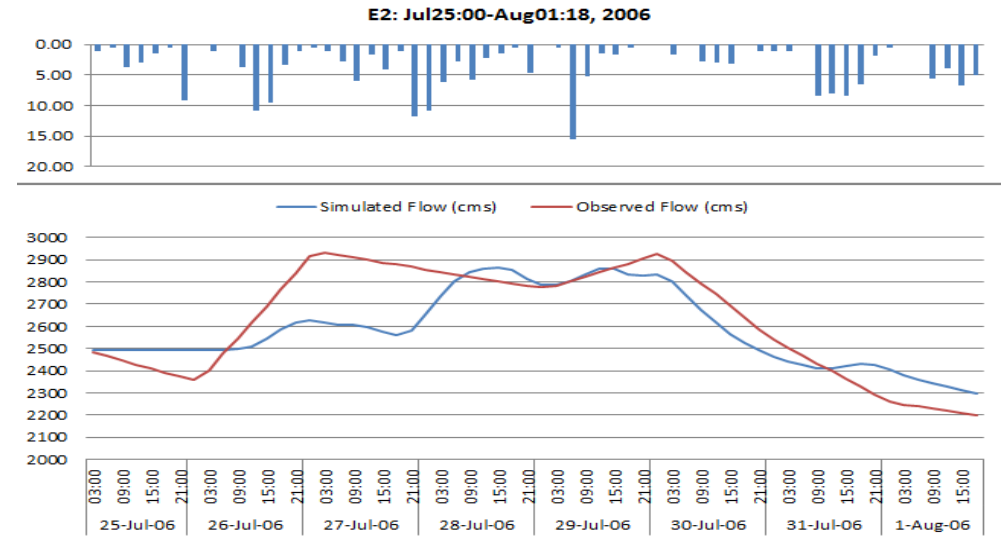

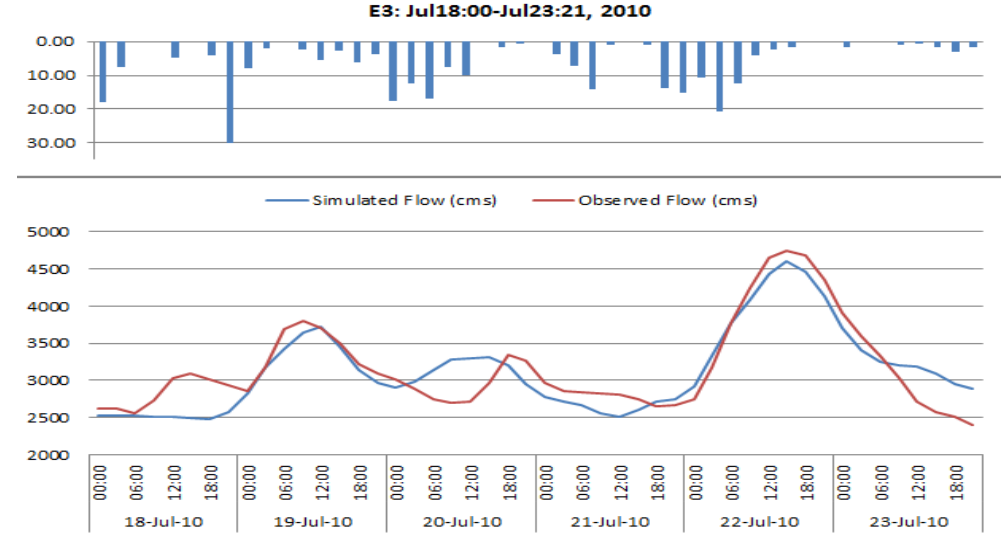

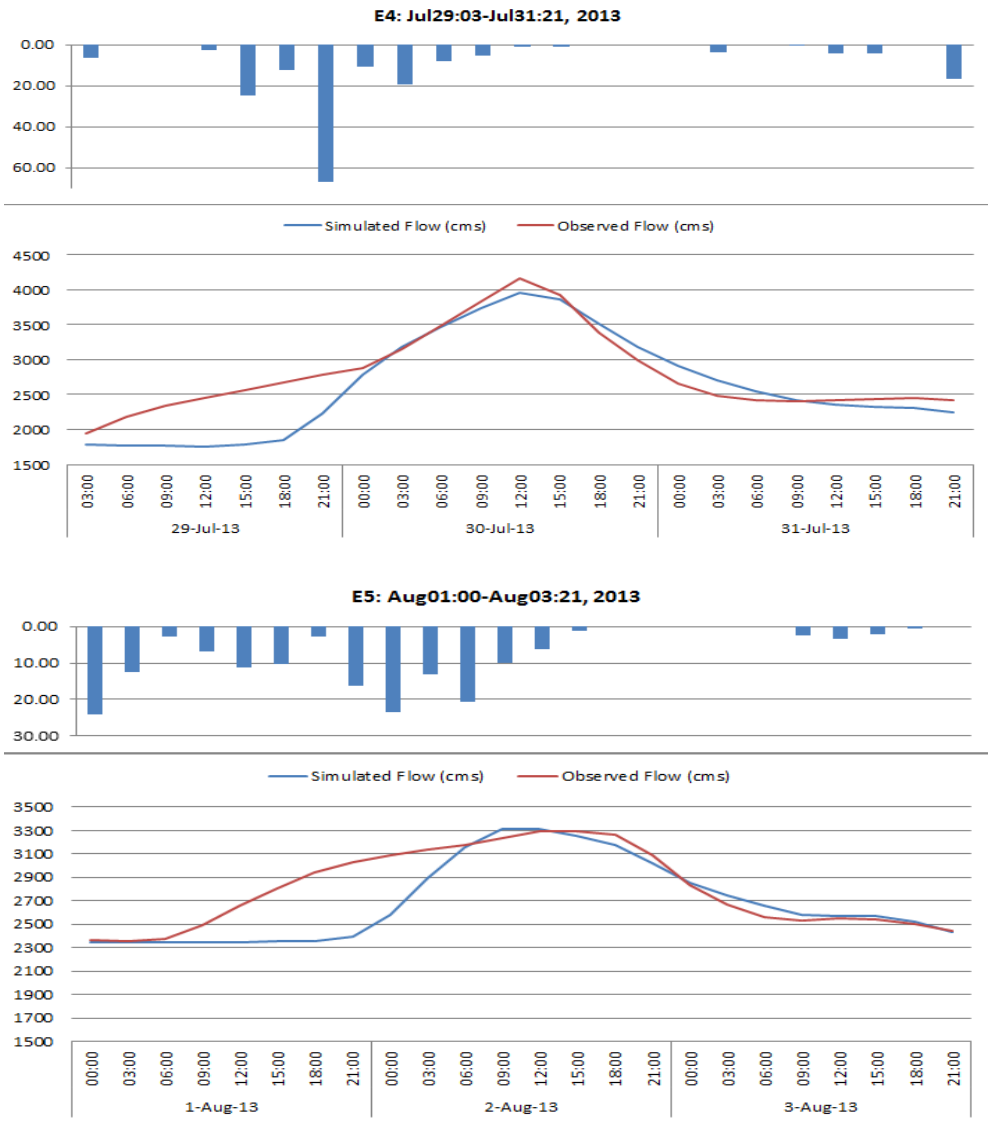

Figure 3.10: Simulated and observed discharges at Marala Barrage for rainfall events, employed for model calibration.

For model validation, optimized parameters were input and the model was run for four other rainfall events. Comparison of simulated and observed discharges for these events has been presented in Figure 3.11. The model estimated the observed flows quite reasonably for the validation phase too, but not as much accurate as in case of calibration events, which is evident from visual inspection of Figure 3.11, as well as from statistical parameters presented in Table 3.5. The percent difference in volume for validation events was found almost within ±6% as compared to about zero to -6% for calibration phase. Percent difference in peak flows was recorded to be up to -5% for calibration events; however, the differences in peaks were on higher side for the validation events with values in ±8% indicating that the peak flows were not as well captured as for the calibration events. NSE values for the validation events,

ranging from 0.299 – 0.679 were also found less than those of calibration phase, with average NSE value of 0.466 for validation events as compared to 0.682 for calibration phase.

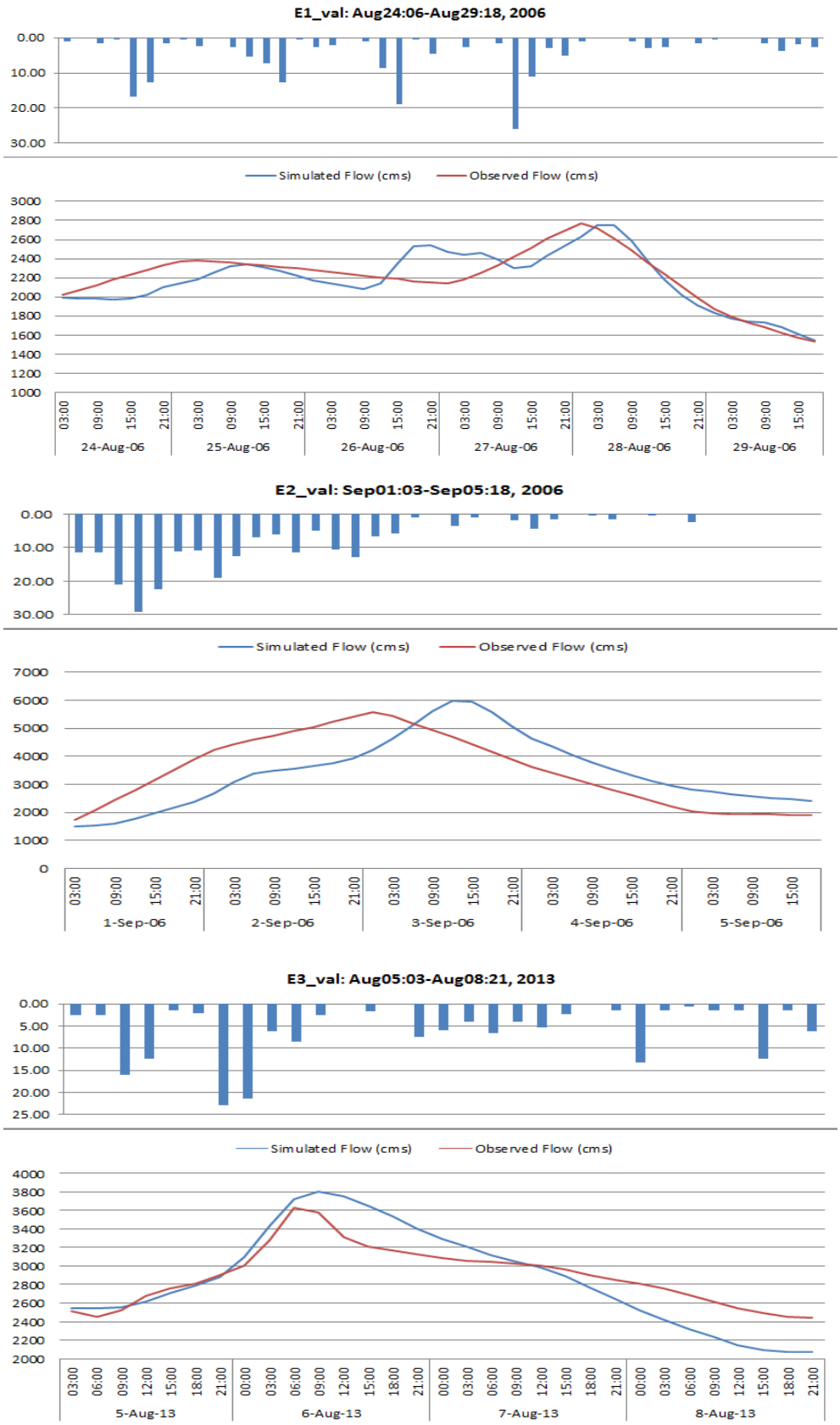

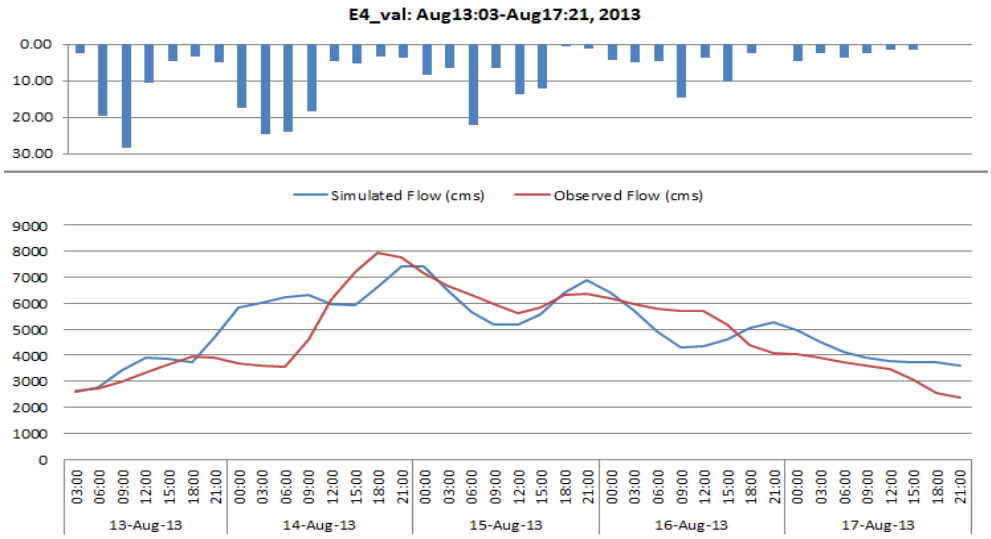

Figure 3.11: Simulated and observed discharges at Marala Barrage for four rainfall events, selected for model validation.

Table 3.5: Statistical parameters for rainfall events during calibration and validation.

Event ID	Start Time Date; Hrs.	End Time Date; Hrs.	D_v (%)	D_p (%)	NSE
Calibration					
E1_2006	July 08; 00	July 11; 06	-1.50	-2.8	0.909
E2_2006	July 25; 00	Aug 01; 18	-1.59	-2.2	0.651
E3_2010	July 18; 00	July 23; 21	-0.76	-3.0	0.757
E4_2013	July 29; 03	July 31; 21	-6.17	-4.8	0.621
E5_2013	Aug 01; 00	Aug 03; 21	-4.03	0.7	0.473
Validation					
E1_val_2006	Aug 24; 06	Aug 29; 18	-1.30	-0.51	0.679
E2_val_2006	Sep 01; 03	Sep 05; 18	-2.18	7.28	0.299
E3_val_2013	Aug 05; 03	Aug 08; 21	-1.30	4.84	0.373
E4_val_2013	Aug 13; 03	Aug 17; 21	5.47	-6.96	0.513

Overall, the NSE values for both calibration and validation events were found to be in acceptable range, but relatively low as compared to those reported by Ali et al. (2011) (0.87 on average) and De Silva et al. (2014) (0.91 on average). Acceptable but comparatively low values of NSE in this study may be attributed to the large size of the catchment (33000 km^2) as compared to only 235 km^2 and 2230 km^2 for Ali et al. (2011) and De Silva et al. (2014), respectively. Moreover, the current study may involve some uncertainties due to satellite

rainfall data too, as compared to conventional rain gauge data based studies. However, it can be considered as a strength of this study to rely on open source rainfall data, which is available in real time and provides uniform spatial coverage for a large catchment with sparse rain gauge network to predict peak flows in real time. It is believed that running and calibrating the model for more events may further refine the parameters' optimization process to increase the accuracy of model for a wider range of rainfall events.

3.9 Conclusions

This study presented a methodology to assess hydrologic response of a transboundary river catchment by integrating HEC-HMS model with open source land cover, soil and rainfall datasets. Main objective in this study was to calibrate and evaluate the open source data based model for runoff simulations due to individual rainfall events so that the model may predict any peak flows or flood situation in real time before or during a rainfall event.

There was found consistency between simulated and observed flows with percent difference in volume to be -6.17% to 5.47% and percent difference in peak flows to be in the range of -6.96% to 7.28%. Values of Nash-Sutcliffe Efficiency were found ranging from 0.299 to 0.909 with average value of 0.586 for all events.

It can be concluded that the model was found well capable of capturing the hydrologic response of the catchment in result of a rainfall event. Moreover, such a distributed hydrologic model, developed and calibrated for the whole catchment, is very helpful in determining the individual contributions of any un-gauged sub-basin. Based on the real time or forecasted rainfall data, such modeling approach can be helpful in providing alerts of peak flows or floods in real time for the whole catchment as well as for any sub-basin.

Results regarding optimized parameters revealed that a lead time of about 30–36 hours is available for the catchment to predict peak flows at the outlet for a rainfall event occurring in major rainfall-runoff generating part of the catchment. Thus, use of real time rainfall data, available about 6-8 hours after its acquisition, may help providing alerts using such modeling approach with a lead time of about 24-28 hours. However, an exceptionally intense rainfall event in the downstream sub-basins like W15 or W16 may cause a flash flood situation with a lead time of only 10-12 hours. In such cases, the integration of forecasted rainfall data with such modeling approach may be helpful in providing timely alerts of peak flows or floods.

Chapter 4

Reference Water Bodies and Flood Hazard Delineation using MODIS

1. Overview of the Chapter

Activities related to floods detection, flooded areas identification and resulting emergency management may employ different methodologies depending upon the topography of the area, data availability and its accuracy, as well as the ease and scope of their use in an area. Hydrologic modeling has been and still is an important traditional approach to assess the hydrologic response in terms of flows of a river catchment, combined with the hydraulic modeling approaches to route the flow through a river and identify the normal flow as well as the flood wave patterns along the whole length of a river. However, a number of unknown parameters to be measured and the complexity involved in the hydrologic modeling, as well as the need for the investigation of each river catchment separately, create space for the alternate flood hazard detection and management techniques. An important such approach may be the use of daily remote sensing images along with statistical analysis for the identification of reference and seasonal water bodies and flooded areas.

Hydrologic modeling is particularly an effective tool for the upper river catchments, having mountainous topography, where low or medium resolution images cannot perform well to identify the narrow river beds and steep gradients. Development and evaluation of a hydrologic model in such areas might be the feasible approach, as described in the previous chapter. On the other side, analysis of the historical archive of the remotely sensed images for flood hazard mapping can be very beneficial in plain areas with wider river beds and large areal extents, due to their large coverage and simplicity to avoid complex hydrologic and hydraulic procedures.

An automated MODIS water bodies' classification tool has been developed at ITHACA, which is used with MODIS daily surface reflectance products to develop reference water bodies and the flooded areas. This chapter presents the implementation and testing of this approach for the plain areas of Pakistan. The chapter proceeds with literature review and problem statement, followed by the description of MODIS products and the detailed

methodology. Results regarding reference water and flooded areas extraction have been presented in the end along with their comparison and validation with the observed peak flows, as well as their application for determining associated critical rainfall depths.

2. Literature Review and Problem Statement

Disaster management and long-term planning activities related to floods can greatly benefit from the availability of information on reference water bodies, as well as on the real extent of past flood events and the monitoring of flood extent during ongoing events. Such information of reference and seasonal water bodies and flooded areas can be obtained by the historical analysis of an area using daily satellite images.

Identification of water bodies on a scene acquired by the optical sensors installed on satellite platforms is based on simple but effective histogram threshold techniques; these techniques exploit the behavior of water in the infrared bands where it has high absorption rates. Such methods based on optical sensors are simple to apply but several disadvantages are associated with them too. Shadows due to the local morphology or the presence of clouds are classified wrongly as water bodies, and threshold values cannot be defined uniquely but adapted to the conditions of a region and the moment of the acquisition (Disabato, 2010).

In addition to histogram thresholds, there are several other techniques to classify water and/ or other land covers, which are based on indices derived from the differential band ratios. Two most commonly used indices to identify and classify the flooded areas are Normalized Differential Water Index (NDWI) and Normalized Difference Vegetation Index (NDVI).

A unique definition of NDWI does not exist and it has been utilized by different scientists for different bands, probably due to its adaptation to the different characteristics of spectral sensors mounted on satellite platform for their use for such applications. The most commonly used definition of NDWI, described by Chowdary et al. (2008), McFeeters (1996), Chatterjee et al. (2005), Jain et al. (2006), Purba et al. (2006), and Hui et al. (2008), is based on reflectivity in the green and near-infrared bands:

$$NDWI = (\rho_{GREEN} - \rho_{NIR})/(\rho_{GREEN} + \rho_{NIR}) \qquad (4.1)$$

Where ρ_{GREEN} and ρ_{NIR} stand for the spectral reflectance measurements acquired in the green and near-infrared regions, respectively. This index reduces the commission errors during

classification due to vegetation and the bare soil classes. However, Zhuowei (2007), Hui et al. (2008) and Fengming et al. (2008) highlighted the low reliability of this index in urban areas, and proposed a Modified Normalized Difference Water Index (MNDWI) to minimize also the errors due to the presence of shadows:

$$MNDWI = (\rho_{GREEN} - \rho_{SWIR})/(\rho_{GREEN} + \rho_{SWIR}) \quad (4.2)$$

Where ρ_{GREEN} and ρ_{SWIR} stand for the spectral reflectance measurements acquired in the green and short-wavelength infrared regions, respectively.

Huggel (2002) proposed an NDWI definition based on reflectivity in the blue and near-infrared bands, especially for the identification of mountain lakes, as follows:

$$NDWI = (\rho_{NIR} - \rho_{BLUE})/(\rho_{NIR} + \rho_{BLUE}) \quad (4.3)$$

Where ρ_{BLUE} and ρ_{NIR} stand for the spectral reflectance measurements acquired in the blue and near-infrared regions, respectively.

Fadhil (2006) and Sakamoto et al. (2007) used red and short-wavelength infrared (SWIR) bands to address the residual influence of humid soils:

$$NDWI = (\rho_{RED} - \rho_{SWIR})/(\rho_{RED} + \rho_{SWIR}) + 1 \quad (4.4)$$

where ρ_{RED} and ρ_{SWIR} stand for the spectral reflectance measurements acquired in the red and short-wavelength infrared regions, respectively.

Gao (1996) and De Alwis et al. (2007) proposed the following NDWI definition for the identification of water saturated soils:

$$NDWI = (\rho_{NIR} - \rho_{SWIR})/(\rho_{NIR} + \rho_{SWIR}) \quad (4.5)$$

where ρ_{NIR} and ρ_{SWIR} stand for the spectral reflectance measurements acquired in the near-infrared and short-wavelength infrared regions, respectively.

Thus, there exists a vast diversity in NDWI definition, with the basic concept as the use of differential ratios for those bands, which provide increasing relative reflectivity differences of the water spectral signature.

Other most commonly used index, NDVI, is generally used for vegetation classification and analysis, but it is also useful for the detection of water bodies. It is defined as:

$$NDVI = (\rho_{NIR} - \rho_{RED})/(\rho_{NIR} + \rho_{RED}) \quad (4.6)$$

Where ρ_{RED} and ρ_{NIR} stand for the spectral reflectance measurements acquired in the red and near-infrared regions, respectively.

In most cases, healthy vegetation may have spectral reflectance quite similar to that of water, and histogram thresholds may not be helpful to differentiate between water and vegetation. In such cases, NDVI provides great help to classify water without wrongly classifying vegetation as water. However, NDVI presents low values not only in correspondence of the flooded areas in IR band, but also in correspondence of bare soils, which have similar characteristics both in the visible and IR bands. Therefore, in order to correctly extract water bodies, NDVI values are often combined with IR histogram thresholds, which allow masking both vegetation and bare sole areas during water bodies' classification.

Moderate-resolution Imaging Spectroradiometer (MODIS) data products have been utilized worldwide for different regional level studies. Thenkabail et al. (2005) analyzed near-continuous time-series (8-day), 500 m resolution 7-band MODIS land data for 2001–2002 to develop land use/land cover (LULC) and irrigated area maps in the Ganges and Indus river basins. Disabato (2010) developed automated water bodies' classification tool and analyzed 10-years historical archive of MODIS daily surface reflectance products for developing reference water bodies, as well as the MODIS rapid response system datasets for real time applications. The classification was performed by extraction of water bodies using suitable indices and thresholds, and compositing into decades for reducing the effects of cloud cover. The methodology was tested and applied for the area of Bangladesh to delineate seasonal water and flooded areas. Forsythe et al. (2012) analyzed the interannual variability in climate using MODIS snow-covered area (SCA) and land surface temperature (LST) products and assessed its impacts on runoff sensitivity in the Upper Indus Basin (UIB). Ajmar et al. (2012) analyzed the TRMM precipitation anomalies for identifying flood events and integrated them with remotely sensed MODIS data for the detection of ground effects of those flood events.

In this phase of study, automated water bodies classification algorithms developed by Disabato (2010) have been employed with NDVI and histogram threshold techniques to investigate the effectiveness of MODIS daily surface reflectance products for floods analysis in Pakistan. Results regarding development of reference water bodies and flooded areas delineation may be helpful for any planning and emergency management activities in the

future. Moreover, comparison of flooded extents detected by this approach with the associated rainfalls may help deciding critical rainfall amounts to provide extreme rainfall alerts.

3. Description of MODIS Data System

The MODIS instrument is a high signal-to-noise instrument designed to satisfy a diverse set of oceanographic, terrestrial, and atmospheric science observational needs. It was completed in 1995 and its two spaceflight units, the Proto Flight Model (PFM) onboard Terra Satellite, and the Flight Model 1 (FM1) onboard Aqua Satellite, were launched on December 18, 1999 and May 4, 2002, respectively.

Terra and Aqua satellites are in a near polar, sun-synchronous orbit at an altitude of 705 km. The Earth scene is perpendicular to the ground track and subtends a scan angle of 110 degrees. The orbits of two satellites are timed so that the Terra satellite passes from north to south across the equator in the morning, while Aqua passes south to north over the equator in the afternoon. Both satellites cover the complete Earth every 16 days and different other instruments are also installed on each satellite in addition to MODIS instrument.

Terra simultaneously studies clouds, water vapor, aerosol particles, trace gases, terrestrial and oceanic properties, the interaction between them and their effect on atmospheric radiation and climate. Aqua data include information on water vapor and clouds in the atmosphere, precipitation from the atmosphere, soil wetness on the land, glacial ice on the land, sea ice in the oceans, snow cover on both land and sea ice, and surface waters throughout the world oceans, bays, and lakes.

4.3.1. MODIS Sensor and Bands

MODIS is a passive imaging spectro-radiometer arranged in 36 spectral bands, which cover the visible and infrared spectrum ranging from 0.412 m to 14.235 m. The acquisition of the narrow-band radiance observations over 36 spectral regions is realized by three internal calibrators and a scan mirror which views the Earth.

All bands are acquired and digitized at 12 bits. Spatial resolution depends on the considered band acquired: two bands (bands 1-2) are imaged at a nominal resolution of 250 m at nadir, five (bands 3-7) at 500 m and the remaining (bands 8-36) at 1000 m (Table 4.1). In case of 1000 m bands, 10 detectors are arranged in an along track linear array, while there are 20 and

40 detectors arranged in an along track linear array for 500 m bands (bands 3-7) and 250 m bands (bands 1 & 2), respectively.

Table 4.1: MODIS Bands and their Characteristics with Possible Uses.

Band	Band Width (nm)	Radiometric Resolution	Geometric Resolution (m)	Primary Use
1	620 – 670	12 bits	250	Land/ Cloud/ Aerosols
2	841 – 876	12 bits	250	Boundaries
3	459 – 479	12 bits	500	Land/ Cloud/ Aerosols
4	545 – 565	12 bits	500	Properties
5	1230 – 1250	12 bits	500	
6	1628 – 1652	12 bits	500	
7	2105 – 2155	12 bits	500	
8	405 – 420	12 bits	1000	Ocean Color/ Phytoplankton/
9	438 – 448	12 bits	1000	Biogeochemistry
10	483 – 493	12 bits	1000	
11	526 – 536	12 bits	1000	
12	546 – 556	12 bits	1000	
13	662 – 672	12 bits	1000	
14	673 – 683	12 bits	1000	
15	743 – 753	12 bits	1000	
16	862 – 877	12 bits	1000	
17	890 – 920	12 bits	1000	Atmospheric Water Vapor
18	931 – 941	12 bits	1000	
19	915 – 965	12 bits	1000	
20	3660 – 3840	12 bits	1000	Surface/ Cloud Temperature
21	3929 – 3989	12 bits	1000	
22	3929 – 3989	12 bits	1000	
23	4020 – 4080	12 bits	1000	
24	4433 – 4498	12 bits	1000	Atmospheric Temperature
25	4482 – 4549	12 bits	1000	
26	1360 – 1390	12 bits	1000	Cirrus Clouds
27	6535 – 6895	12 bits	1000	Water Vapor
28	7175 – 7475	12 bits	1000	
29	8400 – 8700	12 bits	1000	Cloud Properties
30	9580 – 9880	12 bits	1000	Ozone
31	10780 – 11280	12 bits	1000	Surface/ Cloud Temperature
32	11770 – 12270	12 bits	1000	
33	13185 – 13485	12 bits	1000	Cloud Top Altitude
34	13485 – 13785	12 bits	1000	
35	13785 – 14085	12 bits	1000	
36	14085 – 14385	12 bits	1000	

4.3.2. MODIS Products and their Levels and Formats

MODIS data products can be divided into two categories: primary and the derived ones. The data directly coming from the acquisition are known as primary products. Primary products are made of the raw images of radiance/reflectance and geolocation files, which contain geometric references every kilometer. Products generated after processing on the primary products are known as derived products, which contain information at different spatial and temporal resolutions designed to meet the needs of the research community. Derived products are further divided into three classes as follows:

- Atmospheric data products: data concerned with the atmospheric events like cloudiness, precipitation and aerosols;
- Land data products: data regarding phenomena like energy balance of earth, coverage of the soil, land thermal properties, etc.; and
- Ocean data products: data containing information about temperature, ocean primary productivity, presence of phytoplankton, etc.

MODIS data products are provided in a variety of levels. Primary data are stored in the first three levels, while derived products are provided in the next ones.

Levels of storage of the primary data are:

- Level 0: Reconstructed unprocessed instrument data at full resolution. Level 0 data are straight from the instrument consisting of raw radiance values. This form is not friendly to most image processing systems and requires custom code to transform it into something more end user friendly. This product is not made available to the general public.
- Level 1A: Reconstructed unprocessed instrument data at full resolution; time referenced, and annotated with ancillary information, including radiometric and geometric calibration coefficients and geo-referencing parameters computed and appended, but not applied to the Level 0 data. The Level 1A code organizes a 2-hour Level 0 file into a set of scenes, each containing approximately 5 minutes of MODIS data.
- Level 1B: Level 1A data that have been processed to sensor units. The Level 1B software, starting from Level 1A data, implements calibration algorithms to correct raw Earth view-sector data for all known instrumental effects and to transform the

corrected data into calibrated products, organizes the calibrated data into a scene, and performs quality assurance tests on the raw and calibrated data.

The secondary or derived data products are stored in the following three levels:

- Level 2: Derived geographic variables at the same resolution and location as the Level 1 source data. These products are corrected for atmospheric contamination.

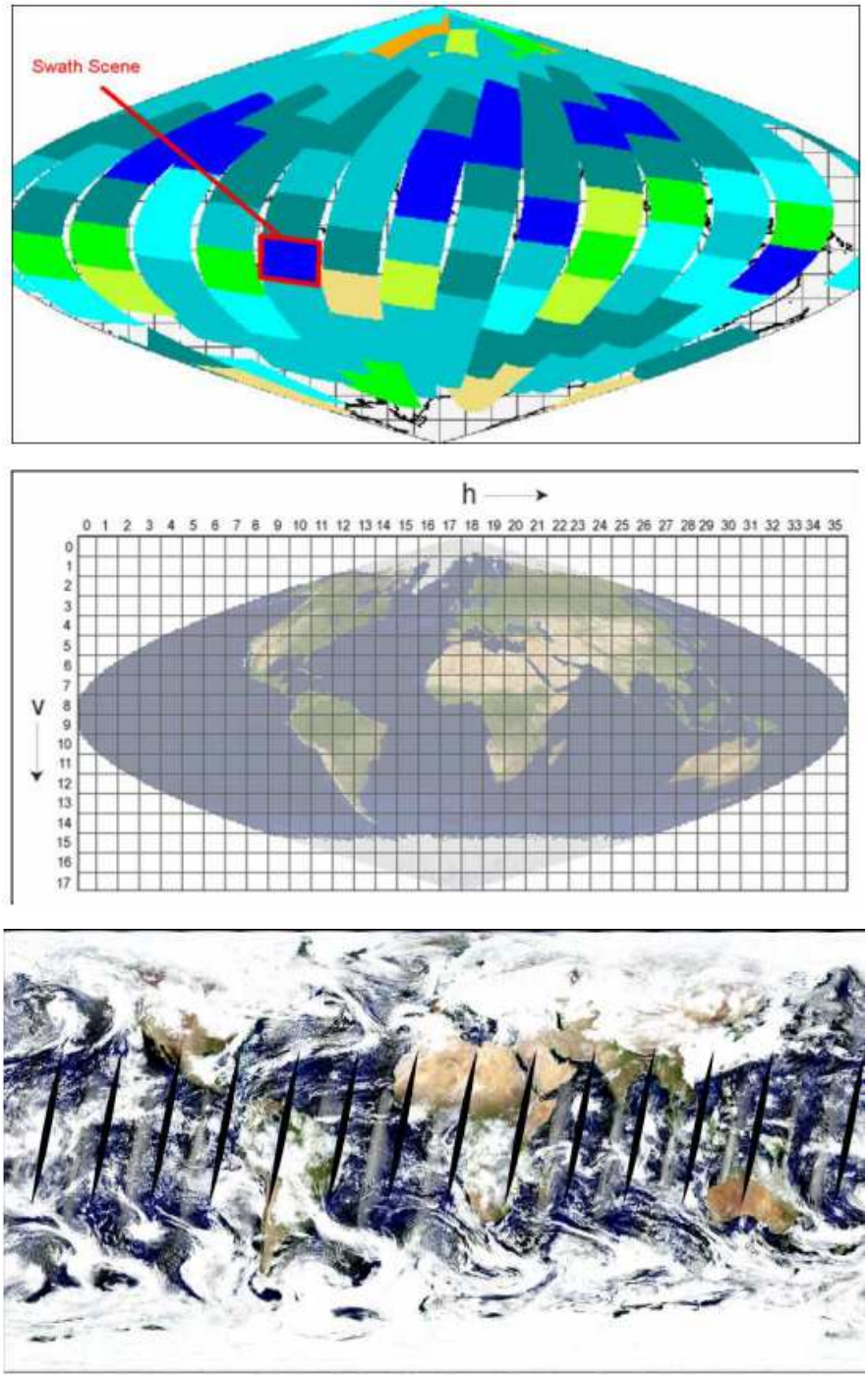

Figure 4.1: Formats of MODIS products; (a) Swath scenes, (b) MODIS Sinusoidal Grid (MSG), and (c) MODIS Climatic Grid (MCG).

- Level 3: Variables mapped on uniform space-time grid scales, usually with some completeness and consistency.
- Level 4: Model output or results from analyses of lower level data (e.g. variables derived from multiple measurements).

MODIS derived products can be stored in two different data formats viz. swath and grid. Level 2 data can be available in both the formats, while level 3 and level 4 data are available only in grid format.

The Swath format is not a projection; rather it is the view as the sensor "sees" the Earth (Figure 4.1a). One swath scene is the result of a 5-minute scan. Since one scan of the MODIS mirror takes 1.4771 seconds, there are typically 203 full scans within a 5-minute product file and occasionally 204 full scans. The use of an occasional 204-scan file keeps the number of 5-minute granules or swath scenes per day at 288, assuming no data gaps. Although this product is available to the end user, special tools are still required to manipulate these data into a map projection and to correct it for the MODIS panoramic distortion (Disabato, 2010, pp. 28-29).

The Grid format used to store the MODIS secondary products may be of two types, viz. Sinusoidal and the Climate Modeling Grid (CMG).The sinusoidal projection is a pseudo-cylindrical equal area projection, with no distortion on the central meridian. Products mapped into the sinusoidal projection are then gridded into 10-degree units called tiles (Figure 4.1b). These files are geometrically corrected and are easily read by image processing software and manipulated by an end user. Products in the Climate Modeling Grid (CMG) provide information on the whole earth surface with a spatial resolution of 0.05 degrees, which corresponds to about 5.6 km (Figure 4.1c).

4.3.3. MODIS Products Utilized in Current Study

In order to perform analysis at a regional scale, MODIS daily surface reflectance products (MOD09GQ and MYD09GQ) were utilized due to their high spatial resolution of 250 m. These products provide a daily estimate of the surface spectral reflectance for two bands; the red one (620-670 nm) and the IR one (841-876 nm). The products are provided in the Sinusoidal Grid format (Figure 4.1b), and different regions of the earth are represented by different squares of the grid (tiles) of 10°x10° dimensions. The tile coordinate system starts at (0, 0) (horizontal tile number, vertical tile number) in the upper left corner and proceeds right (horizontal) and downward (vertical), with the tile number (35, 17) in the bottom right corner.

For the current study, four tiles covering the whole area of Pakistan were employed, namely h23v05, h23v06, h24v05 and h24v06. Daily images for these four tiles were downloaded and used for both Aqua (MOD09GQ) and Terra (MYD09GQ) products since their launch up to September 30, 2014, which allowed developing and analyzing a historical archive of 15 years.

4. Methodology and Implementation of Procedures

The development and analysis of historical archive of reference water bodies was achieved adopting following methodology:

- NDVI index calculation using MODIS spectral bands 2 and 1 of products MOD09GQ and MYD09GQ, which have only two bands of interest and a spatial resolution of 250 m;
- Masking of bare soil areas, clouds, snow, etc. and identification of water bodies through histogram thresholds set for the visible and infrared bands;
- Masking of vegetation areas by setting NDVI thresholds;
- Time compositing of daily classified images for 10 day periods to remove negative effects of clouds and their shadows.

Step by step implementation of the procedures to follow the formulated methodology has been described in detail in the following sections.

4.4.1. Downloading of Data

The data regarding selected MODIS tiles were obtained from NASA's Land Processes Distributed Active Archive Center (LP DAAC), which was established as part of NASA's Earth Observing System's Data and Information System (EOSDIS) initiative to process, archive, and distribute land-related data collected by EOS sensors.

The first step was to select the suitable tiles covering the whole area of Pakistan. As described earlier, four tiles namely h23v05, h3v06, h24v05 and h24v06 were selected for downloading from February 2000 to September 30, 2014. For this purpose, the data was requested through http://reverb.echo.nasa.gov/reverb/ and downloaded using Mozilla DownThemAll extension to automatically download the whole archive. After downloading, an automatic check was performed using an IDL routine to find out the missing files, so that they can be downloaded manually to complete the archive.

4.4.2. Data Pre-processing and Classification

In this phase the images downloaded were projected to the required reference system and resized on the area of interest. As there were more than one images to cover the whole area, a phase of data mosaicking was also involved before re-projection and resizing operations.

These pre-processing operations can be performed in MODIS Reprojection Tool (MRT) developed by LPDAAC. The MRT is a software designed to help individuals work with MODIS data by reprojecting MODIS images (Level-2G, Level-3, and Level-4 land data products) into more standard map projections. Main part of the MODIS Reprojection Tool is the resampler and MRT-mosaic executable program that may be run either from the command-line or from the MRT Graphical User Interface. The command line option was used for the elaboration of the data of the archive, as it allows background processing of large MODIS data files. Therefore, the MRT Tool was called in a batch mode by an IDL routine to perform the three operations of mosaicking, reprojection, and resizing on daily basis for both MOD09GQ and MYD09GQ products. Figure 4.2 shows a daily satellite image after the mosaicking of four tiles, their reprojection and resizing to the study area.

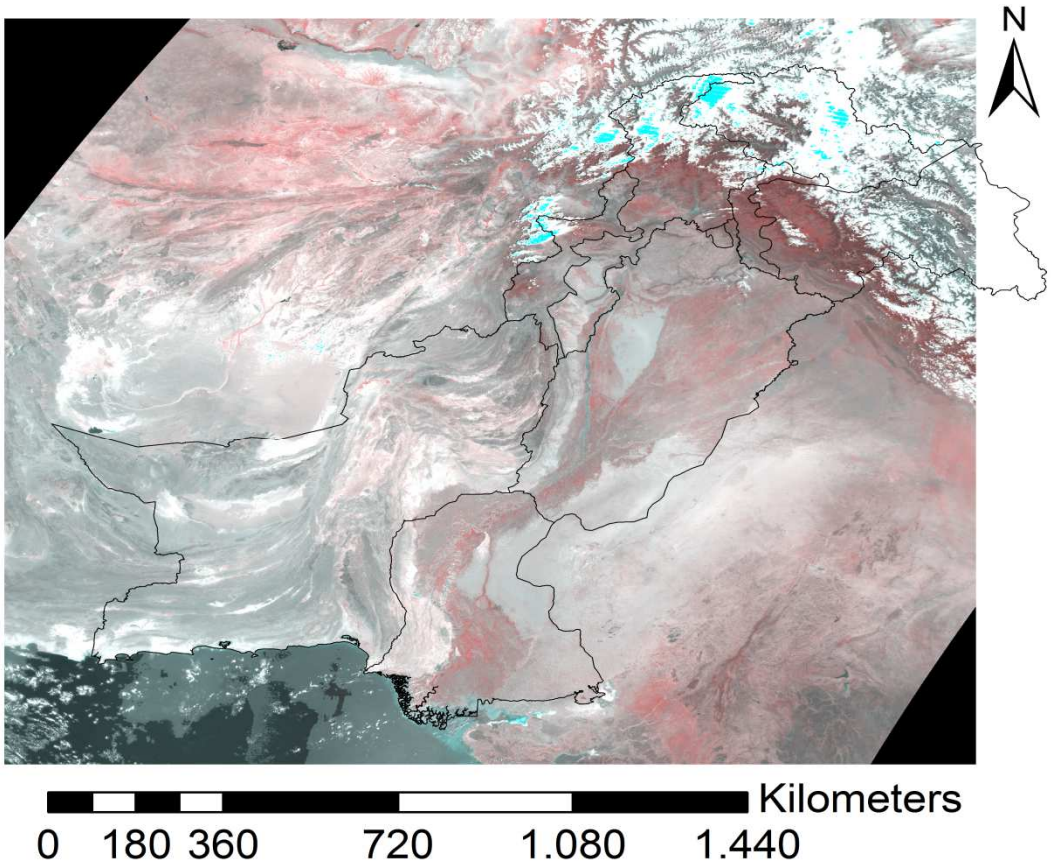

Figure 4.2: MODIS daily image after pre-processing operations.

After the resize on the area of interest, the two daily images (one coming from Terra satellite and the other from Aqua) were classified using the NDVI and IR thresholds. The thresholds were set after preliminary analysis on spectral signatures of different land covers for about 20 randomly selected images. The thresholds set based on this preliminary analysis were used for classification of water bodies and their testing. However, initial testing revealed a lot of noise in some parts and the process of classification was refined by lowering the limits of IR thresholds for water. The results regarding this spectral analysis and the preliminary and finalized thresholds for classification are presented in Table 4.2. The red highlighted values in the Table show the importance of NDVI for differentiating between vegetation and water, which have similar characteristics in IR band and would have been mixed up in the absence of NDVI. In order to provide information on the cloud coverage, the class cloud was also included in the classification of the daily images. Thus, a first archive of couples of daily classified images (one for Terra and one for Aqua) containing information on water bodies and cloud extent was built for 15 years of MODIS data. Figure 4.3 shows the results of classification for one of the classified images of the historical archive of 15 years.

Table 4.2: Surface reflectance and selection of thresholds for different objects.

Description		**Band 1**	**Band 2**	**NDVI**
Black color (water) upper limit	Mean	19.1	19.76	8.93
	St. Dev.	2.74	4.47	7.43
Brownish (bare soils/rocks) lower limit	Mean	25.75	31.22	
	St. Dev.	4.60	3.02	
Reddish (vegetation) lower limit	Mean	8.44	34.69	51.2875
	St. Dev.	3.29	6.21	12.568
Greyish white/white (clouds) lower limit	Mean	51.82	55.75	
	St. Dev.	9.43	9.07	
Initial Thresholds setting to classify water, dry land and clouds:				
Water		< 20	< 25	< 17
Clouds		> 41	> 46	
Final Thresholds set to classify water, dry land and clouds:				
Water		**< 18**	**< 21**	**< 17**
Clouds		**> 34**	**> 41**	

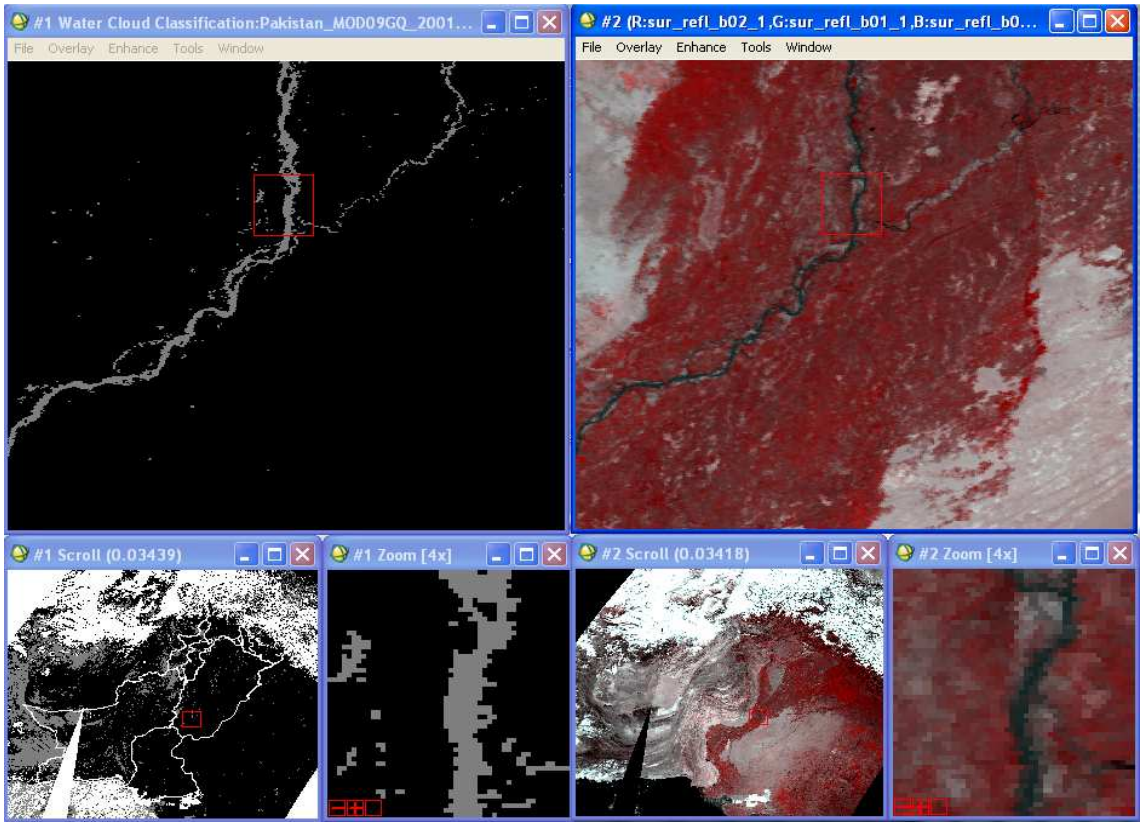

Figure 4.3: Water classification results for one of the daily classified images.

4.4.3. Time Compositing

Time compositing is considered necessary to extract water bodies correctly, which allows filling the daily missing information and removing clouds effects. Apart from cloud coverage, presence of cloud shadows also creates noise in the results, as dark cloud shadows have spectral characteristics quite similar to those of water bodies (Luo et al. 2008). Therefore, the chosen algorithm (Disabato, 2010) adopts an approach that is first aimed at the classification of the available daily images and later composites them into 10-day periods. The steps performed by this compositing algorithm are as follows:

- Automated detection of water bodies from daily satellite imagery;
- Combining information on water bodies coming from the 2 daily images of MODIS Terra and Aqua satellites;
- Compositing of ten daily analyses results into one decadal file, with application of a threshold regarding number of times a pixel should be classified as water in order to assign it to the class of water for that decade;
- Extraction of water bodies using that time compositing threshold.

In this way, water bodies are first detected on every available image, and then in the phase of combination of Terra and Aqua data, each pixel of the image which results to be covered by water in at least one of the two daily available images is considered as water body. The time compositing is performed by counting the number of days a pixel results to be covered by water in the compositing period of ten days, as explained in Figure 4.4. For setting threshold regarding number of days a pixel should be covered by water to assign it as water in the compositing period, it is assumed that the probability that a pixel will be covered by cloud shadows for more than that threshold-percentage of the compositing period (e.g. for more than 1 day over a 10 days compositing period, as used by Disabato (2010)) is extremely low. The same threshold was applied here in this study for Pakistan, and all the pixels that resulted to be covered by water for more than this threshold period ($\geq$ 2 over 10) were considered as areas under water.

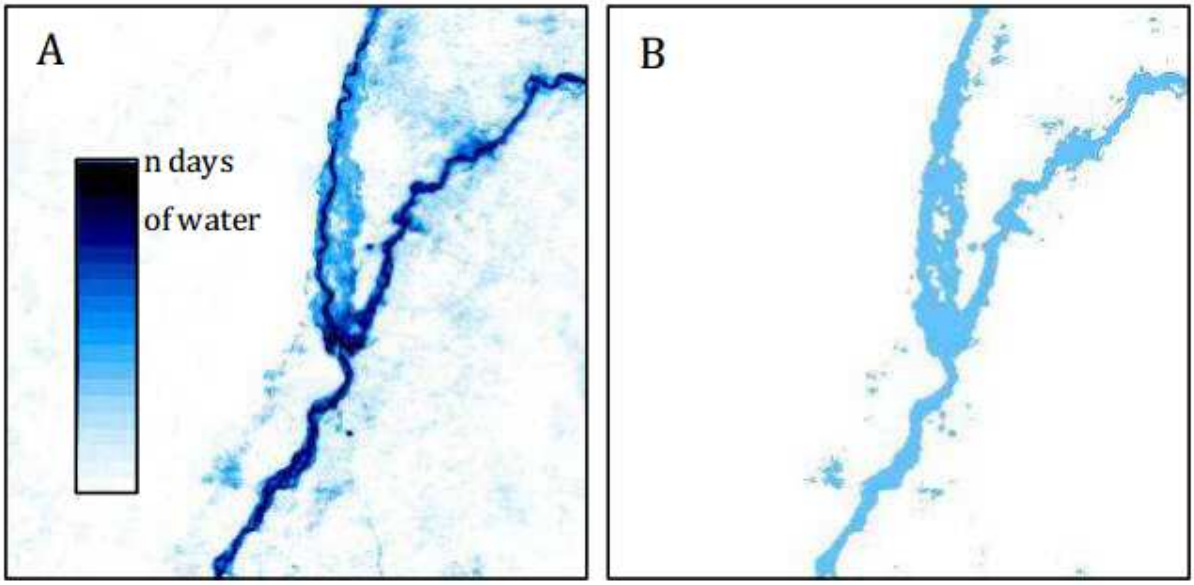

Figure 4.4: (A) Time compositing, and (B) result of classification using temporal threshold approach (Disabato, 2010).

4.4.4. Masking of Areas

It is worth mentioning that the MODIS classification approach did not show encouraging results for high mountainous northern areas and Baluchistan Plateau. This is because the 250 m spatial resolution was not found enough to capture and classify the narrow streams and the surrounding dry areas with steep gradients. Moreover, rocky mountains (in case of Baluchistan) and mountains' shadows resulted in poor classification of water bodies in preliminary analysis phase generating lot of noise. Therefore, the northern areas and

Baluchistan part were masked out in the final analysis, suggesting that the higher resolution radar data like ESA's Sentinel Missions might be helpful to perform similar analysis with good results for such areas.

4.4.5. Use of Automated Procedures and Processing Times Considerations

To perform the above mentioned pre-processing, classification and time-compositing steps automatically, the automated water bodies' classification tool developed at ITHACA by designing a routine in IDL was employed. The outputs of this procedure were three types of temporal composites containing information on how many times in a compositing period, a pixel resulted to be covered by (i) water, (ii) clouds, or (iii) there was no information on a pixel (to check the number of missing information). Thus, in addition to extracting water and no-water areas, if a pixel resulted for more than 80% of the compositing period to be covered by clouds or no data were available on this point, it was marked as covered by clouds or with no available information, respectively.

The developed procedures for the classification of water bodies allowed a good degree of automation to deal with large amount of data and processing operations. For the development of historical archive a dataset corresponding to 15 years of acquisition of MODIS data was processed. As the area of Pakistan was covered by four tiles of the MODIS sinusoidal grid, the number of processed files was as follows:

- About 21000 tiles (images) of the product MOD09GQ (MODIS Terra product from 2000 to 2014);
- About 17500 tiles (images) of the product MYD09GQ (MODIS Aqua product from 2002 to 2009);

Total space occupied by the geo-referenced base data as well as the classified files was about 2.50 Tb. The download and processing of the whole archive took a time of around three months, with downloading and geo-referencing phases being the most critical, while the classification and temporal composite production requiring significantly less processing times. The developed historical archive can be used for different applications viz. real time flooded areas detection by comparison with reference water, and use of seasonal and flooded areas maps for planning disaster management activities.

5. Results and Discussion

Extraction of water bodies and the development of historical archive of reference water areas may be useful for performing different types of beneficial analyses. In order to obtain information on flooded areas, water bodies' extensions during a flood event are generally compared to a layer of reference water. Since the available global hydrographic references are generally static layers, which do not take into account the variability of water bodies during the year, the developed archive by the methodology adopted in this study possesses the advantage to detect the variability of water bodies during the year and consequently to create a reference water information for different periods of the year. The implementation of water bodies' extraction procedures resulted in developing archive of 15 years of MODIS classified data to provide information on different aspects, such as:

- Daily classifications (three classes: water, clouds and soil) both of Terra and Aqua satellites.
- 36 decadal (10-days) synthesis files for every year containing information on the number of times a pixel results to be covered by water, clouds or no data in the 10 days taken into consideration.
- 36 decadal classifications indicating if a pixel is covered by water, clouds or no data.

The daily or decadal classifications may be used to compare flood inundation extents with the observed peak flows to see the on ground effects of a peak flow or flood situation. Such comparative analysis has been made for few points in the study area (Pakistan), which has been presented in the end. In addition, these outputs have been analyzed to extract statistical information derived from the historical archive regarding seasonal and flooded areas analysis.

4.5.1. Reference and Seasonal Water and Flooded Areas Analysis on Annual Basis

Starting from February 2000 up to September 2014, there were 525 total decades. Figure 4.5 presents the number of times in which a pixel results to be classified as water in 525 decadal periods. The histogram analysis of Figure 4.5, presented in Figure 4.6, allows detecting following three classes of water cover:

- Permanent or Reference water, defined as the areas classified as water for more than 75% of 525 decadal periods in 15 years.

- Seasonal water, defined as the areas classified as water for more than 25% and less than 75% of the 525 decadal periods in 15 years. This water has a limited, but almost regular occurrence during the year.
- Historical flooded areas, defined as the areas classified as water for more than 3% and less than 25% of the 525 decadal periods in 15 years (3% was considered the residual error of the procedure). This is the water due to flood events.

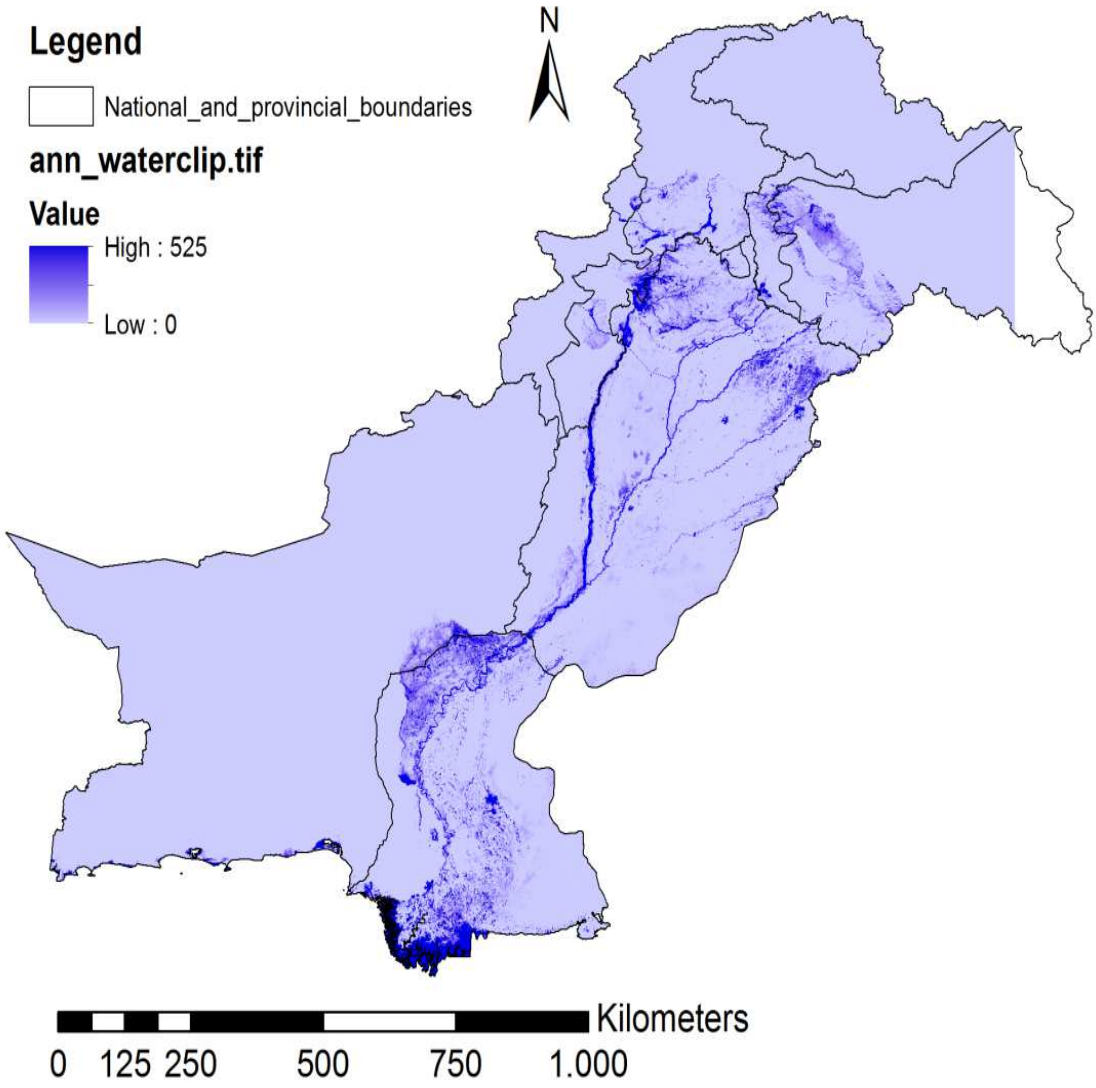

Figure 4.5: Number of times a pixel results to be classified as water over 525 decades in 15 years reference period.

The slicing of histogram analysis into three classes has been presented in Figure 4.6. It can be seen that at 75%, there is a little rise in the frequency values, which indicates the lower limit of the reference water. Similarly, there is a sudden rise in frequency below 25% indicating the

flooded areas. Results of this histogram slicing in the form of three classes have been shown in Figure 4.7.

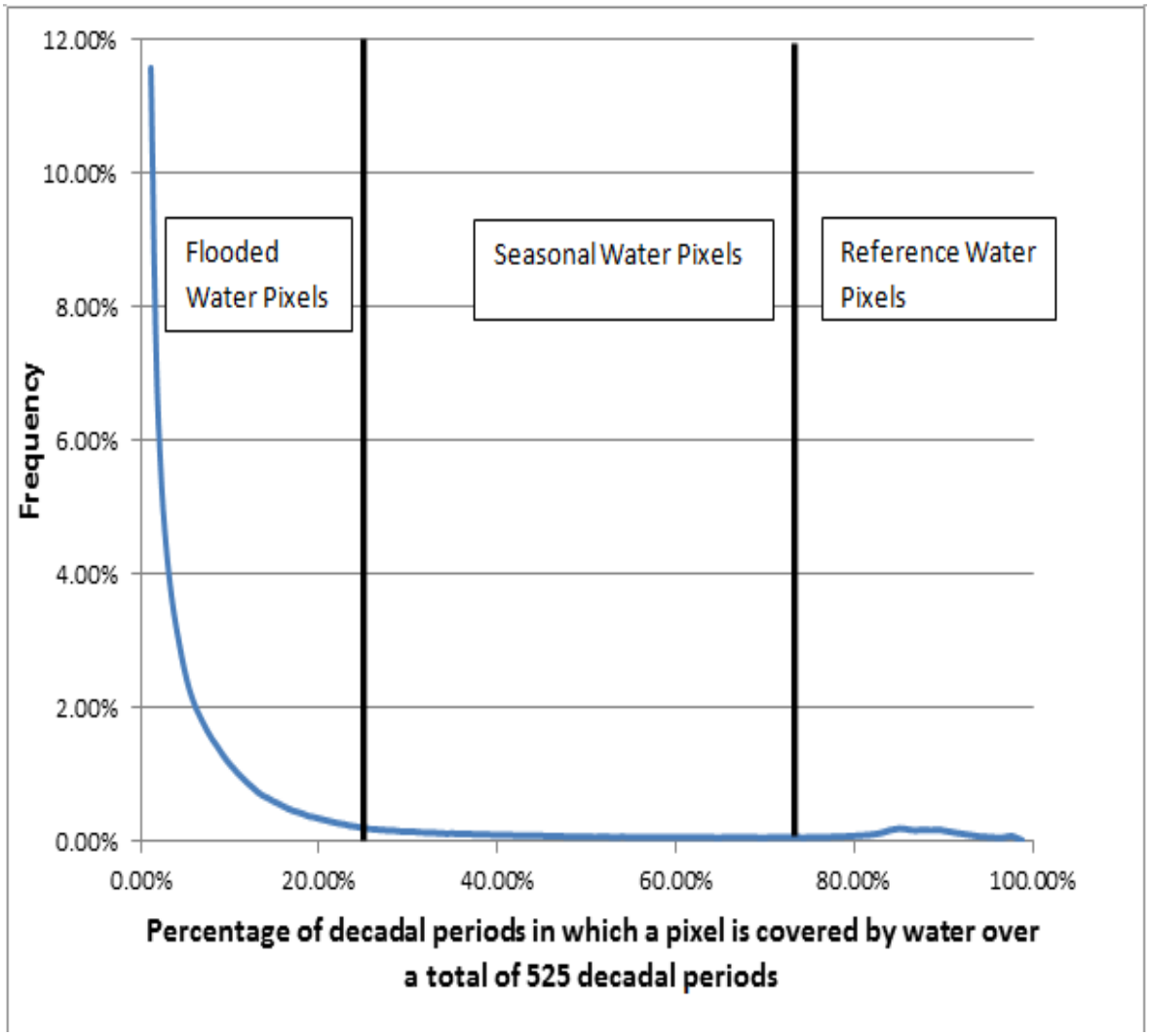

Figure 4.6: Frequency histogram of water bodies for whole year.

4.5.2. Seasonal Reference Water and Flooded Areas Analysis for Monsoon Season

It was observed in the seasonal and reference water analysis on annual basis that there was noise in delineating the flooded areas, which was basically due to biases in the winter months. Areas found highly prone to such noise were the Jhelum valley in Kashmir and some areas in the southern Sind province (as pointed out in Figure 4.7). Possible reasons of noise in the winter months for Jhelum valley may be the high soil moisture and snowfall in these months, while the noise in southern Sind province may possibly be due to absence of vegetation but presence of high moisture in the bare soils of these areas in these months. Results regarding

classification in summer and rainy months were found quite accurate. Therefore, it was decided to perform the same reference water and flooded areas extraction approach only for summer and monsoon season months (April to September), while excluding the winter months.

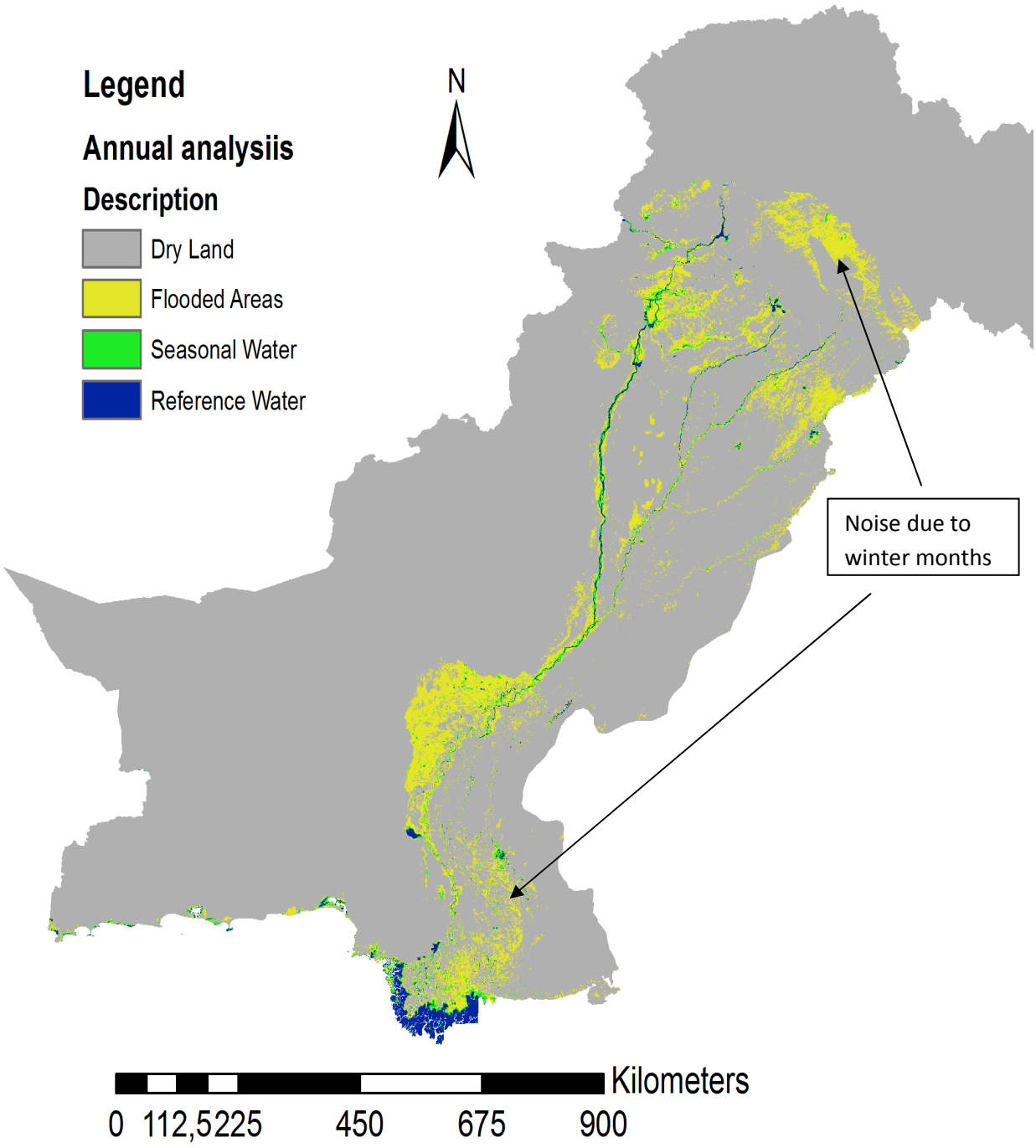

Figure 4.7: Results of histogram slicing in Figure 4.6; reference water, seasonal water, and flooded areas for whole year analysis.

For the monsoon seasonal analysis, total number of decades was 270 for the 15 years archive, and the histogram analysis and slicing approach resulted in following two classes of water:

- Reference water, defined as the areas that have been classified as water for more than 45% of the 270 decadal periods in 15 years. This category represents the areas which are regularly covered by water in almost every monsoon season.
- Historical flooded areas, defined as the areas that have been classified as water for more than 3% and less than 45% of 270 decadal periods in 15 years (3% was considered the residual error of the procedure). This represents the water due to flood events.

The slicing of histogram analysis into two classes has been presented in Figure 4.8, indicating a sudden rise in frequency below 45%. Results of this seasonal histogram analysis in the form of two classes have been shown in Figures 4.9 and 4.10.

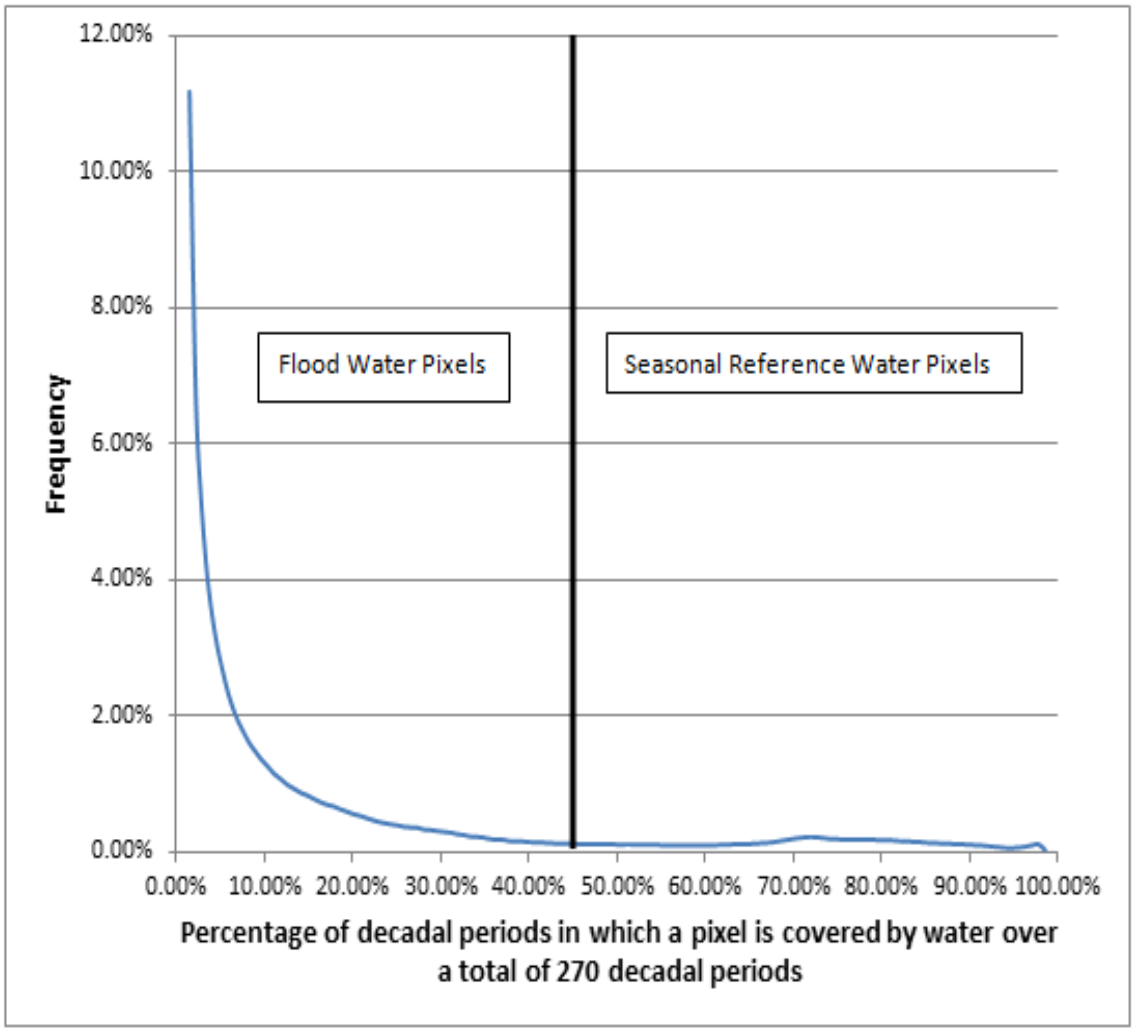

Figure 4.8: Frequency histogram of water bodies for monsoon seasonal analysis.

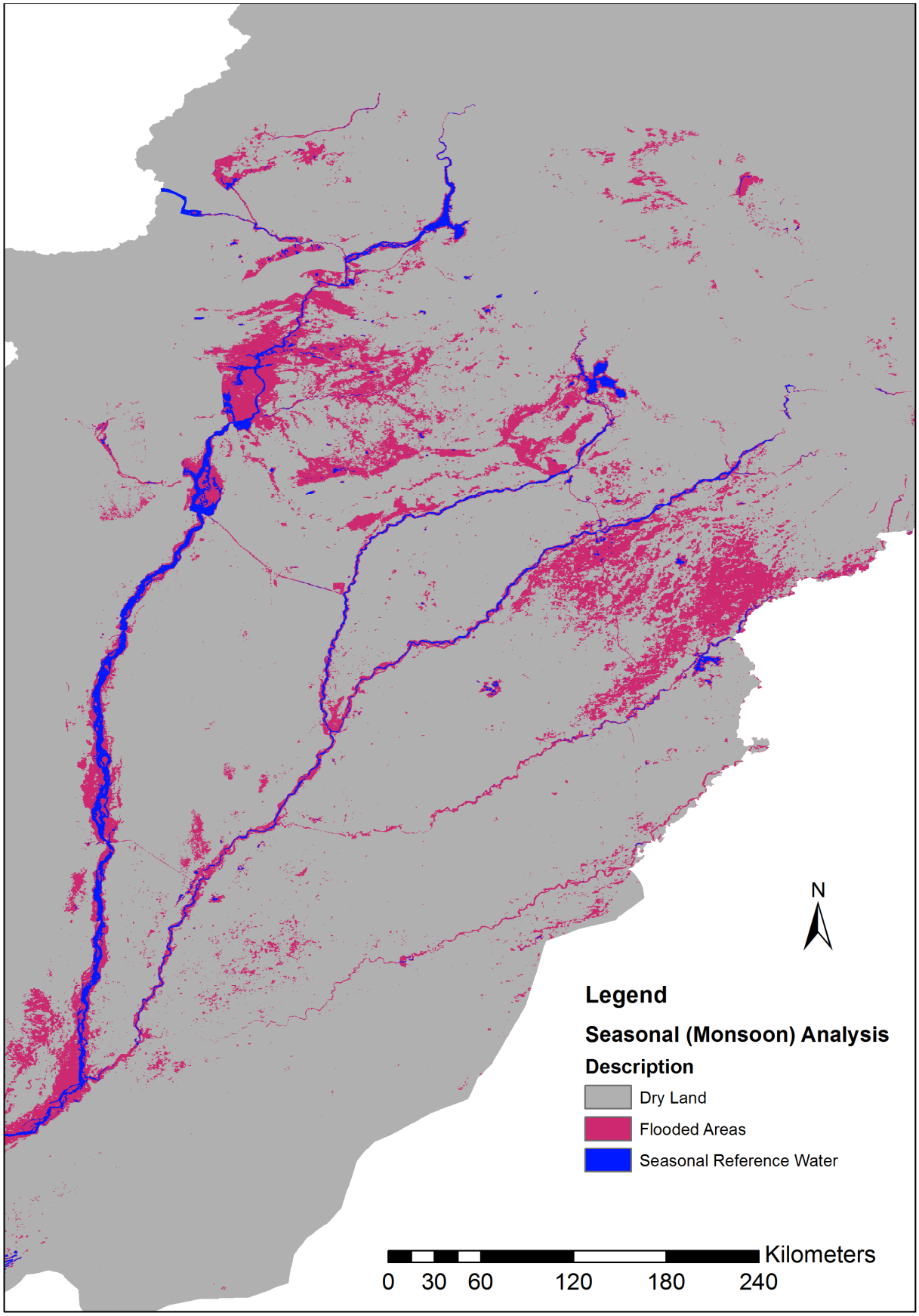

Figure 4.9: Results of histogram slicing analysis in Figure 4.8; reference water and flooded areas for the upper areas and Punjab province.

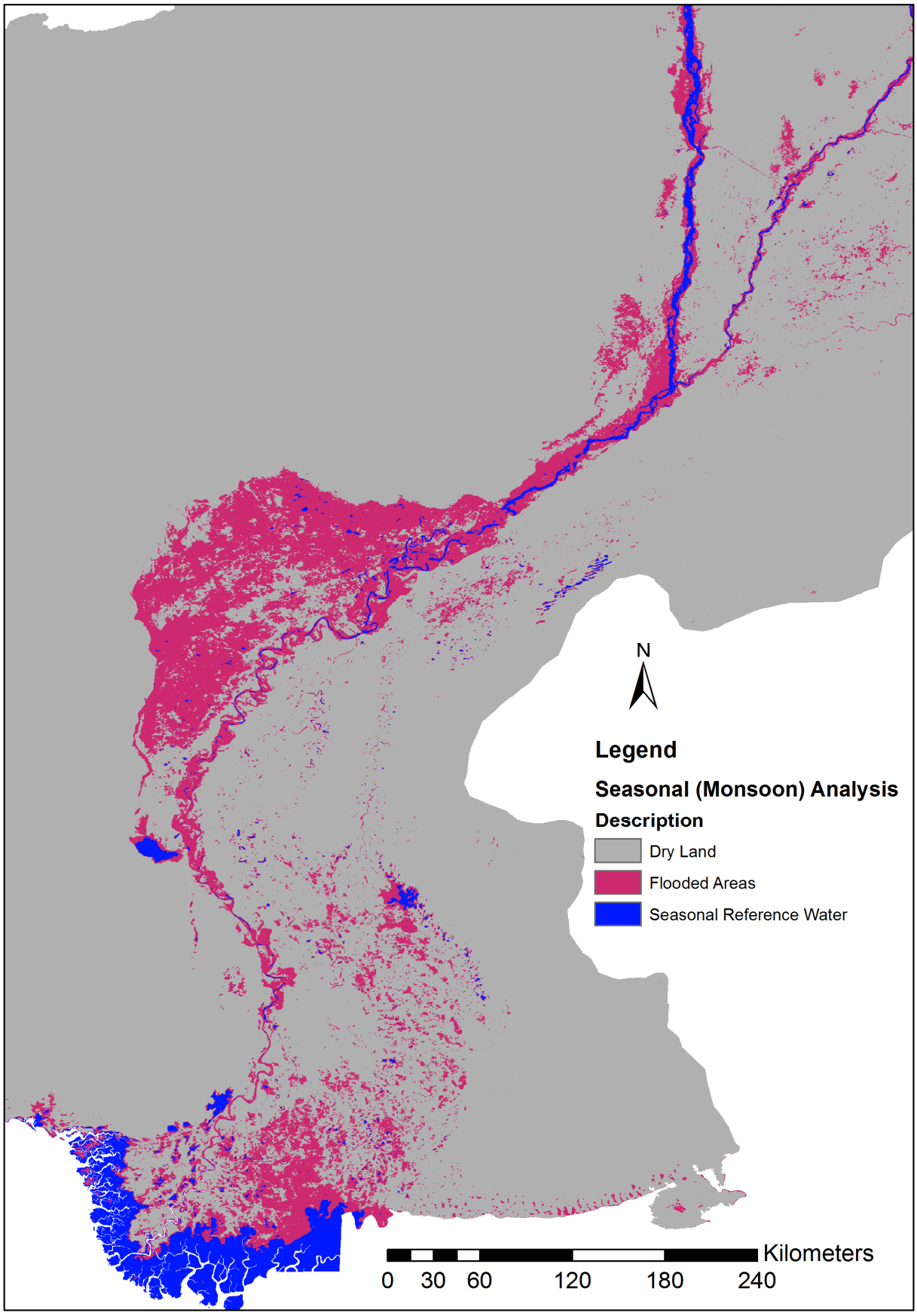

Figure 4.10: Results of histogram slicing analysis in Figure 4.8; reference water and flooded areas for the lower Punjab and Sind provinces.

From Figure 4.9, it can be seen that a considerable reduction in noise in Jhelum valley due to winter months was achieved, whereas Figure 4.10 also shows a significant reduction in noise for southern Sind province.

4.5.3. Areas under Water on Decadal and Monthly Basis

In addition to reference water and flooded areas analysis on annual and seasonal basis, information about areas under water on decadal and monthly basis may provide further insight into temporal variation of reference water and flooded areas. Figure 4.11 presents four sample decades out of 36 total decades to just have an overview of variations in the areas under water, whereas Figure 4.12 presents the analysis on monthly basis.

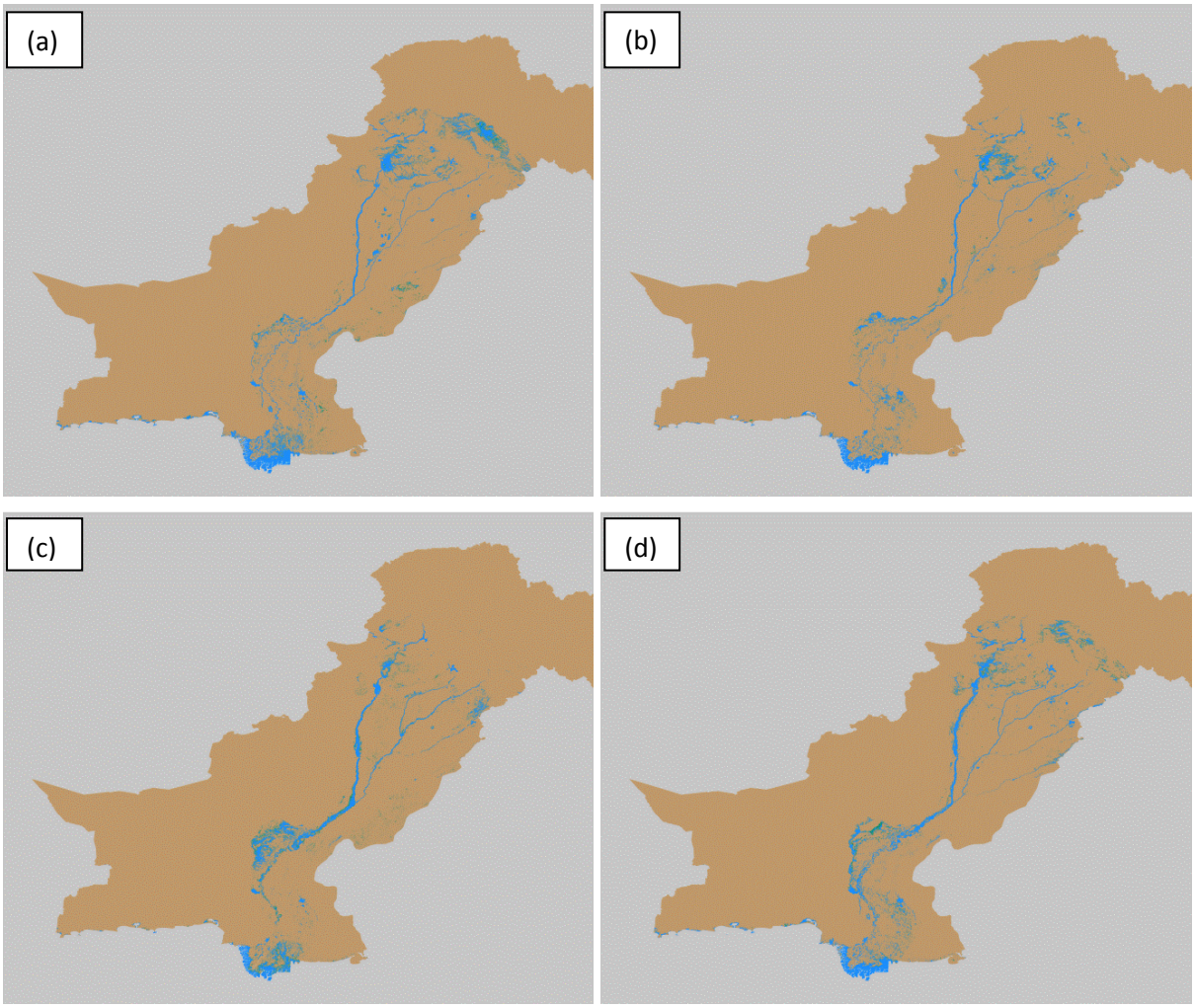

Figure 4.11: Decadal flood hazard maps for a flood event occurring once in five years, extracted from 15 years archive of MODIS classified data; decades no. (a) 4, (b) 13, (c) 22, and (d) 31.

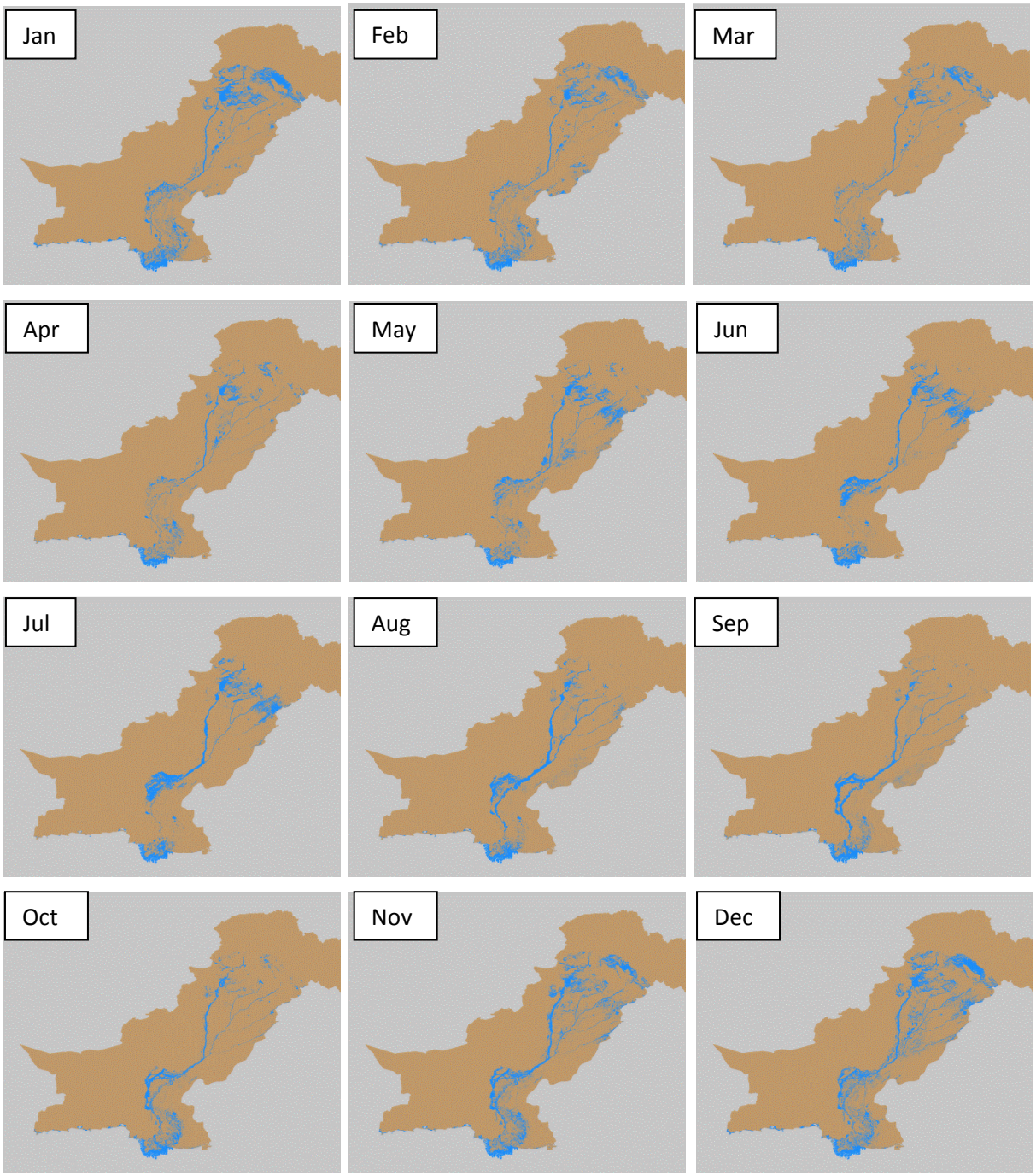

Figure 4.12: Monthly flood hazard maps for floods occurring once in five years, extracted from 15 years archive of MODIS classified data.

Such decadal and monthly analyses were performed by estimating the number of times in which a pixel resulted to be classified as water during a 10-days period, and similarly during a month by uniting the information of three respective decades for a month. For both types of analyses, a pixel was classified as water for a decade or month, if it resulted to be covered by water for more than 20% (3 years) of the time of same decade or month for 15 years. Thus, the resulted decadal and monthly files provide information about areas which may be under

water due to flood occurring once in every five years, as well as the variation in these areas from decade to decade and month to month. The monthly variations are basically a derived form of decadal analysis, but are helpful for the ease of planners to just deal with 12 reference files regarding areas under water.

Figure 4.11 shows that noise was observed, particularly for the upper areas, for decades in winter months, i.e. decade no. 4 and 31 representing first decades of February and November, respectively. The summer months decades, on the other hand, provided very good classification information, as can be seen especially in case of Figure 4.11(c) representing first decade of July. Such comparative analysis regarding accuracy of classification may be given further insight from Figure 4.12, representing the monthly files for all the 12 months. The biases or noise due to wrong classification of some areas as water can be observed easily for the winter months; however, results of classification and such analyses were found quite encouraging for the monsoon months from July-September, with reasonable performance for the other summer months (April-June) too.

Similar analyses can be performed using several different thresholds to determine the on-ground effects of floods with different return periods, as well as using threshold of 45% (based on Figure 4.8 for reference water) to determine the variations in reference water areas from decade to decade. A complete comparison of reference water and the areas under water due to a flood of 5 years return period has been presented in Appendix B for whole monsoon season (Decades' No. 10–27). Such information may be helpful for estimating the intensity and damage (in terms of flooded areas) of a real time flood event by comparing real time images with the 15 years reference water information for that specific decade or month.

4.5.4. Comparison of Flood Inundated Areas with the Observed Peak Flows and TRMM Rainfall

This section presents the comparison of inundation extents (Ha) derived by the MODIS classification approach with the respective discharge (cms) and different durations rainfall depth (mm) values for the selected points on the rivers. At first stage comparison of annual peak discharge values and respective flood inundation extents was made, and the index of correlation (R^2) was used to investigate relationship trends and consistency between the two parameters. Such comparison may provide an indication of the accuracy of classification methodology by relating water inundation extent with the respective discharge data.

Discharge data regarding annual peak flows at different points on the rivers in Pakistan were collected from Flood Forecasting Division (FFD) of Pakistan Meteorological Department (PMD). FFD also provides the dates when these peak flows were recorded in a year for each considered gauging station. It is worth mentioning that these annual peak flows may not always be representing a flood situation, e.g., in case of a dry year when these flow values may not be above the discharge flood limits. However, such peak flows are still useful for developing relation between the discharge (cms) and areal inundation extent (Ha) for different points on the rivers.

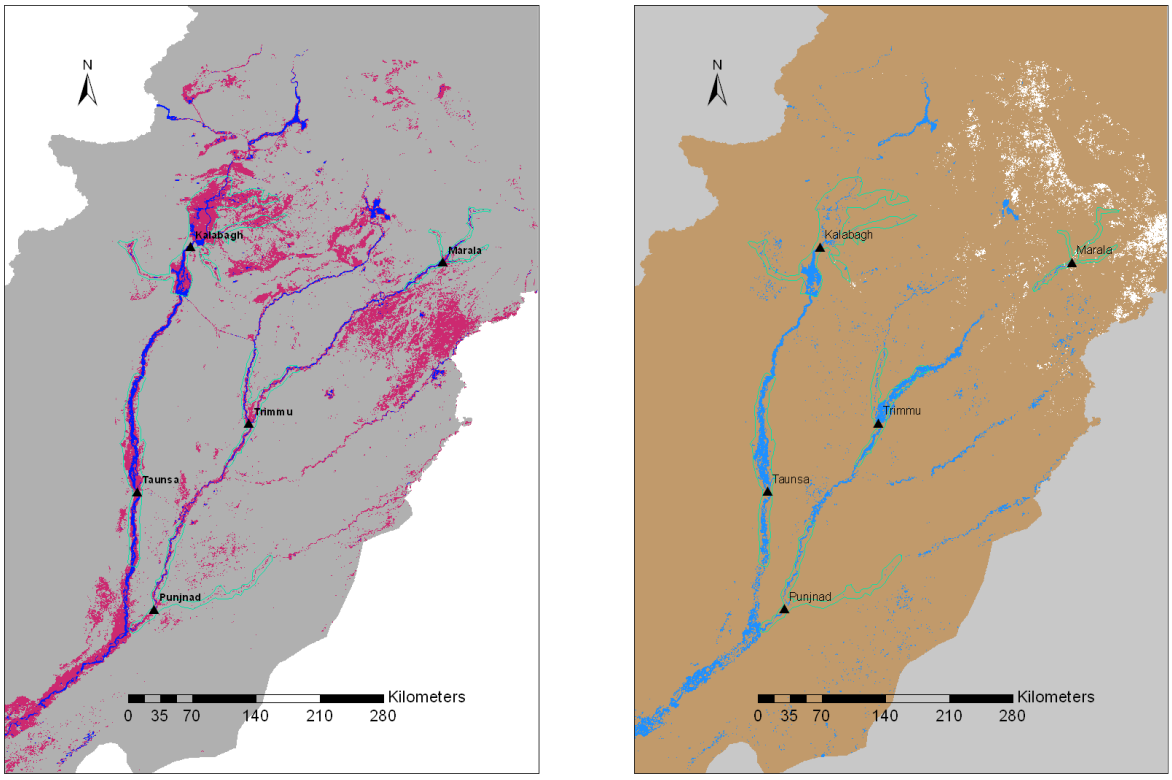

Figure 4.13: (A) Delineation of AOIs based on seasonal and flooded areas, and (B) example of extraction of inundation extent (Ha) for AOIs (Decade 23 of 2013, when most of the peak flows for that year occurred).

For such comparative analysis, five points (barrages/ head-works) namely Kalabagh, Taunsa, Marala, Trimmu and Punjnad were selected and shape files were generated defining the areas of interest (AOIs) of these points (Figure 4.13). These AOIs were delineated based on the seasonal and flooded areas information developed in this study, as well as keeping in view the hydro-morphologically defined catchments based on DEM analysis. It is believed that the use of a fixed AOI for a point to compare all of its annual peak flows with respective inundation extents (Ha) may provide a good indication of having some relationship between the discharge (cms) and inundation extent (Ha). The annual peak flows (cms) on specific dates

were compared with the flood extents (Ha) for the respective decades covering those dates, for all the five points for 14 years from 2000 to 2013.

Figure 4.14 presents the results of comparison for all the five points, with three colored lines indicating the flood limits as defined by PMD. Specifically, the green lines indicate the low flood limit, while the orange and red lines indicating the medium and high flood limits, respectively. There was found a good relationship between the two parameters for Trimmu and Punjnad with R^2 values of 0.72 and 0.92, respectively. For other three points, there were observed some biases with R^2 values as 0.68, 0.65 and 0.61 for Kalabagh, Taunsa and Marala, respectively.

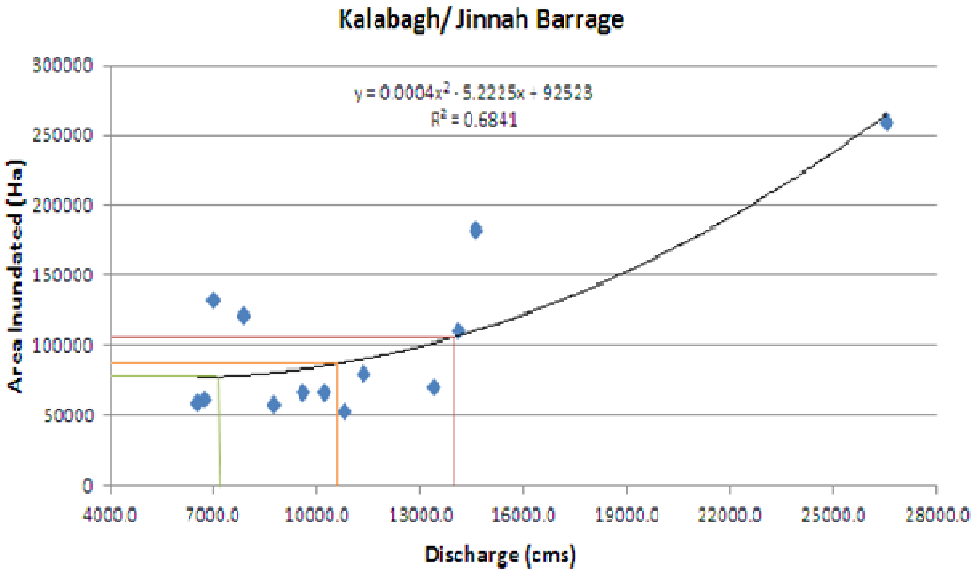

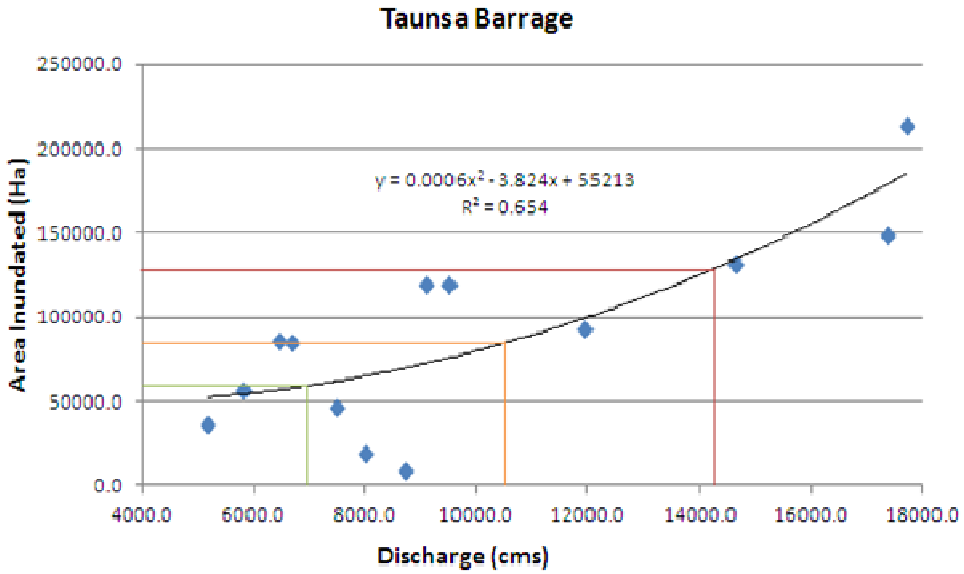

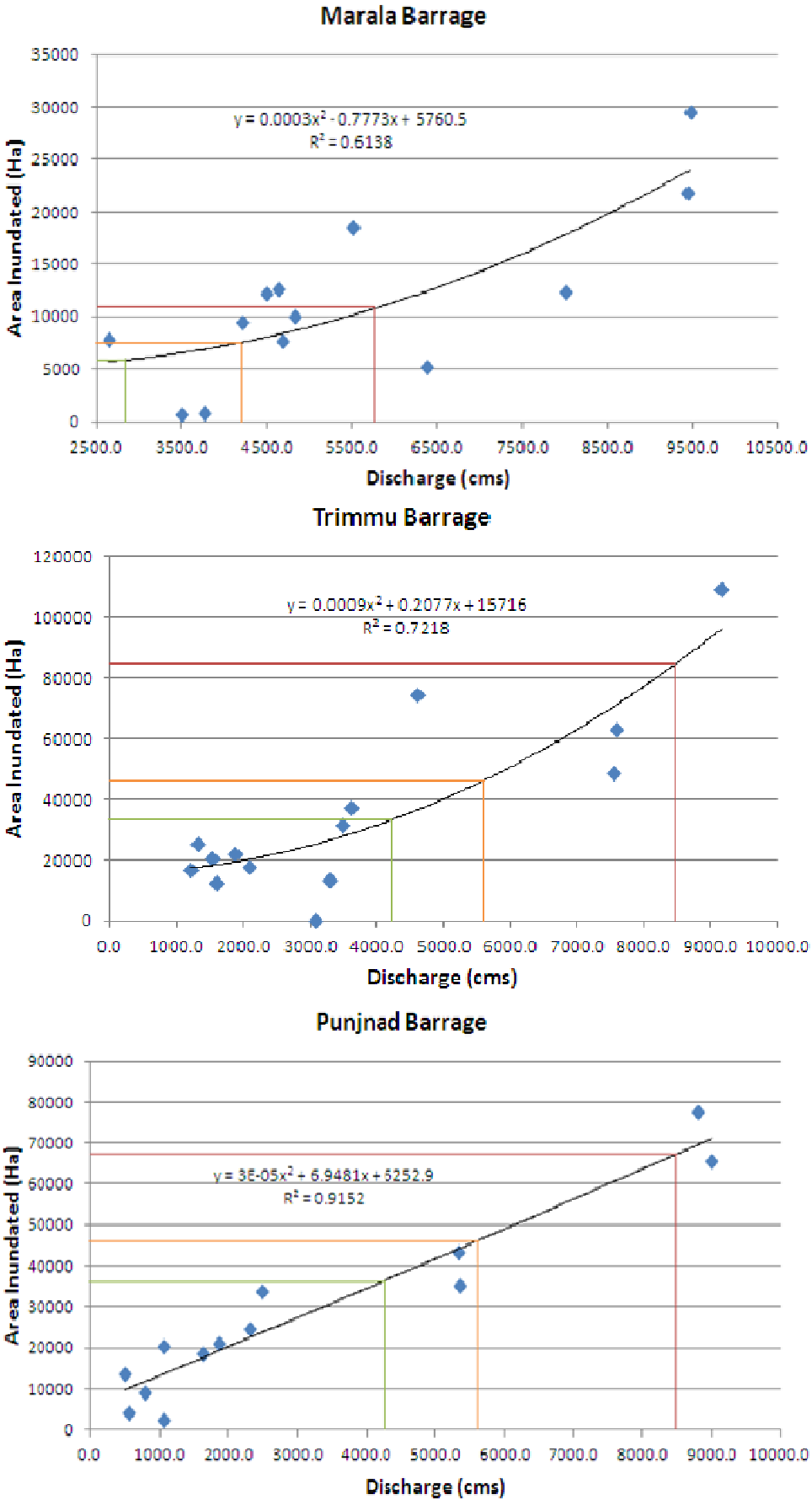

Figure 4.14: Comparison of annual peak flows (cms) with flood extent (Ha) on ground.

Reasons for relatively low correlation values between discharge and the area inundated at these points may be their vicinity to the mountainous regions, which may cause quick variations in the flows at these points. This was not the case for the other two stations, i.e. Trimmu and Punjnad, which lie in the plain areas. It is important to mention that this comparison was made just for 14 years annual peak flow values; however, this small sample can give a preliminary view of the relationship between the two parameters. More number of points, if discharge data is made available, may help investigating the correlations with more confidence. Moreover, such comparison along with defining flood limits in terms of inundation extents (Ha) may be used to employ these flood inundation extents (Ha) for comparison with rainfall amounts and defining levels of floods (low, medium, high, etc.) in the absence of discharge data.

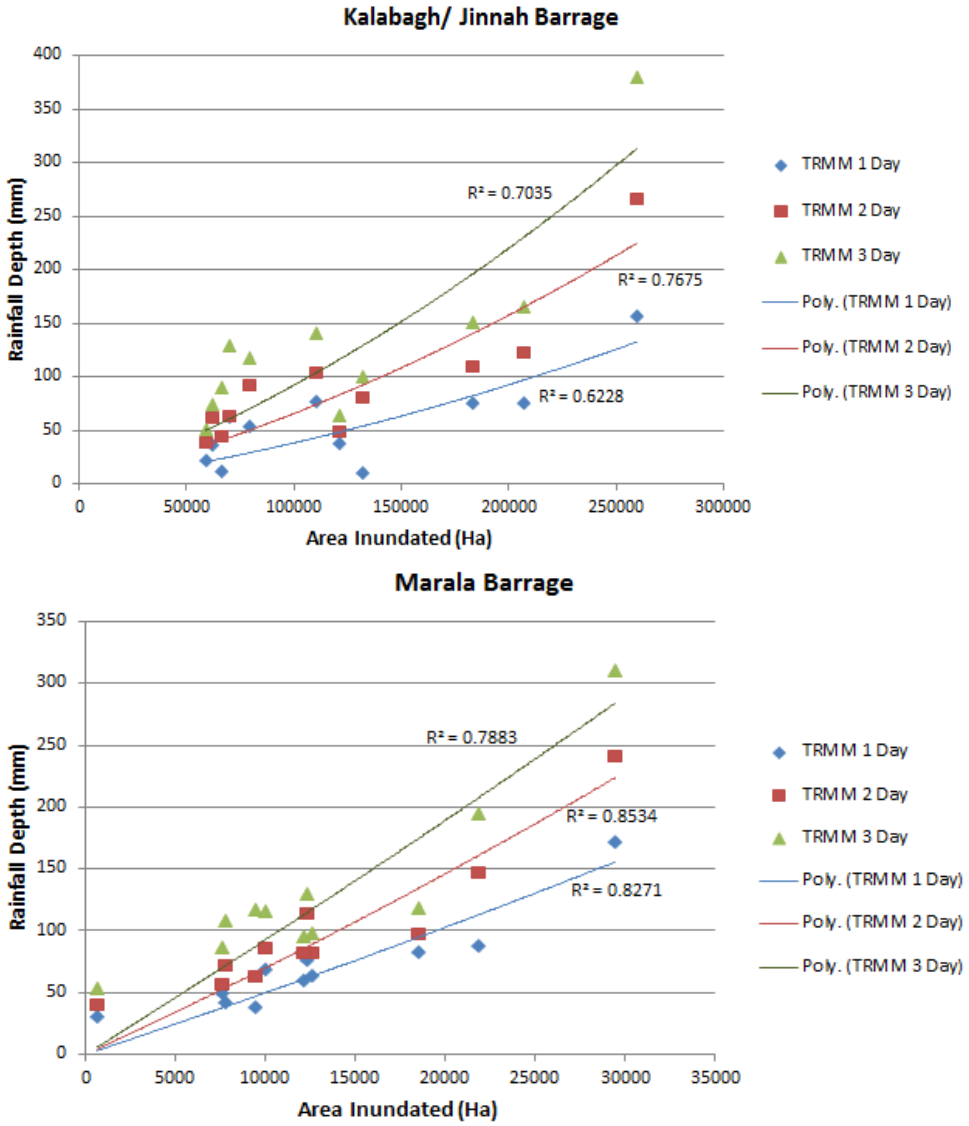

Figure 4.15: Comparison of inundation extents (Ha) with respective rainfall depths (mm) for different durations.

In the next stage, comparison of inundation extents (Ha) was made with respective TRMM rainfall depths for 1-day, 2-days and 3-days durations. It was observed that a direct relationship between areal rainfalls and flooded extents may exist only for the upstream points like Kalabagh and Marala, which are directly affected by the rainfall in their respective river catchments. In case of downstream points, other hydraulic or hydrologic factors like their distance from upper catchment and influence of flow regulations at upstream control stations may create some mismatch between the rainfall and its impacts on ground in the form of inundation extent. Therefore, to avoid such errors, the comparison of rainfall (mm) and inundation extents (Ha) was made for only two points, viz. Kalabagh and Marala, as shown in Figure 4.15. The Figure shows that good relationships were found between rainfall depths (mm) and inundation extents (Ha), and the correlation values were found best for 2-days duration.

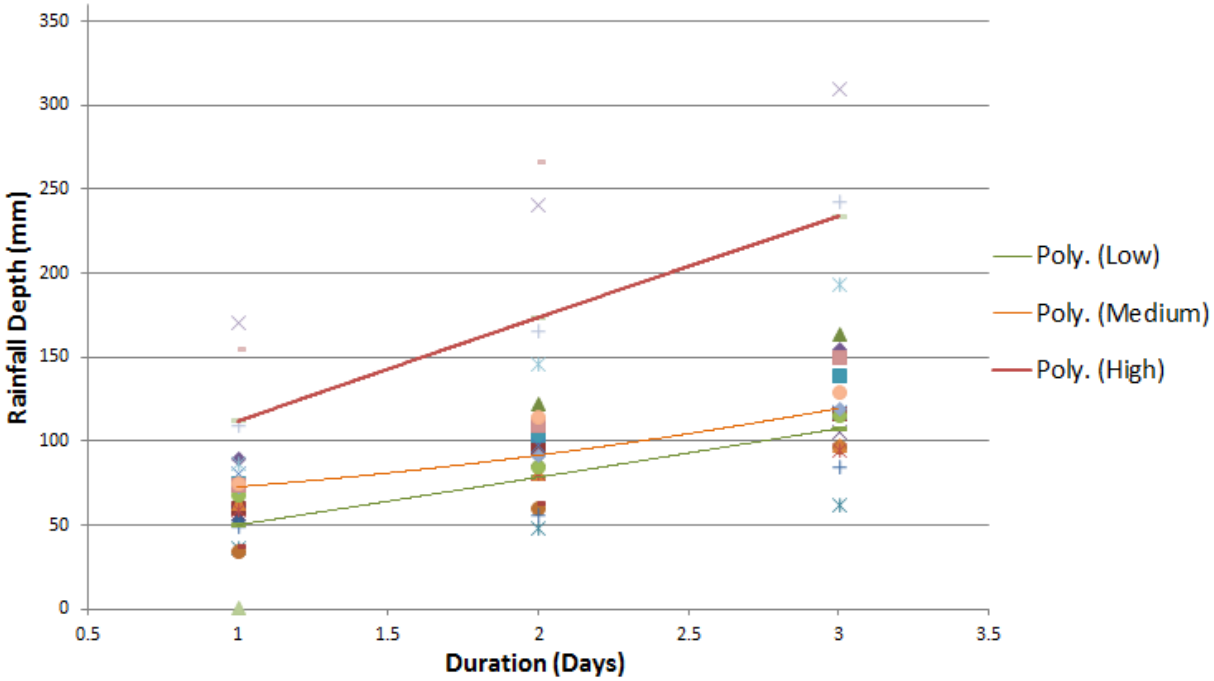

Figure 4.16: Critical rainfall depths for different durations for low, medium and high floods.

Figure 4.16 shows a joint graph of all flood events for both Kalabagh and Marala. The events were categorized into Low, Medium and High flood classes according to the discharge and inundation extents, and the respective rainfall depths were plotted against the durations. The average rainfall depths for each flood class were also plotted to have depth-duration curves for all the three classes of floods, i.e. low, medium and high. Such analysis may be used as a guideline to check the rainfall thresholds already being used by different extreme rainfall alert

systems like Extreme Rainfall Detection System (ERDS) developed by ITHACA. The critical rainfall depths for different durations and flood levels obtained through this analysis (Figure 4.16) are presented in Table 4.3 along with the thresholds already being used by ERDS for Pakistan.

Table 4.3: Critical rainfall depths for different durations and levels of floods.

Sr. #	Flood Level	Rainfall thresholds being used in ERDS for Pakistan for 24-hr duration (mm)	Critical rainfall depths (mm) for different durations obtained through this analysis		
			1-Day	2-Days	3-Days
1	Low	52	50	78	108
2	Medium	88	73	92	120
3	High	130	112	174	234

From Figure 4.16 and Table 4.3, it is evident that the critical rainfall amounts for one day (24 hours) were found to be 50 mm, 73 mm and 112 mm for the low, medium and high flood limits, respectively. The thresholds being used in ERDS for these areas of Pakistan are 52 mm, 88 mm and 130 mm for the three types of floods, respectively. In addition to have a check and finding close agreement between one day critical rainfall depths resulting from this analysis and being used in ERDS, the analysis also helped developing guidelines for critical rainfall depths for 2-days and 3-days durations. However, these guidelines may be used just to have an initial idea of critical rainfall depths for the study area due to limited number of data points. For further refining the results regarding setting of rainfall thresholds for an area, it is suggested to have intensive comparative analysis using increased number of data points in terms of discharge data. Moreover, traditional approach of statistical analysis of historical rainfall data to develop depth-duration-frequency curves may provide insight into the critical rainfall depths with more confidence.

6. Conclusions

In this chapter, a case study was presented for Pakistan to assess the scope of MODIS water bodies' classification approach for developing historical archive of reference water and delineating flood hazard maps. Automated procedures developed by Disabato (2010) were utilized to download, process and analyze the MODIS daily surface reflectance images (MOD09GQ and MYD09GQ) for Pakistan. Preliminary analysis revealed that in addition to

IR thresholds, use of NDVI is necessary to well differentiate between water and vegetation. Thus, combination of IR and NDVI thresholds were utilized for classification of water bodies.

Morphological analysis and preliminary classification results indicated relatively poor performance of MODIS for Baluchistan Plateau due to bare rocks and for Northern Areas due to steep slopes and narrow river channels. Due to steep gradients, such areas are less prone to flood water inundation, and high stream flows pass through these areas quickly to inundate the areas in the southern foothills and the plains of Punjab and Sind provinces. Therefore, it was decided to mask out the northern areas and Baluchistan Plateau due to inability of this approach to correctly detect water in such areas, as well as due to less importance of these areas regarding flood water inundation.

To remove the negative effects of clouds and their shadows, time compositing approach of 10-days period was employed, and threshold of more than or equal to 2 days was tested and found suitable to be used for Pakistan.

The analysis produced good results regarding reference and seasonal water and flooded areas delineation. There was observed noise in the winter months as a result of over-classification of some areas as water, possibly due to moist bare-soils in these months. However, classification results regarding summer months were found very encouraging, particularly for rainy months of July to September, which constitute the flood season for Pakistan. Thus, it can be concluded that the MODIS classification approach was found well capable for its application for floods detection in plain areas of Pakistan.

The classification results were also evaluated by comparison of annual peak flows for some gauging stations with the respective flood inundation extents and a good relationship was found between two parameters. In addition, the inundation extents were also compared with respective rainfall depths for two gauge stations. There was found good correlation between these two parameters too, and the analysis provided valuable indications regarding critical rainfalls for different levels of floods.

The outcomes of this analysis regarding reference and seasonal water and flood hazard maps may be helpful for planning any management interventions in the flood prone areas. Moreover, the temporally dynamic reference water and flood hazard maps (for different return periods) on decadal basis should be helpful for comparing any real time flood event imagery with the respective reference map to determine the intensity of the flood event as well as performing vulnerability analysis and planning disaster management activities.

Summary and Conclusions

The work of this thesis was aimed at developing and evaluating different open source data based methodologies for floods detection and analysis in Pakistan. Specifically, the research work was conducted for developing and evaluating a hydrologic model being able to run in real time based on satellite rainfall data, as well as to perform flood hazard mapping by analyzing seasonality of flooded areas using MODIS classification approach. Moreover, the outcome of this research work was aimed at providing guidelines regarding critical rainfall depths which may cause different levels of floods in Pakistan. The work of the thesis was divided into three phases:

Phase I: Performance Evaluation of TRMM Precipitation Estimates

At first step, monthly satellite rainfall data (TMPA 3B43 product) was evaluated for Pakistan by comparison with rain gauge data, as well as by further focusing on its analysis and evaluation for different time periods and climatic zones of Pakistan.

It was concluded that TRMM data are quite reliable for their direct and real time use for conducting any rainfall-based studies. For conducting high accuracy studies, these can be further calibrated by adopting suitable calibration techniques. However, for high mountainous areas with heavy orographic rainfalls, regional calibration should be performed very carefully and for limited areal extents using as much dense and uniformly distributed rain gauge network as possible.

Results regarding TRMM evaluation were further evaluated by performing zonal analysis, which again resulted in high NSE values (0.59 – 0.98) indicating the reliability of TRMM data for its direct use in any real time study for Pakistan.

Phase II: Hydrologic Modeling to Predict Peak Flows in Real Time

In this phase, hydrologic modeling was performed using HEC-HMS model for Chenab river catchment, an eastern tributary of Indus River. Keeping in view the mandate of this dissertation to develop and use open source data based procedures, TRMM rainfall data and other open source datasets like digital soil map and global land cover map were utilized to develop and evaluate an event-based hydrologic model, which may be capable to be run in real time for predicting peak flows or floods in the river.

There was found consistency between simulated and observed flows with percent difference in volume to be -6.17% to 5.47% and percent difference in peak flows to be in the range of -6.96% to 7.28%. Values of Nash-Sutcliffe Efficiency were found ranging from 0.299 to 0.909 with average value of 0.586 for all events.

It can be concluded that the model was found well capable of capturing the hydrologic response of the catchment in result of a rainfall event. Moreover, such a distributed hydrologic model, developed and calibrated for the whole catchment, is very helpful in determining the individual contributions of any un-gauged sub-basin. Based on the real time or forecasted rainfall data, such modeling approach can be helpful in providing alerts of peak flows or floods in real time for the whole catchment as well as for any sub-basin.

Phase III: MODIS Water Bodies Classification and Flood Hazard Mapping

Finally, to broaden the study canvas from a river catchment to the whole country scale, MODIS automated water bodies classification approach with MODIS daily surface reflectance products was utilized to develop a historical archive of reference water bodies and perform seasonal analysis of flooded areas for Pakistan. The comparison of MODIS flooded areas extents with respective peak flow values and TRMM precipitation helped checking and refining the classification approach, as well as developing some guidelines regarding critical rainfall amounts which may cause low, medium or high floods in Pakistan.

Preliminary analysis revealed that in addition to IR thresholds, use of NDVI is necessary to well differentiate between water and vegetation. Thus, combination of IR and NDVI thresholds were utilized for classification of water bodies.

Since MODIS classification approach with 250 m resolution may not be successful in mountainous areas due to steep gradients and narrow river channels, it was decided after preliminary morphological analysis to mask out the Baluchistan plateau and northern areas, and focus more on the areas in the southern foothills and the plains of Punjab and Sind provinces, which are more prone to flood inundation.

The analysis produced good results regarding reference and seasonal water and flooded areas delineation. There was observed noise in the winter months as a result of over-classification of some areas as water. However, classification results regarding summer months were found very encouraging, particularly for rainy months of July to September, which constitute the flood season for Pakistan. It can be concluded that the MODIS classification approach was

found well capable for its application for floods detection in plain areas of Pakistan; whereas the hydrologic modeling approach might be helpful for traditional rainfall-runoff modeling at a river catchment scale, particularly in mountainous topography.

The classification results were also evaluated by comparison of annual peak flows for some gauging stations with the respective flood inundation extents and a good relationship was found between two parameters. In addition, the inundation extents were also compared with respective rainfall depths for two gauge stations. There was found good correlation between these two parameters too, and the analysis provided valuable indications regarding critical rainfalls for different levels of floods.

The outcomes of this phase of analysis regarding reference and seasonal water and flood hazard maps may be helpful for planning any management interventions in the flood prone areas. Moreover, the temporally dynamic reference water and flood hazard maps (for different return periods) on decadal basis will be helpful for comparing any real time flood event imagery with the respective reference map to determine the intensity of the flood event as well as performing vulnerability analysis and planning disaster management activities.

References

Chapter 1

Ajmar, A., Albanese, A., Cristofori, E., & Vigna, R. (2013). Automated extreme rainfall monitoring and forecasting : towards an effective alerts dissemination for humanitarian practitioners. In *13th EMS Annual Meeting*. (Vol. 10).

Archer, D. R., & Fowler, H. J. (2004). Spatial and temporal variations in precipitation in the Upper Indus Basin , global teleconnections and hydrological implications. *Hydrology and Earth System Sciences*, *8*(1), 47–61.

Bookhagen, B., & Burbank, D. W. (2010). Toward a complete Himalayan hydrological budget: Spatiotemporal distribution of snowmelt and rainfall and their impact on river discharge. *Journal of Geophysical Research*, *115*(F03019), 1–25.

Briscoe, J., & Qamar, U. (2005). *Pakistan's Water Economy: Running Dry*. Oxford, UK.

De Groeve, T., Z. Kulger, and G. R. B. (2007). Near real time flood alerting for the global disaster alert and coordination system. In *4th International ISCRAM Conference*. Delft, The Netherlands.

Disabato, F. (2010). *REMOTE SENSING DATA ANALYSIS FOR ENVIRONMENTAL AND HUMANITARIAN PURPOSES: The automation of information extraction from free satellite data*. Politecnico di Torino, Italy. Retrieved from http://porto.polito.it/2496964/

EM-DAT. (2010). *The OFDA/CRED International Disaster Database*. Retrieved from www.emdat.net-Universit Catholique de Louvain?Brussels?Belgium

FAO-Aquastat. (2012). *Irrigation in Southern and Eastern Asia in figures: AQUASTAT Survey - 2011*. Rome.

FIG. (2006). *The contribution of the surveying profession to disaster risk management. A publication of FIG Working Group 8.4, International Federation of Surveyors.*

Guha-sapir, D., Hoyois, P., & Below, R. (2014). *Annual Disaster Statistical Review 2013: The numbers and trends*. Brussels, Belgium.

Hanif, M. (2011). Redistribution of Precipitation (Seasonal Shift) in Pakistan & Super Flood in Pakistan-2010. In *One Day Colloqium on "Water Crisis and Choices", held at University of Agriculture, Faisalabad.*

Horton, A. (2008). Early Warning and Early Impact Analysis: WFP Preparedness in Action. In *European Commission, From Early Warning to Early Action.* (pp. 325–328).

http://erds2.ithacaweb.org/. (n.d.). Retrieved from http://erds2.ithacaweb.org/

IPCC. (2012). *Managing the risks of extreme events and disasters to advance climate change adaptation. A Special Report of Working Groups I and II of IPCC.* Cambridge, UK, and New York, NY, USA.

IPCC. (2014). *IPCC Fifth Assessment Synthesis Report*.

Qureshi, A. S. (2011). Water Management in the Indus Basin in Pakistan□: Challenges and Opportunities. *Mountain Research and Development*, *31*(3), 252–260.

Rees, G. H., & Collins, D. N. (2005). Regional differences in response of flow in glacier-fed-Himalayan rivers to climate warming. *Hydrological Processes*, *20*(10), 2157–2169.

Thielen, J., Bartholmes, J., Ramos, M. H., & De Roo, A. P. J. (2009). The European Flood Alert System Part 1: concept and development. *Hydrology and Earth System Sciences*, *13*, 125–140.

UNISDR. (2009). *UNISDR Terminology on Disaster Risk Reduction.* Geneva, Switzerland.

Van Der Knijff, J. M., Younis, J., & De Roo, A. P. J. (2008). LISFLOOD: A GIS-based distributed model for the river basin scale water balance and Flood simulation. *International Journal of Geographical Information Science.*, 1–24.

Chapter 2

Adeyewa, Z.D., and K. Nakamura. (2003). Validation of TRMM radar rainfall data over major climatic regions in Africa. *Journal of Appl. Meteor. , 42*, 331-347.

Anagnostou, E.N., W.F. Krajewski, and J.A. Smith. (1999). Uncertainty quantification of mean-areal radar-rainfall estimates. *Journal of Atmos. Oceanic Technol. , 16*, 206-215.

Anders, A.M., G.H. Roe, B. Hallet, D.R. Montgomery, N.J. Finnegan, and J. Putkonen. (2006). Spatial patterns of precipitation and topography in the Himalaya. *GSA Spec. Pap. , 398*, 39 - 53.

ANDRÉASSIAN, V., C. PERRIN, C. MICHEL, I. USART-SANCHEZ, and J. LAVABRE. (2001). Impact of imperfect rainfall knowledge on the efficiency and the parameters of watershed models. *Journal of Hydrology , 250*, 206 - 223.

Barros, A.P., G. Kim, E. Williams, and S.W. Nesbitt. (2004). Probing orographic controls in the Himalayas during the monsoon using satellite imagery. *Nat. Hazards Earth Syst. Sci. , 4* (1), 29 - 51.

Bell, T.L., A. Abdullah, R.L. Martin, and G.R. North. (1990). Sampling errors for satellite-derived tropical rainfall: Monte Carlo study using a space-time stochastic model . *Journal of Geophysical Research , 95*, 2195-2206.

Bhatt, B.C., and K. Nakamura. (2005). Characteristics of monsoon rainfall around the Himalayas revealed by TRMM precipitation radar. *Mon. Weather Rev. , 133* (1), 149 - 165 .

Chang, A.T.C., and L.S. Chiu. (1999). Nonsystematic errors of monthly oceanic rainfall derived from SSM/I. *Mon. Wea. Rev., , 127*, 1630-1638.

Cheema, M.J.M., and W.G.M. Bastiaanssen. (2012). Local calibration of remotely sensed rainfall from the TRMM satellite for different periods and spatial scales in the Indus Basin. *International Journal of Remote Sensing , 33* (8), 2603-2627.

Chiu, L.S., D. Short, A. McConnel, and G. North. (1990). Rain estimation from satellites: Effect of finite field of view. *Journal of Geophysical Research , 95*, 2177-2185.

Chokngamwong, R., L. Chiu, and J. Vongsaard. (2005). Comparison of TRMM rainfall and daily gauge data in Thailand. *Spring Meeting 2005 of American Geophysical Union.*

Din, S.U., A.A. Dousari, A. Ramdan, and A.A. Ghadban. (2008). Site-specific precipitation estimate from TRMM data using bilinear weighted interpolation technique: an example from Kuwait. *Journal of Arid Environments , 72*, 1320-1328.

Dinku, T., P. Ceccato, E. Grover-Kopec, M. Lemma, S.J. Connor, and C.F. Popelewski. (2007). Validation of satellite rainfall products over East Africa's complex topography. *International Journal of Remote Sensing , 28*, 1503-1526.

Draper, C.S., J.P. Walker, P.J. Steinle, R.A.M. Dejeu and T.R.H. Holmes. (2009). An evaluation of AMSR-E derived soil moisture over Australia. *Remote Sensing of Environment , 113*, 703 - 710.

Franchito, S.H., V.B. Rao, A.C. Vasques, C.M.E. Santo, and J.C. Conforte. (2009). Validation of TRMM precipitation radar monthly rainfall estimates over Brazil. *Journal of Geophysical Research , 114*.

Hong, Y., K.L. Hsu, H. Moradkhani, and S. Sorooshian. (2006). Uncertainty quantification of satellite precipitation estimation and Monte Carlo assessment of the error propagation into hydrologic response. *Water Resources Research , 42*.

Hossain, F., E.N. Anagnostoub, and A.C. Bagtzoglou. (2006). On Latin hypercube sampling for efficient uncertainty estimation of satellite rainfall observations in flood prediction. *Computers and Geosciences , 32*, 776-792.

Huffman, G. (1997). Estimates of root-mean-square random error for finite samples of estimated precipitation. *J. Appl. Meteor. , 36*, 1191-1201.

Huffman, G.J., R.F. Adler, D.T. Bolvin, G. Gu, E.J. Nelkin, K.P. Bowman, Y. Hong, E.F. Stocker, and D.B. Wolff. (2007). The TRMM Multisatellite Precipitation Analysis (TMPA): Quasi-global, multiyear, combined-sensor precipitation estimates at fine scales. *Journal of Hydrometeorology , 8* (1), 38-55.

Huffman, G.J., R.F. Alder, M.M. Morrissey, D.T. Bolvin, S. Curtis, R. Joyce, B. Mcgavock, and J. Susskind. (2001). Global precipitation at one-degree daily resolution from multisatellite observations. *Journal of Hydrometeorology , 2*, 36-50.

Islam, N.M., and H. Uyeda. (2008). Vertical variations of rain intensity in different rainy periods in and around Bangladesh derived from TRMM observations. *International Journal of Climatology , 28*, 273-279.

Ji, Y., and E. Stocker. (2003). Ground validation of TRMM and AMSU microwave precipitation estimates. *Proceedings of the International Geoscience and Remote Sensing Symposium* (pp. 3157-3159). Toulouse, France: IEEE.

Kousky, V. (1980). Diurnal rainfall variation in northeast Brazil. *Mon. Wea. Rev. , 108*, 488-498.

Kubota, T., S. Shige, H. Hashizume, K. Aonashi, N. Takahashi, S. Seto, Y.N. Takayabu, T. Ushio, K. Nakagawa, K. Iwanami, M. Kachi, and K. Okamoto. (2007). Global precipitation map using satellite-borne microwave radiometers by the GSMap project: Production and validation. *Geoscience and Remote Sensing , 45* (7), 2259-2275.

Kummerow, C. (1998). Beamfilling errors in passive microwave rainfall retrievals. *J. Appl. Meteor. , 37*, 356-357.

Kummerow, C., and Coauthors. (2000). The status of the Tropical Rainfall Measuring Mission (TRMM) after two years in orbit. *J. Appl. Meteor. , 39*, 1965-1982.

Kummerow, C., W. Barnes, T. Kozu, J. Shiue, and J. Simpson. (1998). The Tropical Rainfall Measuring Mission (TRMM) sensor package. *J. Atmos. Oceanic Technol. , 15* (3), 809-817.

Nash, J.E., and J.V. Sutcliffe. (1970). River flow forecasting through cpnceptual models part 1 - a discussion of principles. *Journal of Hydrology , 10*, 282-290.

Sawunyama, T. and D.A. Hughes. (2008). Application of satellite-derived rainfall estimates to extend water resource simulation modelling in South Africa. *Pretoria: Water Research Commission , 34*, 1 - 9.

Tobin, K.J., and M.E. Bennett. (2010). Adjusting satellite precipitation data to facilitate hydrologic modeling. *Journal of Hydrometeorology , 11*, 966-978.

Tustison, B., D. Harris and E. Foufoula-Georgiou. (2001). Scale issues in verification of precipitation forecasts. *J. Geophys. Res. , 106* (D11), 11775 - 11784.

Ushio, T., K. Sasashige, T. Kubota, S. Shige, K. Okamoto, K. Aonashi, T. Inoue, N. Takahashi, and T. Iguchi. (2009). A Kalman filter approach to the Global Satellite Mapping of Precipitation (GSMaP) from combined passive microwave and infrared radiometric data. *J. Meteorol. Soc. Jpn. , 87A* (9), 3084-3097.

Vigna, R. (2011). *Early warning systems for risk management: design and implementation of a global early warning system for heavy rainfall detection.* PhD Thesis, Politecnico di Torino, Department of Land, Environment and Geo-engineering.

Vila, D.A., L.G.G. De Goncalves, D.L. Toll, and J.R. Rozante. (2009). Statistical evaluation of combined daily gauge observations and rainfall satelite estimates over Continental South America. *Journal of Hydrometerology , 10*, 533-543.

Villarini, G., and W.F. Krajewski. (2007). Evaluation of the research version TMPA three-hourly 0.25 x 0.25 rainfall estimates over Oklahoma. *Geophysical Research Letters , 34*.

Chapter 3

Adeyewa, Z. D., & Nakamura, K. (2003). Validation of TRMM Radar Rainfall Data over Major Climatic Regions in Africa. *Journal of Applied Meteorology*, *42*, 331–347.

Ali, M., Khan, S. J., Aslam, I., & Khan, Z. (2011). Landscape and Urban Planning Simulation of the impacts of land-use change on surface runoff of Lai Nullah Basin in Islamabad , Pakistan. *Landscape and Urban Planning*, *102*(4), 271–279. doi:10.1016/j.landurbplan.2011.05.006

Cheema, M. J. M., & Bastiaanssen, W. G. M. (2012). Local calibration of remotely sensed rainfall from the TRMM satellite for different periods and spatial scales in the Indus Basin. *International Journal of Remote Sensing*, *33*(8), 2603–2627.

Chen, Y., Xu, Y., & Yin, Y. (2009). Impact of land use change scenarios on storm-runoff generation in Xitiaoxi basin, China. *Quaternary International*, *1*, 1–8.

De Silva, M. M. G. T., Weerakoon, S. B., & Herath, S. (2014). Modeling of Event and Continuous Flow Hydrographs with HEC – HMS : Case Study in the Kelani River Basin , Sri Lanka. *ASCE Journal of Hydrologic Engineering*, *19*(4), 800–806. doi:10.1061/(ASCE)HE.1943-5584.0000846.

Dinku, T., Ceccato, P., Grover-Kopec, E., Lemma, M., Connor, S. J., & Popelewski, C. F. (2007). Validation of satellite rainfall products over East Africa's complex topography. *International Journal of Remote Sensing*, *28*, 1503–1526.

ESA. (2010). GlobeCover2009 version 2.3. Retrieved from http://due.esrin.esa.int/globcover/

FAO. (2007). Digital Soil Map of World, Version 3.6. Retrieved from http://www.fao.org/geonetwork/srv/en/metadata.show?id=14116

Fleming, M. J., & Doan, J. H. (2010). *HEC-GeoHMS Geospatial Hydrologic Modeling Extension User's Manual, Version 5.0.*

Halwatura, D., & Najim, M. M. M. (2013). Environmental Modelling & Software Application of the HEC-HMS model for runoff simulation in a tropical catchment. *Environmental Modelling and Software*, *46*, 155–162. doi:10.1016/j.envsoft.2013.03.006

Immerzeel, W. W., Droogers, P., de Jong, S. M., & Bierkens, M. F. P. (2009). Large-scale monitoring of snow cover and runoff simulation in Himalayan river basins using remote sensing. *Remote Sensing of Environment*, *113*(1), 40–49.

ITHACA. (2010). *Flood Index in Ethiopia: HEC-HMS Model Implementation.*

Loukas, A., & Quick, M. C. (1996). Physically-based estimation of lag time for forested mountaneous watersheds. *Hydrological Sciences*, *41*(1), 1–19.

Merwade, V. (2012). *Creating SCS Curve Number Grid using HEC-GeoHMS*. Retrieved from http://web.ics.purdue.edu/~vmerwade/tutorial.html

Nash, J. E., & Sutcliffe, J. V. (1970). River Flow Forecasting Through Conceptual Models: Part I - A Discussion of Principles. *Journal of Hydrology.*, *10*, 282–290.

Russel, S. O., Kenning, B. F. I., & Sunnell, G. J. (1979). Estimating design flows for urban drainage. *Journal of Hydraulics Division.*, *105*(1), 43–52.

Shahid, M. A., Boccardo, P., Garcia, W. C., Albanese, A., & Cristofori, E. (2013). Evaluation of TRMM Satellite Data for Mapping Monthly Precipitation in Pakistan by Comparison with Locally Available Data. In *III CUCS Congress - Imagining Cultures of Cooperation: Universities working to face the new developemnt challenges.* Turin, Italy.

Singh, P., Jain, S. K., & Kumar, N. (1997). Estimation of Snow and Glacier-Melt Contribution to the Chenab River, Western Himalaya. *Mountain Research and Development*, *17*(1), 49–56.

Singh, P., Ramasastri, K. S., & Kumar, N. (1995). Topographical Influence on Precipitation Distribution in different ranges of western Himalays. *Nordic Hydrology*, *26*, 259–284.

USACE. (1994). *Flood-Runoff Analysis, Engineer Manual 1110-2-1417.* Washington, USA.

USACE. (2000). *Hydrologic Modeling System (HEC-HMS) Technical Reference Manual* (pp. 36–37). Washington, USA.

USACE. (2008). *Hydrologic Modeling System (HEC-HMS) Applications Guide.*

USDA-NRCS. (1986). *TR-55: Urban Hydrology for Small Watersheds.*

USDA-NRCS. (2007). Chapter 7: Hydrologic Soil Groups. In *National Engineering Handbook of Hydrology (Part 630).*

USDA-NRCS. (2010). *National Engineering Handbook Chapter 15, Time of Concentration.* (pp. 1–29).

Villarini, G., & Krajewski, W. F. (2007). Evaluation of the research version TMPA three-hourly 0.25 x 0.25 rainfall estimates over Oklahoma. *Geophysical Research Letters*, *34*.

Chapter 4

Ajmar, A., Albanese, A., Disabato, F., & Miotto, F. (2012). Integration of satellite and rainfall data for the identification of flood events in developing countries. *Italian Journal of Remote Sensing, 44*(1), 167-180.

Chatterjee, C., Kumar, R., Chakravorthy, B., Lohani, A.K., & Kumar, S. (2005). Integrating remote sensing and GIS techniques with groundwater flow modeling for assessment of waterlogged areas. *Water Resource Management, 19*, 539–554. doi: 10.1007/s11269-005-2071-4.

Chowdary, V.M., Chandran, R. V., Neeti, N., Bothale, R.V., Srivastava, Y.K., Ingle, P., Ramakrishnan, D., Dutta, D., Jeyaram, A., Sharma, J.R., & Singh, R. (2008). Assessment of surface and sub-surface waterlogged areas in irrigation command areas of Bihar state using remote sensing and GIS. *Agricultural Water Management, 95*(7), 754-766.

De Alwis, D.A., Easton, Z.M., Dahlke, H.E., Philpot, W.D., and Steenhuis, T.S. (2007). Unsupervised classification of saturated areas using a time series of remotely sensed images. *Hydrol. Earth Syst. Sci., 11*, 1609–1620.

Disabato, F. (2010). *Remote Sensing Data Analysis for Environmental and Humanitarian Purposes: The automation of information extraction from free satellite data.* Politecnico di Torino, Italy. Retrieved from http://porto.polito.it/2496964/

Fadhil, A.M. (2006). Environmental Change Monitoring by Geoinformation Technology for Baghdad and its Neighboring Areas. *Proceedings of the International Scientific Conference of Map Asia 2006: The 5th Asian Conference in GIS, GPS, Aerial Photography and Remote Sensing. Bangkok, Thailand.*

Fengming, H., Bing, X., Huabing, H., Qian, Y., & Peng, G. (2008). Modeling spatial-temporal change of Poyang Lake using multi-temporal Landsat imagery. *International Journal of Remote Sensing, 29*(20), 5767–5784.

Forsythe, N., Kilsby, C.G., Fowler, H.J., & Archer, D.R. (2012). Assessment of Runoff Sensitivity in the Upper Indus Basin to Inter-annual Climate Variability and Potential Change Using MODIS Satellite Data Products. *Mountain Research and Development, 32*(1), 16-29.

Gao, B.C. (1996). NDWI-A normalized difference water index for remote sensing of vegetation liquid water from space. *Remote Sensing of Environment, 58*(3), 257-266.

Huggel, C., Kääb, A., Haeberli, W., Teysseire, P., & Paul, F. (2002). Remote sensing based assessment of hazards from glacier lake outbursts: A case study in the Swiss Alps. *Canadian Geotechnical Journal, 39*(2), 316–330.

Hui, J.W.C., Cook, B.I., Ravi, S., D'Odorico, P., & Fuentes, J.D. (2008). Dust-rainfall feedbacks in West African Sahel. *Water Resour. Res., 44*, W05202, doi: 10.1029/2008WR006885.

Jain, S.K., Saraf, A.K., Goswami, A., and Ahmad, T. (2006). Flood inundation mapping using NOAA AVHRR data. *Water Resources Management, 20*(6): 949–959.

Luo, Y., Trishchenko, A., & Khlopenkov, K.V. (2008). Developing clear-sky, cloud and cloud shadow mask for producing clear sky composites at 250-meter spatial resolution for the seven MODIS land bands over Canada and North America. *Remote Sensing of Environment, 112*(12), 4167-4185.

Mcfeeters, S.K. (1996). Use of Normalized Difference Water Index (NDWI) in the Delineation of Open Water Features. *International Journal of Remote Sensing, 17*, 1425–1432.

Purba, G.S., et al. (2006). Identification of Flood Affected Areas-Need for a Scientific Approach. *Proceedings of Indian Disaster Management Congress, Organized by National Institute of Disaster Management and Central Water Commission, at Vigyan Bhawan, New Delhi, November 28-30, 2006.*

Sakamoto, T., Nguyen, N. V., Kotera, A., Ohno, H., Ishitsuka, N., & Yokozawa, M. (2007). Detecting temporal changes in the extent of annual flooding within the Cambodia and the Vietnamese Mekong Delta from MODIS time-series imagery. *Remote Sensing of Environment, 109*(3), 295-313.

Thenkabail, P. S., Schull, M., and Turral, H. (2005). Ganges and Indus river basin land use land cover (LULC) and irrigated area mapping using continuous streams of MODIS data. *Remote Sensing of Environment, 95*(3), 317-341.

Zhuowei, H.U., Gong, H., Zhu, L. (2007). Fast flooding information extraction in emergency response of flood disaster. *ISPRS Workshop on Updating Geo-spatial Databases with Imagery & The 5th ISPRS Workshop on DMGISs*.

Appendix A

Hydrologic Response of Individual Sub-basins

Semi-distributed hydrologic modeling helps assessing hydrologic response of the individual sub-basins. This appendix provides the information about individual contribution of each sub-basin to the total flow at outlet for all the rainfall events.

A.1. Summary Table for Event E1; collective peak time: 10-Jul-2006, 03:00.

Hydrologic Element	Drainage Area (km2)	Peak Discharge (cms)	Time of Peak	Volume (mm)
W1	2397.34	586.9	09lug2006, 12:00	26.87
W2	1658.96	205.6	09lug2006, 09:00	19.22
J1	4056.3	773.4	09lug2006, 12:00	23.74
R1	4056.3	758.8	09lug2006, 18:00	24.65
W4	964.19	97.5	09lug2006, 12:00	18.32
W3	879.52	247.2	09lug2006, 12:00	23.82
J2	5900.01	953.5	09lug2006, 18:00	23.49
R2	5900.01	937.7	10lug2006, 03:00	24.66
W5	2610.83	365.4	09lug2006, 12:00	20.76
W6	1497.71	122.8	08lug2006, 00:00	17.53
J3	10008.55	1224.9	10lug2006, 03:00	22.58
R3	10008.55	1217.9	10lug2006, 09:00	23.21
W8	1492.16	122.3	08lug2006, 00:00	16.37
W9	1401.74	147.3	08lug2006, 18:00	19.63
J4	2893.9	250.8	08lug2006, 18:00	17.95
R4	2893.9	244.7	08lug2006, 21:00	18.55
W10	1927.94	158	08lug2006, 00:00	17.05
W7	787.61	73.1	09lug2006, 21:00	19.17
J5	15618	1541.2	10lug2006, 09:00	21.38
R5	15618	1532.1	10lug2006, 12:00	21.86
W12	1003.85	109.8	09lug2006, 15:00	21.05
W11	485.32	39.8	08lug2006, 00:00	16.37
J6	17107.17	1624.1	10lug2006, 12:00	21.66
R6	17107.17	1616.3	11lug2006, 03:00	22.23
W13	3316.22	475.8	09lug2006, 18:00	26.64
W14	1184.23	97	08lug2006, 00:00	16.37
J7	21607.62	1932.4	11lug2006, 03:00	22.59
R7	21607.62	1813.3	10lug2006, 06:00	22.42
W15	2822.43	729.5	10lug2006, 00:00	44.37
W16	1576.87	475.8	09lug2006, 15:00	47.84
J8	26006.92	2889.9	10lug2006, 03:00	26.34

A.2. Summary Table for Event E2; collective peak time: 25-Jul-2006, 03:00.

Hydrologic Element	Drainage Area (km2)	Peak Discharge (cms)	Time of Peak	Volume (mm)
W1	2397.34	229.8	25lug2006, 03:00	33.49
W2	1658.96	159	25lug2006, 03:00	30.35
J1	4056.3	388.9	25lug2006, 03:00	32.21
R1	4056.3	388.9	25lug2006, 03:00	33.75
W4	964.19	92.4	25lug2006, 03:00	30.35
W3	879.52	84.3	25lug2006, 03:00	30.35
J2	5900.01	565.6	25lug2006, 03:00	32.69
R2	5900.01	565.6	25lug2006, 03:00	35
W5	2610.83	448.4	26lug2006, 15:00	37.74
W6	1497.71	150.1	01ago2006, 18:00	33.99
J3	10008.55	1014.5	26lug2006, 15:00	35.56
R3	10008.55	1012.9	26lug2006, 21:00	36.63
W8	1492.16	149.9	26lug2006, 21:00	35.39
W9	1401.74	208.9	26lug2006, 18:00	36.1
J4	2893.9	353.2	26lug2006, 18:00	35.74
R4	2893.9	341.4	27lug2006, 00:00	36.88
W10	1927.94	202.6	27lug2006, 15:00	36.54
W7	787.61	122.1	26lug2006, 18:00	44.27
J5	15618	1633.8	26lug2006, 21:00	37.05
R5	15618	1618.6	27lug2006, 03:00	38.17
W12	1003.85	96.2	25lug2006, 03:00	31.83
W11	485.32	46.5	25lug2006, 03:00	32.27
J6	17107.17	1721.5	27lug2006, 03:00	37.63
R6	17107.17	1707.2	27lug2006, 18:00	41.21
W13	3316.22	317.9	25lug2006, 03:00	30.82
W14	1184.23	120.8	29lug2006, 12:00	37.46
J7	21607.62	2071.5	25lug2006, 03:00	39.41
R7	21607.62	2071.5	25lug2006, 03:00	42.73
W15	2822.43	270.6	25lug2006, 03:00	31.95
W16	1576.87	200	29lug2006, 15:00	56.12
J8	26006.92	2493.2	25lug2006, 03:00	42.37

A.3. Summary Table for Event E3; collective peak time: 23-Jul-2010, 00:00.

Hydrologic Element	Drainage Area (km2)	Peak Discharge (cms)	Time of Peak	Volume (mm)
W1	2397.34	235.9	20lug2010, 12:00	30.55
W2	1658.96	161.5	18lug2010, 00:00	29.16
J1	4056.3	394.9	18lug2010, 00:00	29.98
R1	4056.3	394.9	18lug2010, 00:00	31.67
W4	964.19	136.7	20lug2010, 15:00	33.24
W3	879.52	303.3	20lug2010, 09:00	43.06
J2	5900.01	659.1	20lug2010, 09:00	33.63
R2	5900.01	627.0	20lug2010, 18:00	35.99
W5	2610.83	557.8	22lug2010, 12:00	47.59
W6	1497.71	289.7	20lug2010, 15:00	37.76
J3	10008.55	1267.1	20lug2010, 18:00	39.28
R3	10008.55	1256.8	21lug2010, 00:00	40.57
W8	1492.16	258.8	20lug2010, 12:00	45.96
W9	1401.74	415.3	21lug2010, 12:00	49.71
J4	2893.9	629.2	21lug2010, 12:00	47.77
R4	2893.9	593.2	21lug2010, 18:00	48.67
W10	1927.94	314.1	21lug2010, 15:00	48.17
W7	787.61	207.2	21lug2010, 12:00	67.78
J5	15618	1899.1	21lug2010, 18:00	44.38
R5	15618	1890.6	21lug2010, 21:00	45.37
W12	1003.85	188.9	22lug2010, 12:00	47.45
W11	485.32	70.1	22lug2010, 09:00	43.82
J6	17107.17	2036.0	21lug2010, 21:00	45.45
R6	17107.17	2018.5	22lug2010, 12:00	47.90
W13	3316.22	475.7	22lug2010, 12:00	44.12
W14	1184.23	237.1	22lug2010, 06:00	51.53
J7	21607.62	2696.0	22lug2010, 12:00	47.52
R7	21607.62	2664.7	23lug2010, 00:00	48.38
W15	2822.43	405.1	19lug2010, 12:00	50.10
W16	1576.87	334.3	19lug2010, 09:00	76.85
J8	26006.92	3106.5	23lug2010, 00:00	50.29

A.4. Summary Table for Event E4; collective peak time: 30-Jul-2013, 15:00.

Hydrologic Element	Drainage Area (km2)	Peak Discharge (cms)	Time of Peak	Volume (mm)
W1	2397.34	164.3	29lug2013, 03:00	12.17
W2	1658.96	113.7	29lug2013, 03:00	12.17
J1	4056.3	278	29lug2013, 03:00	12.17
R1	4056.3	278	29lug2013, 03:00	12.91
W4	964.19	66.1	29lug2013, 03:00	12.17
W3	879.52	60.3	29lug2013, 03:00	12.17
J2	5900.01	404.4	29lug2013, 03:00	12.68
R2	5900.01	404.4	29lug2013, 03:00	13.67
W5	2610.83	179	29lug2013, 03:00	12.17
W6	1497.71	102.7	29lug2013, 03:00	12.17
J3	10008.55	686	29lug2013, 03:00	13.05
R3	10008.55	686	29lug2013, 03:00	13.62
W8	1492.16	182.7	30lug2013, 09:00	17.21
W9	1401.74	169.8	30lug2013, 09:00	16.21
J4	2893.9	352.5	30lug2013, 09:00	16.72
R4	2893.9	338.1	30lug2013, 15:00	16.81
W10	1927.94	428.4	30lug2013, 09:00	24.29
W7	787.61	191.8	30lug2013, 06:00	26.44
J5	15618	1454.9	30lug2013, 12:00	16.18
R5	15618	1450.9	30lug2013, 15:00	16.51
W12	1003.85	115.8	30lug2013, 09:00	17.94
W11	485.32	88.3	30lug2013, 06:00	23.26
J6	17107.17	1620.9	30lug2013, 15:00	16.78
R6	17107.17	1614	31lug2013, 06:00	17.39
W13	3316.22	580.4	30lug2013, 12:00	26.45
W14	1184.23	713.2	30lug2013, 03:00	61.49
J7	21607.62	2267.3	31lug2013, 03:00	21.2
R7	21607.62	2255.7	31lug2013, 18:00	20.33
W15	2822.43	922.4	30lug2013, 12:00	46.41
W16	1576.87	766.5	30lug2013, 09:00	63.38
J8	26006.92	3738.2	30lug2013, 15:00	25.77

A.5. Summary Table for Event E5; collective peak time: 03-Aug-2013, 09:00.

Hydrologic Element	Drainage Area (km2)	Peak Discharge (cms)	Time of Peak	Volume (mm)
W1	2397.34	216.6	01ago2013, 00:00	17.53
W2	1658.96	149.9	01ago2013, 00:00	17.07
J1	4056.3	366.5	01ago2013, 00:00	17.34
R1	4056.3	366.5	01ago2013, 00:00	18.37
W4	964.19	87.1	01ago2013, 00:00	17.07
W3	879.52	79.5	01ago2013, 00:00	17.07
J2	5900.01	533.1	01ago2013, 00:00	17.96
R2	5900.01	533.1	01ago2013, 00:00	19.37
W5	2610.83	436.3	02ago2013, 09:00	25.61
W6	1497.71	348	01ago2013, 18:00	25.89
J3	10008.55	1269.8	01ago2013, 18:00	21.98
R3	10008.55	1263.8	02ago2013, 00:00	22.75
W8	1492.16	157.5	01ago2013, 09:00	20.17
W9	1401.74	266.7	01ago2013, 18:00	24.77
J4	2893.9	398.3	01ago2013, 18:00	22.4
R4	2893.9	378.6	01ago2013, 21:00	23
W10	1927.94	473.1	02ago2013, 12:00	38.59
W7	787.61	255.5	02ago2013, 12:00	46.45
J5	15618	2122.8	02ago2013, 00:00	25.95
R5	15618	2059.4	02ago2013, 03:00	26.48
W12	1003.85	191	02ago2013, 12:00	28.16
W11	485.32	97.9	02ago2013, 12:00	31.35
J6	17107.17	2224.1	02ago2013, 18:00	26.72
R6	17107.17	2215.2	03ago2013, 09:00	27.64
W13	3316.22	750.5	02ago2013, 15:00	37.06
W14	1184.23	151.9	02ago2013, 09:00	22.96
J7	21607.62	3038.3	02ago2013, 18:00	28.83
R7	21607.62	3023.1	03ago2013, 09:00	27.89
W15	2822.43	255	01ago2013, 00:00	19.46
W16	1576.87	469.1	02ago2013, 12:00	45.04
J8	26006.92	3531.8	03ago2013, 09:00	28.02

A.6. Summary Table for Event E1_val; collective peak time: 28-Aug-2006, 03:00.

Hydrologic Element	Drainage Area (km2)	Peak Discharge (cms)	Time of Peak	Volume (mm)
W1	2397.34	211.3	26ago2006, 00:00	19.73
W2	1658.96	127.1	24ago2006, 00:00	17.9
J1	4056.3	310.8	24ago2006, 00:00	18.98
R1	4056.3	310.8	24ago2006, 00:00	20.42
W4	964.19	112.8	24ago2006, 21:00	22.22
W3	879.52	200.2	25ago2006, 21:00	34.48
J2	5900.01	452.1	24ago2006, 00:00	22.81
R2	5900.01	452.1	24ago2006, 00:00	24.3
W5	2610.83	356	24ago2006, 21:00	32.81
W6	1497.71	428	24ago2006, 21:00	52.6
J3	10008.55	1187.6	24ago2006, 21:00	30.76
R3	10008.55	1150.5	25ago2006, 06:00	31.88
W8	1492.16	147.6	25ago2006, 21:00	28.2
W9	1401.74	122.7	24ago2006, 21:00	21.55
J4	2893.9	221.8	24ago2006, 00:00	24.98
R4	2893.9	221.8	24ago2006, 00:00	26.23
W10	1927.94	164.9	25ago2006, 00:00	25.47
W7	787.61	65.1	24ago2006, 21:00	34.46
J5	15618	1570.9	25ago2006, 06:00	30.17
R5	15618	1570.2	25ago2006, 12:00	31.05
W12	1003.85	107	24ago2006, 21:00	29.15
W11	485.32	37.2	24ago2006, 00:00	28.09
J6	17107.17	1685.7	25ago2006, 12:00	30.86
R6	17107.17	1672.2	26ago2006, 06:00	33.4
W13	3316.22	494.3	25ago2006, 00:00	44.51
W14	1184.23	533	27ago2006, 18:00	69.8
J7	21607.62	2052.2	26ago2006, 06:00	37.1
R7	21607.62	2043.9	26ago2006, 18:00	38.2
W15	2822.43	627.1	28ago2006, 00:00	55.61
W16	1576.87	364.9	27ago2006, 21:00	67.94
J8	26006.92	2751.6	28ago2006, 03:00	41.89

A.7. Summary Table for Event E2_val; collective peak time: 03-Sep-2006, 12:00.

Hydrologic Element	Drainage Area (km2)	Peak Discharge (cms)	Time of Peak	Volume (mm)
W1	2397.34	364.6	01set2006, 21:00	21.31
W2	1658.96	203.6	01set2006, 18:00	18.12
J1	4056.3	541.8	01set2006, 18:00	20.01
R1	4056.3	535.3	02set2006, 03:00	20.88
W4	964.19	98.6	01set2006, 18:00	16.78
W3	879.52	210.4	01set2006, 18:00	29.16
J2	5900.01	692	02set2006, 00:00	21.44
R2	5900.01	679.1	02set2006, 09:00	22.32
W5	2610.83	424	01set2006, 15:00	31.24
W6	1497.71	482.7	01set2006, 18:00	54.82
J3	10008.55	1197.7	01set2006, 18:00	29.51
R3	10008.55	1193.8	02set2006, 00:00	29.91
W8	1492.16	820.8	01set2006, 21:00	88
W9	1401.74	815.1	01set2006, 18:00	78.6
J4	2893.9	1590.2	01set2006, 18:00	83.45
R4	2893.9	1543.4	02set2006, 03:00	81.92
W10	1927.94	866	02set2006, 06:00	88.8
W7	787.61	288.5	01set2006, 21:00	73.6
J5	15618	3799.2	02set2006, 03:00	49.02
R5	15618	3797.9	02set2006, 09:00	48.75
W12	1003.85	339.9	01set2006, 18:00	64.64
W11	485.32	155.9	01set2006, 18:00	70.1
J6	17107.17	4111.1	02set2006, 09:00	50.28
R6	17107.17	4099.9	03set2006, 03:00	48.74
W13	3316.22	1294.4	02set2006, 06:00	87.32
W14	1184.23	394.8	01set2006, 18:00	57.15
J7	21607.62	5270.5	03set2006, 03:00	55.12
R7	21607.62	5247.7	03set2006, 15:00	53.55
W15	2822.43	403.1	02set2006, 12:00	38.43
W16	1576.87	679.9	02set2006, 00:00	88.98
J8	26006.92	5969.7	03set2006, 12:00	54.06

A.8. Summary Table for Event E3_val; collective peak time: 06-Aug-2013, 09:00.

Hydrologic Element	Drainage Area (km2)	Peak Discharge (cms)	Time of Peak	Volume (mm)
W1	2397.34	235.4	05ago2013, 00:00	17.76
W2	1658.96	162.9	05ago2013, 00:00	19.56
J1	4056.3	398.2	05ago2013, 00:00	18.49
R1	4056.3	398.2	05ago2013, 00:00	20.12
W4	964.19	121.8	08ago2013, 03:00	24.27
W3	879.52	217	08ago2013, 03:00	31.1
J2	5900.01	579.2	05ago2013, 00:00	22.44
R2	5900.01	579.2	05ago2013, 00:00	23.94
W5	2610.83	398.1	08ago2013, 03:00	31.96
W6	1497.71	162.6	07ago2013, 15:00	29.84
J3	10008.55	982.6	05ago2013, 00:00	26.92
R3	10008.55	982.6	05ago2013, 00:00	27.95
W8	1492.16	146.5	05ago2013, 00:00	25.02
W9	1401.74	175.5	05ago2013, 15:00	23.93
J4	2893.9	315.4	05ago2013, 15:00	24.5
R4	2893.9	306.4	06ago2013, 00:00	25.91
W10	1927.94	189.3	05ago2013, 00:00	22.87
W7	787.61	77.3	05ago2013, 00:00	30.34
J5	15618	1533.3	05ago2013, 00:00	27.07
R5	15618	1533.3	05ago2013, 00:00	27.75
W12	1003.85	98.6	05ago2013, 00:00	25.49
W11	485.32	47.6	05ago2013, 00:00	27.36
J6	17107.17	1679.5	05ago2013, 00:00	27.61
R6	17107.17	1679.5	05ago2013, 00:00	29.75
W13	3316.22	333.7	06ago2013, 06:00	30.73
W14	1184.23	140	07ago2013, 03:00	29.73
J7	21607.62	2135.5	06ago2013, 06:00	29.9
R7	21607.62	2133.6	06ago2013, 15:00	31.25
W15	2822.43	866.5	06ago2013, 09:00	61.46
W16	1576.87	831.6	06ago2013, 09:00	86.04
J8	26006.92	3805.2	06ago2013, 09:00	37.85

A.9. Summary Table for Event E4_val; collective peak time: 15-Aug-2013, 00:00.

Hydrologic Element	Drainage Area (km2)	Peak Discharge (cms)	Time of Peak	Volume (mm)
W1	2397.34	272.3	16ago2013, 21:00	24.97
W2	1658.96	165.6	13ago2013, 00:00	24.06
J1	4056.3	405	13ago2013, 00:00	24.6
R1	4056.3	405	13ago2013, 00:00	26.01
W4	964.19	96.3	13ago2013, 00:00	23.58
W3	879.52	89.7	13ago2013, 12:00	29.69
J2	5900.01	589	13ago2013, 00:00	26.17
R2	5900.01	589	13ago2013, 00:00	27.72
W5	2610.83	484.2	13ago2013, 18:00	56.95
W6	1497.71	202.4	13ago2013, 18:00	40.41
J3	10008.55	1240.1	13ago2013, 18:00	37.25
R3	10008.55	1221.8	14ago2013, 03:00	38.2
W8	1492.16	302.5	14ago2013, 21:00	52.87
W9	1401.74	282.4	14ago2013, 18:00	48.08
J4	2893.9	584.8	14ago2013, 18:00	50.55
R4	2893.9	575.8	15ago2013, 03:00	51.53
W10	1927.94	842.1	15ago2013, 09:00	82.33
W7	787.61	555.5	15ago2013, 09:00	106.84
J5	15618	2753.8	15ago2013, 09:00	49.58
R5	15618	2752.4	15ago2013, 15:00	49.89
W12	1003.85	600.6	15ago2013, 12:00	126.44
W11	485.32	194.1	15ago2013, 12:00	83.67
J6	17107.17	3505.4	15ago2013, 15:00	55.34
R6	17107.17	3448.9	16ago2013, 09:00	55.41
W13	3316.22	3011.5	14ago2013, 12:00	170.06
W14	1184.23	611.4	14ago2013, 09:00	102.43
J7	21607.62	6005.9	14ago2013, 12:00	75.58
R7	21607.62	5943.3	15ago2013, 00:00	74.45
W15	2822.43	1505.5	14ago2013, 09:00	98.43
W16	1576.87	1818.9	14ago2013, 09:00	174.47
J8	26006.92	7404	15ago2013, 00:00	83.12

Appendix B

Reference Water and Flood Hazard Maps on Decadal Basis for Summer/ Monsoon Season.

Reference Water | Flood with return period of 5 year

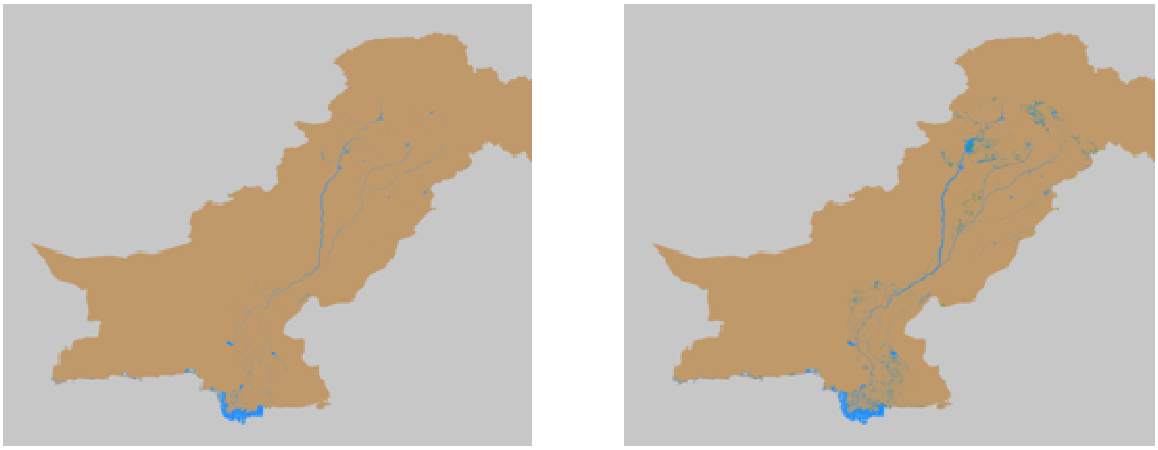

Decade 10: April, 1-10.

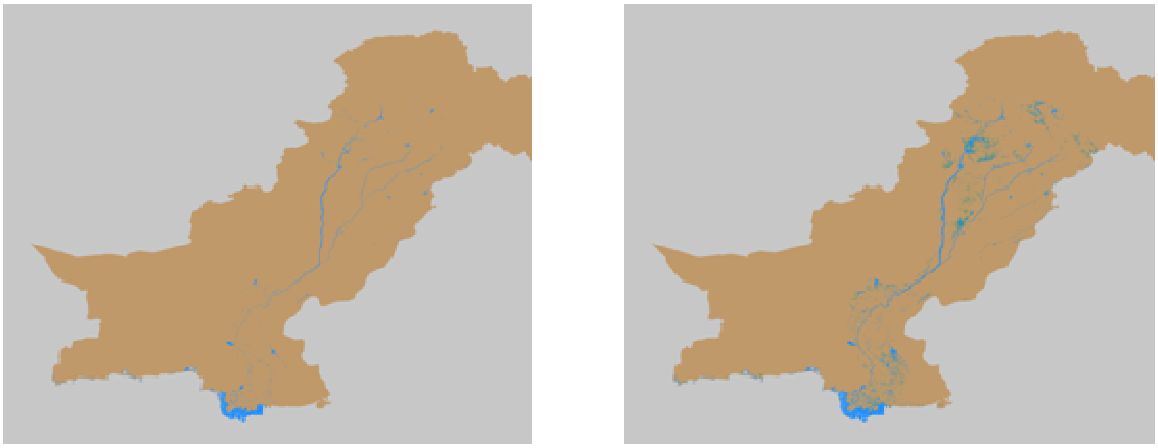

Decade 11: April, 11-20.

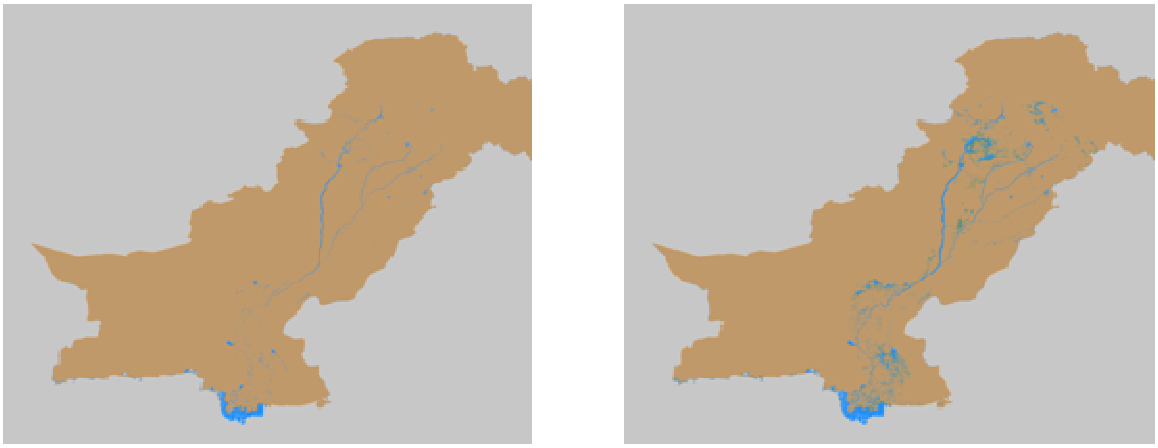

Decade 12: April, 21-30.

Reference Water **Flood with return period of 5 years**

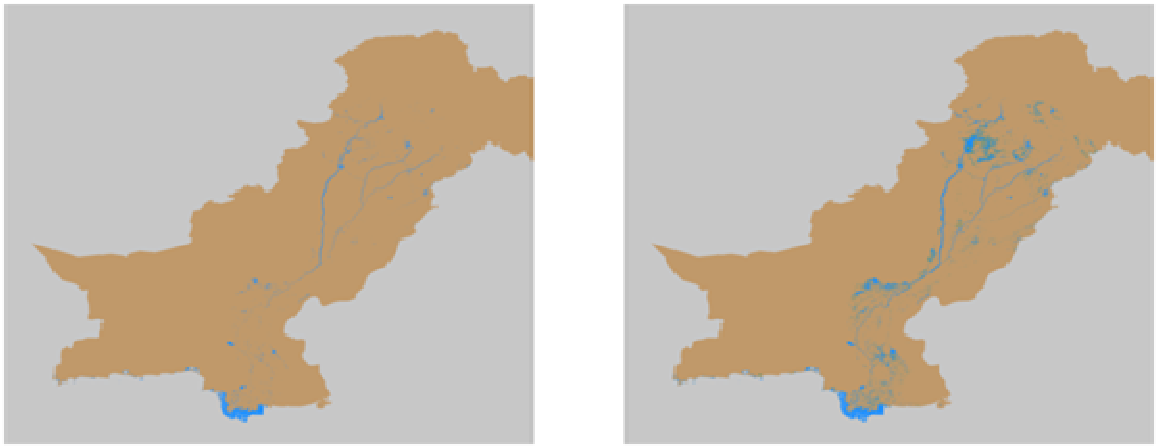

Decade 13: May, 1-10.

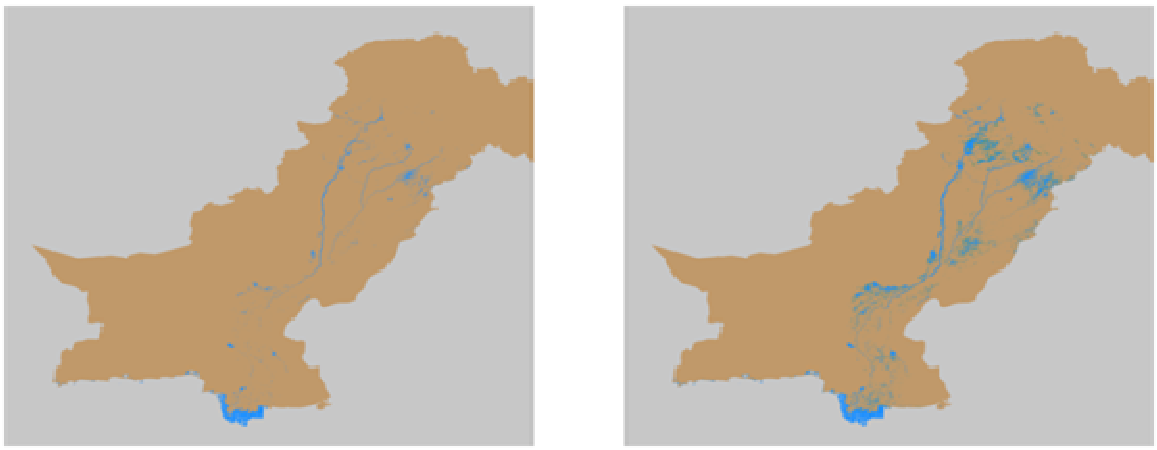

Decade 14: May, 11-20.

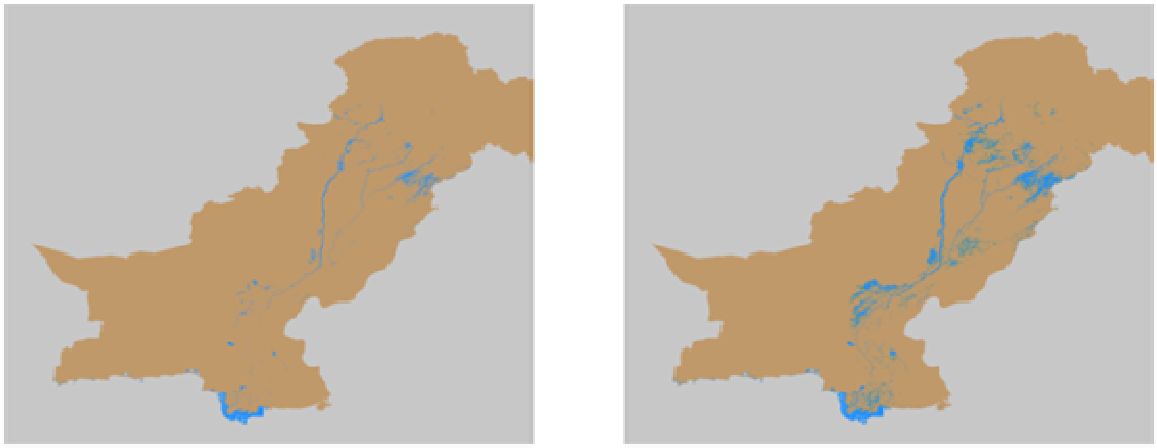

Decade 15: May, 21-31.

Reference Water **Flood with return period of 5 years**

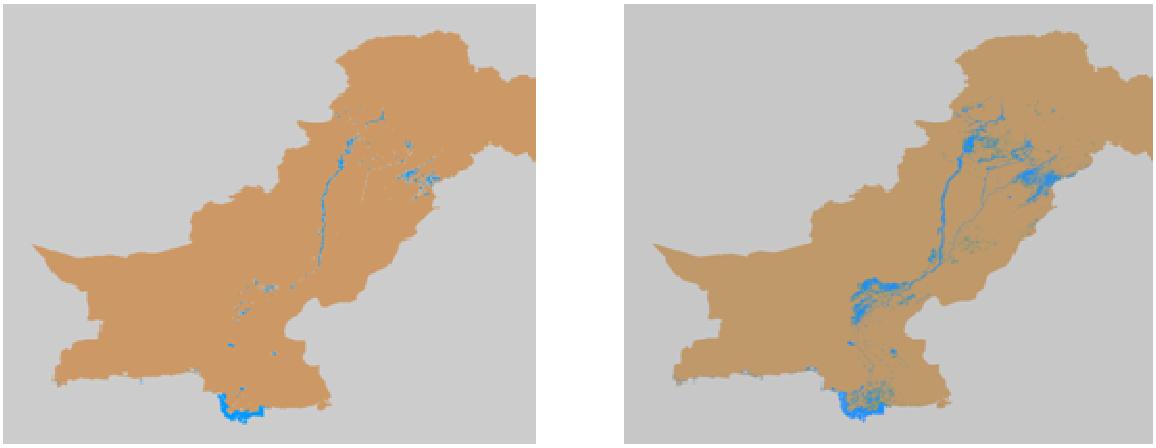

Decade 16: June, 1-10.

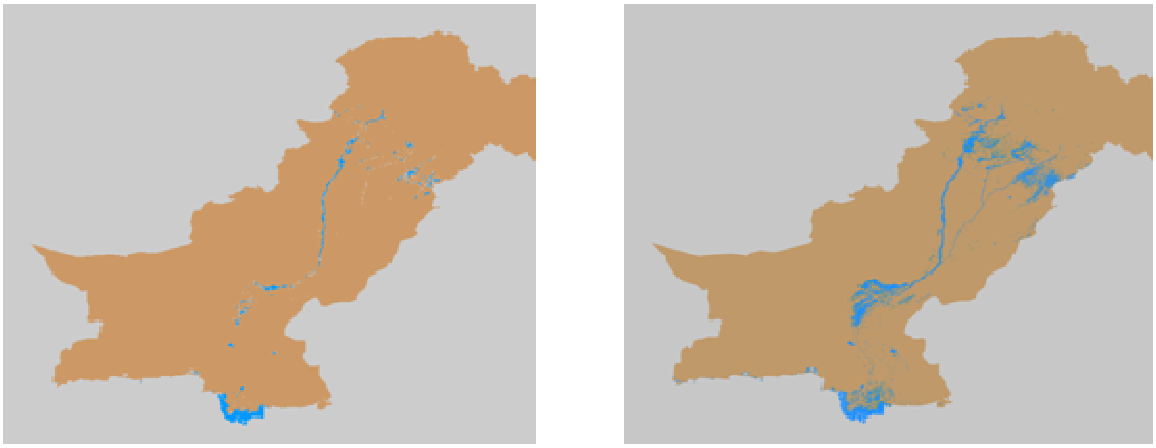

Decade 17: June, 11-20.

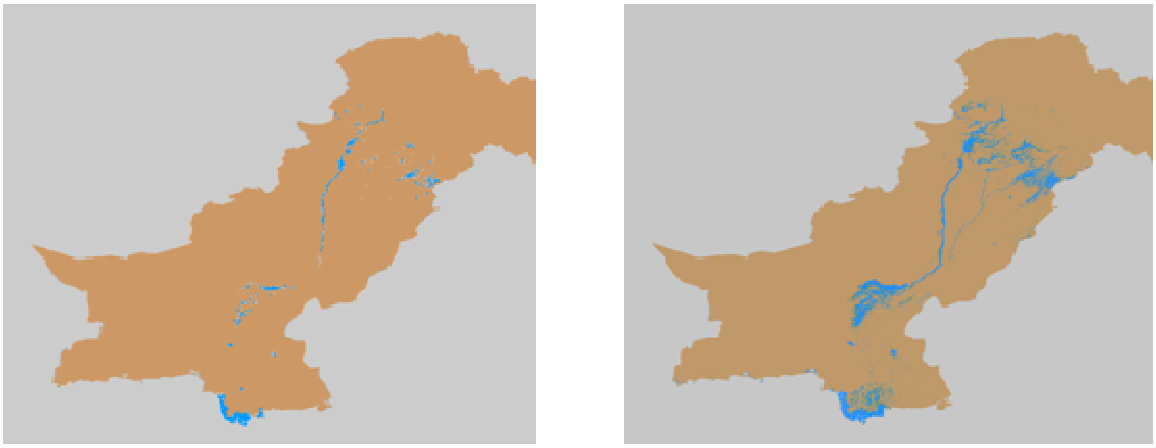

Decade 18: June, 21-31.

Reference Water **Flood with return period of 5 years**

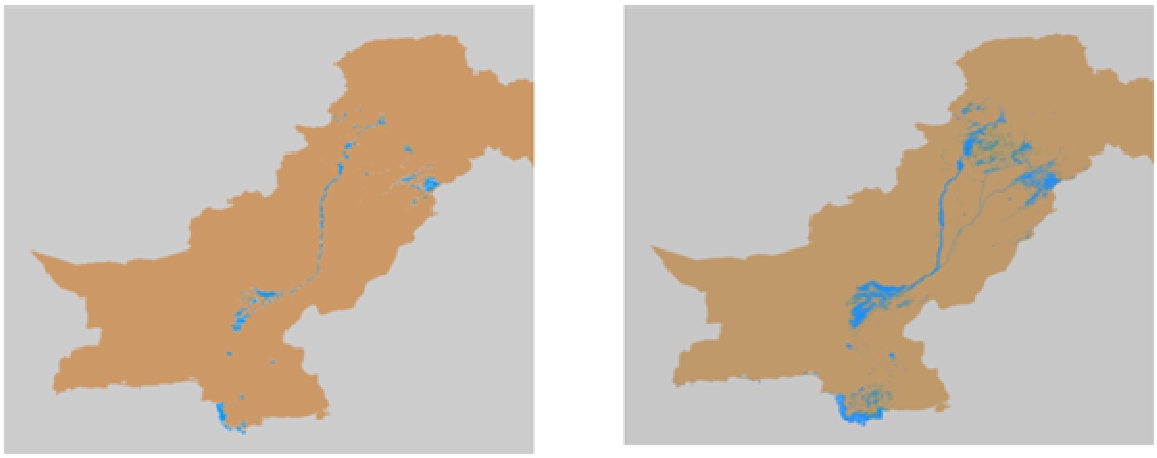

Decade 19: July, 1-10.

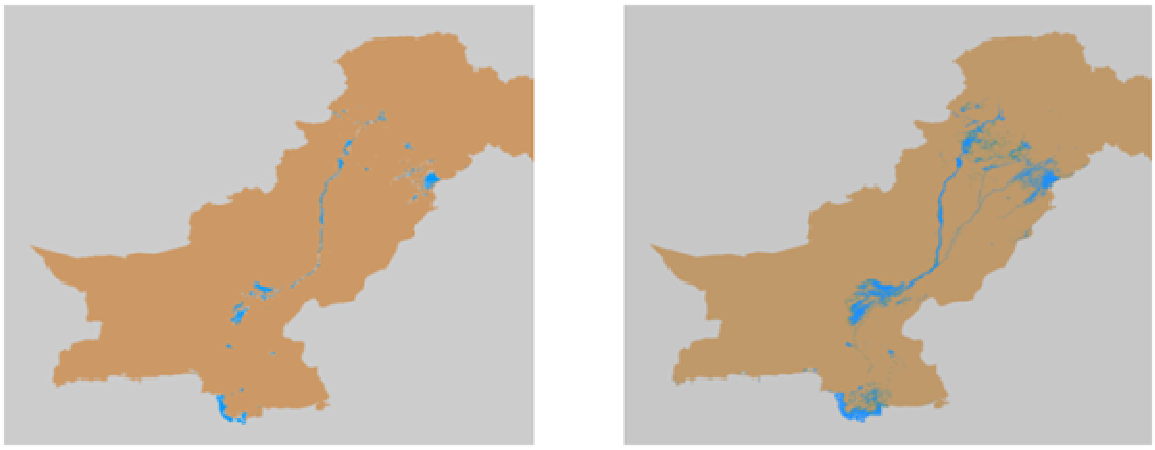

Decade 20: July, 11-20.

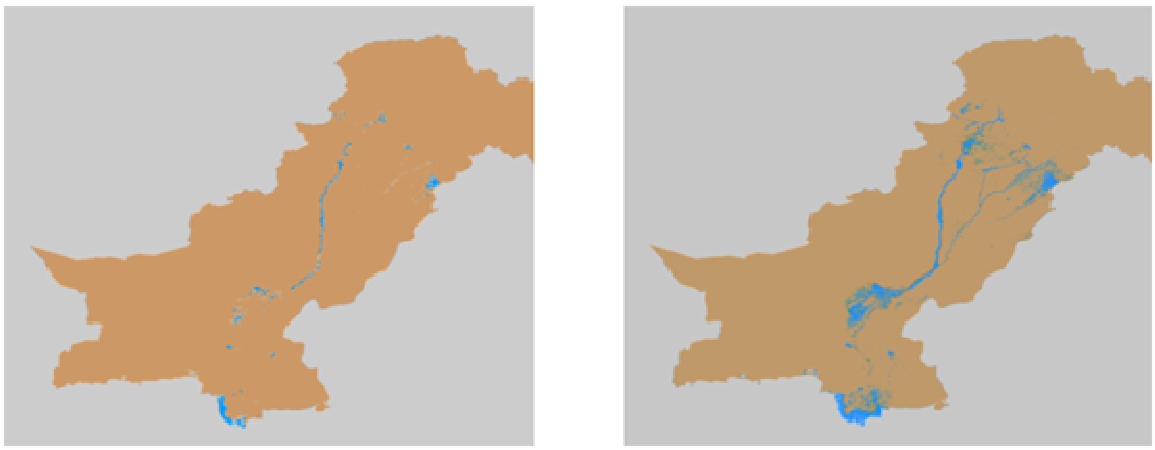

Decade 21: July, 21-31.

Reference Water **Flood with return period of 5 years**

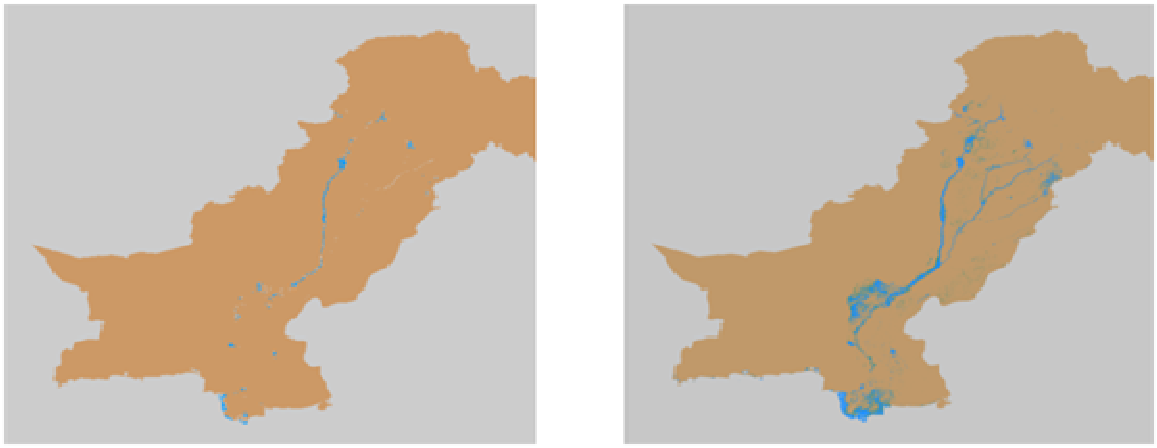

Decade 22: August, 1-10.

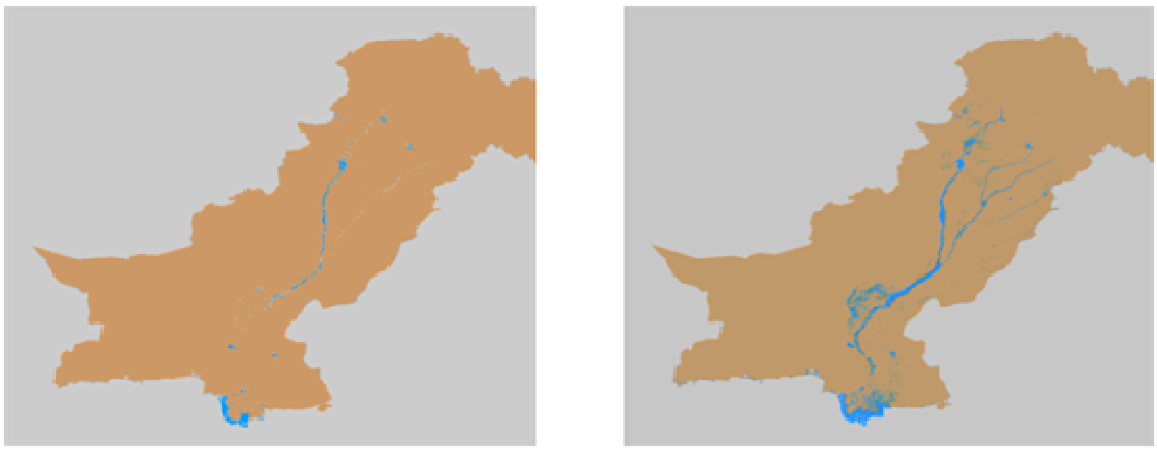

Decade 23: August, 11-20.

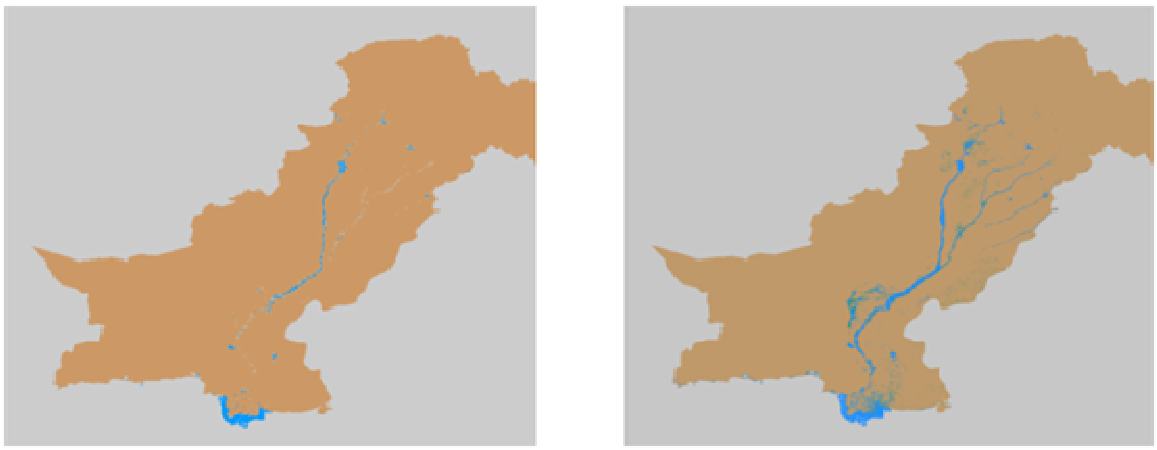

Decade 24: August, 21-31.

Reference Water **Flood with return period of 5 years**

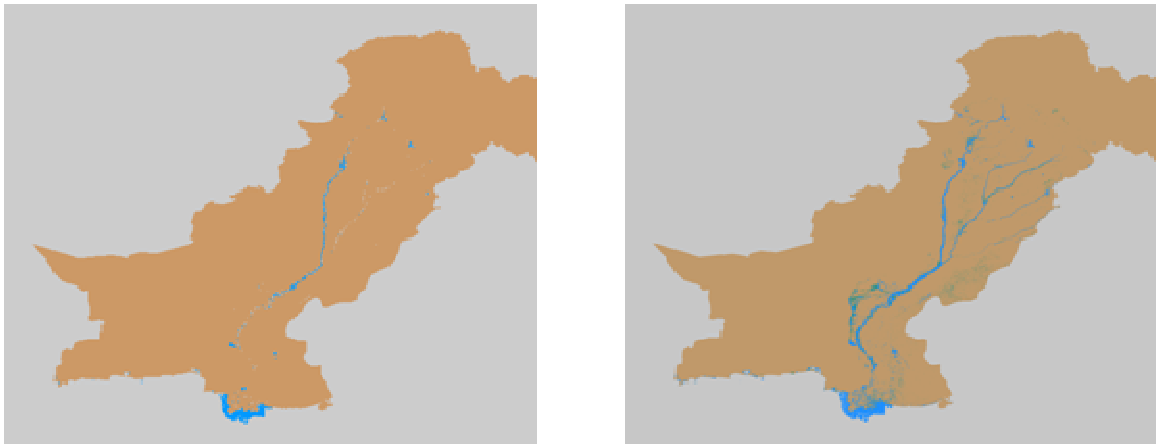

Decade 25: September, 1-10.

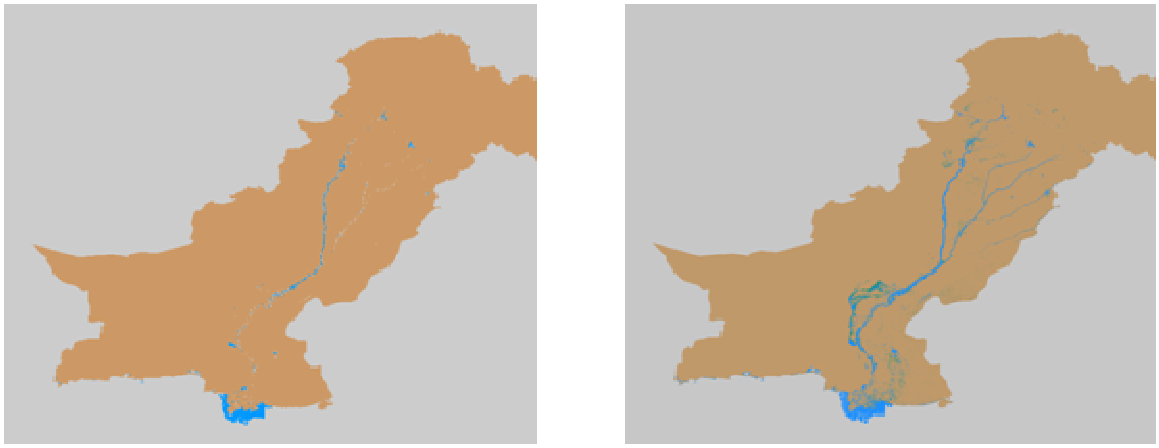

Decade 26: September, 11-20.

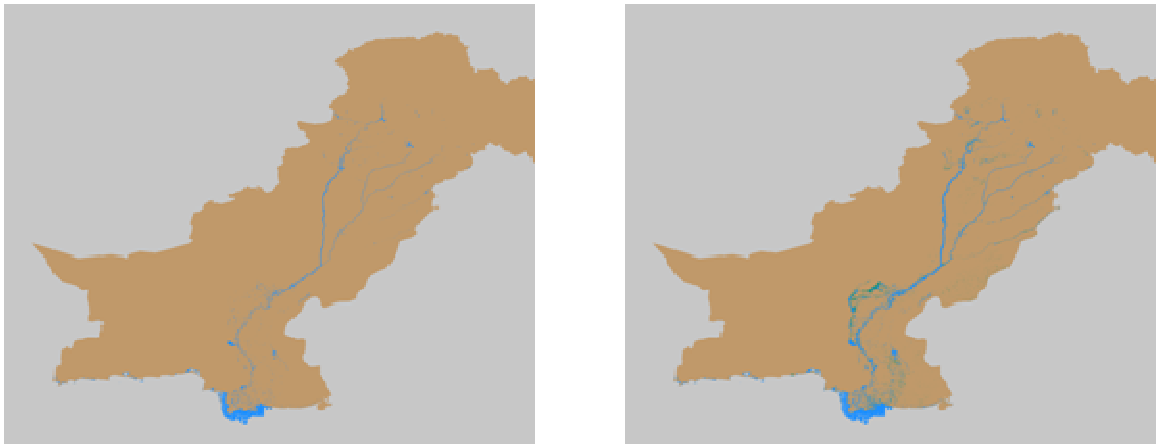

Decade 27: September, 21-30.